NBS TECHNICAL NOTE 1160

U.S. DEPARTMENT OF COMMERCE/National Bureau of Standards

NBS Reactor: Summary of Activities July 1980 Through June 1981

NATIONAL BUREAU OF STANDARDS

The National Bureau of Standards[1] was established by an act of Congress on March 3, 1901. The Bureau's overall goal is to strengthen and advance the Nation's science and technology and facilitate their effective application for public benefit. To this end, the Bureau conducts research and provides: (1) a basis for the Nation's physical measurement system, (2) scientific and technological services for industry and government, (3) a technical basis for equity in trade, and (4) technical services to promote public safety. The Bureau's technical work is performed by the National Measurement Laboratory, the National Engineering Laboratory, and the Institute for Computer Sciences and Technology.

THE NATIONAL MEASUREMENT LABORATORY provides the national system of physical and chemical and materials measurement; coordinates the system with measurement systems of other nations and furnishes essential services leading to accurate and uniform physical and chemical measurement throughout the Nation's scientific community, industry, and commerce; conducts materials research leading to improved methods of measurement, standards, and data on the properties of materials needed by industry, commerce, educational institutions, and Government; provides advisory and research services to other Government agencies; develops, produces, and distributes Standard Reference Materials; and provides calibration services. The Laboratory consists of the following centers:

Absolute Physical Quantities[2] — Radiation Research — Chemical Physics — Analytical Chemistry — Materials Science

THE NATIONAL ENGINEERING LABORATORY provides technology and technical services to the public and private sectors to address national needs and to solve national problems; conducts research in engineering and applied science in support of these efforts; builds and maintains competence in the necessary disciplines required to carry out this research and technical service; develops engineering data and measurement capabilities; provides engineering measurement traceability services; develops test methods and proposes engineering standards and code changes; develops and proposes new engineering practices; and develops and improves mechanisms to transfer results of its research to the ultimate user. The Laboratory consists of the following centers:

Applied Mathematics — Electronics and Electrical Engineering[2] — Manufacturing Engineering — Building Technology — Fire Research — Chemical Engineering[2]

THE INSTITUTE FOR COMPUTER SCIENCES AND TECHNOLOGY conducts research and provides scientific and technical services to aid Federal agencies in the selection, acquisition, application, and use of computer technology to improve effectiveness and economy in Government operations in accordance with Public Law 89-306 (40 U.S.C. 759), relevant Executive Orders, and other directives; carries out this mission by managing the Federal Information Processing Standards Program, developing Federal ADP standards guidelines, and managing Federal participation in ADP voluntary standardization activities; provides scientific and technological advisory services and assistance to Federal agencies; and provides the technical foundation for computer-related policies of the Federal Government. The Institute consists of the following centers:

Programming Science and Technology — Computer Systems Engineering.

[1] Headquarters and Laboratories at Gaithersburg, MD, unless otherwise noted;
mailing address Washington, DC 20234.

[2] Some divisions within the center are located at Boulder, CO 80303.

NBS technical note

NBS Reactor: Summary of Activities July 1980 Through June 1981

Frederick J. Shorten, Editor

Reactor Radiation Division
National Measurement Laboratory
National Bureau of Standards
Washington, DC 20234

U.S. DEPARTMENT OF COMMERCE, Malcolm Baldrige, Secretary
NATIONAL BUREAU OF STANDARDS, Ernest Ambler, Director

Issued June 1982

National Bureau of Standards Technical Note 1160
Nat. Bur. Stand. (U.S.), Tech. Note 1160, 204 pages (June 1982)
CODEN: NBTNAE

U.S. GOVERNMENT PRINTING OFFICE
WASHINGTON: 1982

FOREWORD

The National Bureau of Standards Reactor was built not only to serve the needs of the NBS but also those of other government agencies and the greater Washington scientific community. The Reactor Radiation Division was established to operate the reactor and to foster its scientific and technological use. Toward this end, the Division has a small nucleus of scientists experienced in the use of reactors for a wide range of scientific and technical problems. In addition to pursuing their own research and developing sophisticated experimental facilities, they actively seek out and encourage collaboration with other scientists engaged in challenging programs whose work can benefit from use of the reactor, but who as yet do not have the reactor experience necessary to take full advantage of the facilities available. The Division also provides irradiation services to a wide variety of users as well as engineering and other technical services.

The reactor operates at 10 MW and is designed to provide more than 25 experimental facilities ranging from intense neutron beams to extensive irradiation facilities, making it one of the most versatile high flux research reactors in the country. Thus, it is able to serve a large number of scientists and engineers in a broad range of activities both within and outside the NBS.

This report attempts to summarize all the work done which is dependent on the reactor including a large number of programs outside the Division. The first section summarizes these programs carried out by scientists in the Reactor Radiation Division and their collaborators. The second section summarizes NBS work originating entirely outside the RRD which requires no collaboration with RRD scientists. The section entitled, "Service Programs," covers those programs originating outside NBS but for which RRD provides irradiation services. The remaining sections are self-explanatory.

FOREWORD

Appreciation is extended to F. J. Shorten of the Reactor Radiation Division for his extensive contributions to the editing, organization, and preparation of this report, and T. Mangum, L. Sprecher, and S. Long for efforts in typing manuscripts.

R. S. Carter

R. S. Carter
Chief, Reactor Radiation Division
National Bureau of Standards

ABSTRACT

This report summarizes all those programs which depend on the NBS reactor. It covers the period from July 1980 through June 1981. The programs range from the use of neutron beams to study the structure and dynamics of materials through nuclear physics and neutron standards to sample irradiations for activation analysis, isotope production, radiation effects studies, neutron radiography, and nondestructive evaluation.

Key words: Activation analysis; crystal structure; diffraction; isotopes; molecular dynamics; neutron; neutron radiography; nondestructive evaluation; nuclear reactor; radiation.

DISCLAIMER

TABLE OF CONTENTS

TABLE OF CONTENTS

TABLE OF CONTENTS

A. REACTOR RADIATION DIVISION AND COLLABORATIVE PROGRAMS

SURFACE VIBRATIONAL SPECTROSCOPY WITH NEUTRON INELASTIC SCATTERING

R. D. Kelley
(Surface Science Division)

R. R. Cavanagh
(Molecular Spectroscopy Division)

and

J. J. Rush

Neutron inelastic scattering (NIS) has been used to measure the vibrational spectra of hydrogen and carbon monoxide chemisorbed on Raney nickel (a high surface area nickel powder). The neutron spectra were measured using the BT-4 triple-axis spectrometer at the NBS Reactor. A cold (77 K) beryllium-filter analyzer was used which transmits only scattered neutrons of energies ≤ 5.2 meV and thus provides a "fixed" final energy of ~ 3 meV. The energy resolution was about 5.5 to 6 percent over the whole energy range (e.g., $\Delta E \sim 5.5$ meV at 80 meV and 12 meV at 200 meV). The sample, approximately 90 g of a commercial Raney nickel, was contained in a stainless steel cell and mounted in a variable temperature cryostat which allows "in situ" gas dosing.

In agreement with previous work, the spectrum of a monolayer of hydrogen adsorbed at 300 K has peaks at 72, 117, and 142 meV. These peaks were assigned (based on theoretical predictions) to the vibrational fundamentals of multiply-bonded atomic hydrogen on nickel. We have now combined a) measurements of the vibrational spectra as a function of hydrogen coverage and b) neutron scattering intensity calculations of model hydrogen-nickel adsorption geometries to conclude that the predominant binding site for hydrogen adsorbed on the nickel powder is one of three-fold symmetry.

Measurements of the scattering intensity at 10 percent, 50 percent, and 100 percent of a monolayer of hydrogen chemisorbed on the Raney nickel indicate that the two dominant high-frequency vibrational modes

(117 and 142 meV) track the H coverage very closely at a constant intensity ratio of 2:1. The low-frequency mode (∿74 meV) has a maximum intensity at ∿10 percent of an H monolayer.

Figure 1 is the NIS vibrational spectrum of H(10 percent of a monolayer) + D(20 percent of a monolayer) which had been chemisorbed at 300 K. The hydrogen-nickel vibrational modes are found at 138 meV, 123 meV, and 72 meV (the analogous deuterium modes are shifted by $\sim\sqrt{2}$, and occur at 104 meV, 86 meV, and ∿50 meV). The frequency changes and the narrowing of the peak widths at low coverage are thought to be the result of adsorbate-adsorbate (in particular H.....H) interactions and are discussed in another paper. The peak at ∿172 meV is believed to be due to the first overtone of the 86 meV Ni-D vibration.

The fact that the 117 and 142 meV peak intensities vary directly with hydrogen coverage at a constant ratio strongly suggests that they originate from vibrations at a single type of site. Further, since these two features dominate the incoherent scattering, such a site must dominate the sites available for hydrogen chemisorption. As discussed below, we believe this to be a three-fold site. The low-frequency mode (72 meV) has been assigned -- based on theoretical calculations, neutron scattering and neutron diffraction studies of hydrogen in transition metals, and an EELS-LEED study of H on Ni(100) -- to the symmetric stretching vibration of a hydrogen chemisorbed on a four-fold site.

1. Intensity calculations of model hydrogen-nickel geometries

The assignment of the two higher frequency modes is facilitated by the non-electrodynamic nature of the NIS process (no dipole or polarizability selection rules). Both the frequency and the NIS intensity of the normal modes involving hydrogen motions can be calculated, the required parameters being the effective force constants, the bond lengths, and the symmetry of the hydrogen bonding sites. Using model geometries for the H-Ni system and a normal mode analysis, one can attempt to reproduce the observed NIS spectrum. Such calculations have been

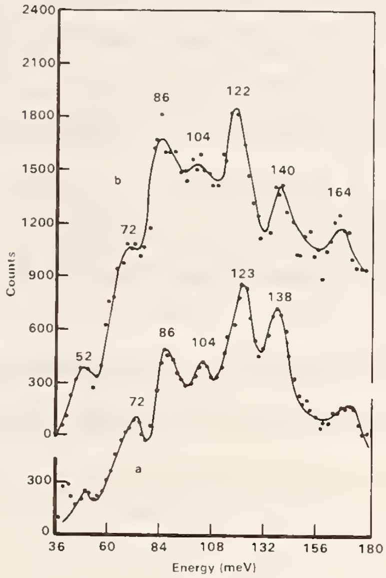

Figure 1. NIS spectra (scattering intensity vs. energy transfer) for H(10 percent of a monolayer) + D(20 percent of a monolayer) chemisorbed on Raney nickel.

performed. Binding in a three-fold symmetric site demands a two to one intensity ratio for the observed spectral features. That is, the site symmetry requires a degenerate set of modes independent of the chosen force constants or bond lengths. Only one set of force constants and bond lengths are consistent with the observed NIS features. Specifically, $d_{Ni-H} = 1.89$ Å; k = 0.58 mdyne/Å. This bond length is in good agreement with the bond length found in LEED experiments for H on Ni(111). Thus, the 117 meV feature can be assigned to a doubly degenerate mode parallel to the surface plane and 142 meV feature to the vibrational mode perpendicular to the surface plane in the three-fold symmetric site.

When a monolayer of CO is co-adsorbed with a monolayer of H at 120 K, virtually no change is observed in the NIS spectrum of the chemisorbed hydrogen (the inelastic neutron scattering cross section of CO is very low relative to hydrogen). This observation demands that the chemisorbed CO does not displace H and further that the chemisorption binding site for CO is not the three-fold symmetry preferred by hydrogen. At higher temperatures the hydrogen spectrum changes indicating interactional effects between H and CO. At room temperature, increased intensity at low frequency (<70 meV) and at high frequency (>150 meV) suggests the presence on the surface of hydrocarbon fragments.

Extensive measurements on the temperature dependence of the chemisorption of ethylene and acetylene have also been obtained and are being analyzed.

These experiments are indicative of the potential of NIS for not only identifying surface species but of using chemisorbed hydrogen to characterize the structure of high surface area polycrystalline metals (i.e., catalysts) and of molecules adsorbed on their surfaces.

LITHIUM SELF DIFFUSION IN THE IONIC CONDUCTOR LiAl

T. O. Brun and S. Susman
(Argonne National Laboratory, Argonne, IL)

and

J. J. Rush and J. M. Rowe

The properties of nearly stoichiometric β-phase LiAl are of considerable interest both for scientific and technological reasons. This fast-ion conductor is used as an electrolyte in proposed lithium-based batteries now being developed for use in automobiles. A key property for this use is the self diffusion of lithium ions through the lattice. There exist no reliable measurements of the macroscopic diffusion constant in this material, and little is known about the mechanisms for Li-ion diffusion. It is known that vacancies on the Li-sublattice are connected to the diffusion process, but little is known about the dynamics and microscopic mechanisms of this phenomenon.

Since Li-7 cross section is half incoherent (.76 out of 1.26), this substance is a difficult but natural candidate for study by neutron quasi-elastic scattering. In fact, it is an excellent model system for such studies, since in no other substance is the vacancy concentration so high. We have completed a detailed study of the Li self diffusion mechanism in a single crystal of $^{7}Li_{.49}Al_{.51}$, using the BT-4 triple axis spectrometer at NBSR. With a crystal of less than 1 cm^3 in volume, we have studied the neutron quasielastic scattering at 800K along the principal symmetry axes, with an energy resolution of 90 μeV. The results for the lineshapes have been compared to a model based upon vacancy diffusion, which is in excellent agreement with the experimental results, thus confirming the basic diffusion mechanism. A diffusion constant of 7.9×10^{-6} cm^2/sec has been derived at 800K from the results, which is the first quantitative measurement of this fundamental property.

ROTATION-TRANSLATION COUPLING IN IONIC AND MOLECULAR CRYSTALS

1. Critical Dynamics in Nd_4Br[1]

J. M. Rowe, J. J. Rush, R. Pynn*, A. Heidemann*, K. H. Michel**

We have successfully measured the coherent critical quasielastic neutron scattering in a single crystal of ND_4Br at 225 K (T_c + 7 K) using the IN-10 back reflection spectrometer at the Institut Laue Langevin in Grenoble, France. The measurements were performed at the point (0.5, 0.5, 1.0) in the cubic brillouin zone. This point becomes a superlattice reflection in the low temperature γ phase in which the $(ND_4)^+$ ions are fully orientationally ordered. The results are shown in figure 1, where the solid line represents the results of a least squares fit of a Lorentzian fitted to the data. From this fit, we obtain an intrinsic quasielastic width of 0.28 ± .1 μeV for this scattering, compared to a predicted width of 0.50 μeV from simple theory. (The dashed line in the figure is the result of a measurement below T_c where the scattering is elastic, and thus represents the resolution.) The present result shows clearly that the simple theory which ignores all collective effects except those included by mean-field theory is inadequate to explain the results. In this simple theory, the single particle reorientations are the source of the translation-rotation coupling which leads to the phase transition. The results obtained here suggest that many-body effects on the transport coefficients cannot be neglected. Further experiments are planned.

2. KCN_xKBr_{1-x} Structure and Dynamics

J. M. Rowe, J. J. Rush, S. Susman[†], D. G. Hinks[†], K. H. Michel[**] and M. Klein[#]

In the past year, many new results have been obtained in the mixed crystal system. Single crystal diffraction measurements on pure KCN as a function of temperature have been completed at 300, 250, 200, and 170 K. These results agree well with earlier measurements at 300 K and 175 K. The salient result from this study is that the orientations of the $(CN)^-$ ion become more isotropic as the temperature is lowered, a result in direct contradiction to expectations based upon a static crystal field potential. These results can be understood qualitatively on the basis of an effective potential for $(CN)^-$ orientations which includes the effect of lattice strains coupled to orientations. The effective potential due to such strains has deep minima along cubic [100] directions, in contrast to the static crystal field potential which has minima along [111] directions. The final potential, which is the sum of these two potentials is nearly isotropic and depends critically on the parameters used to describe the ion-ion potentials. In addition, there is a direct interaction between $(CN)^-$ ions due to quadrupole-quadrupole coupling which favors [100] orientations. In lowest order, the effective potential is temperature independent, but when self-consistent methods are applied, the magnitude of the strain-mediated potential becomes strongly temperature-dependent, leading to a temperature dependent total potential. Thus, as the temperature is lowered, the $(CN)^-$ orientations change from predominantly [111] towards [100]. However, the first-order phase transition at 168 K interrupts this process before [100] orientations

---

[*] Institut Laue Langevin, Grenoble, France.
[**] Universiteit Instelling Antwerp, Antwerp, Belgium.
[#] National Research Council of Canada, Ottawa, Canada.
[†] Argonne National Laboratory, Argonne, Illinois.

become favored. In the low-temperature structure (which is orthorhombic), the ions orient along cubic [110] axes. In addition to the theoretical work on the strain-mediated interactions, we have initiated a program to do molecular dynamics simulations of the alkali-cyanides and mixed cyanide-halide systems. The results of these simulations were critical to the new understanding of the behavior of KCN outlined above. A key result was the finding that the inclusion of the quadrupole-quadrupole interaction was essential. In fact, the comparison of experiment and simulation showed that the quadrupole moment in KCN was reduced by at least a factor of two from its value in the free ion. This astonishing result led to quantum calculations of the properties of the $(CN)^-$ ion which showed that induced quadrupole moments were also important and that the free molecule was not linear, a result in accord with very recent experiments.

We have also completed a single crystal diffraction study of $(KCN)_{0.5}(KBr)_{0.5}$ at several temperatures between 10 and 300 K. For this mixed crystal, we also find that the $(CN)^-$ ion orientations are predominantly [111] at 300 K, and tend continuously towards [100] as the temperature

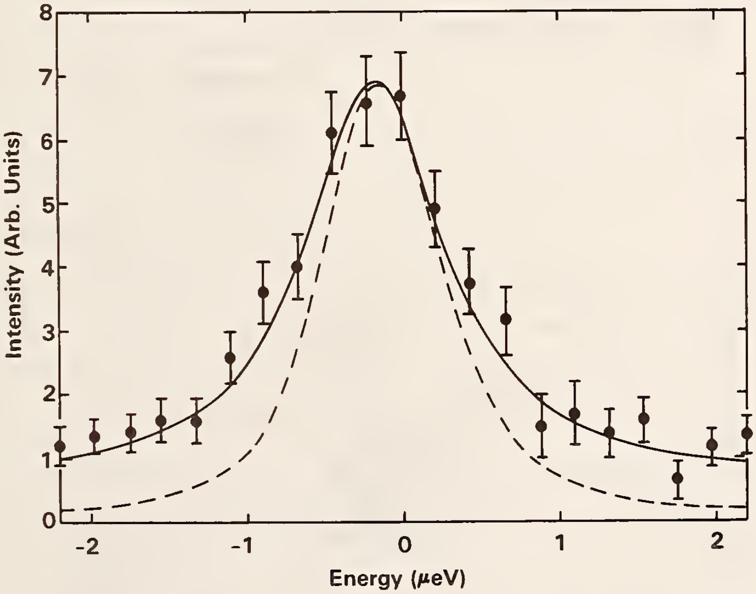

Figure 1. Measured spectra for ND_4Br. Points measured at 225 K (7 K above T_c) and dashed line at 213 K (errors for this are too small to show) are both normalized to equal peak intensity. The solid line is the result of the least squares fit to the data described in the text.

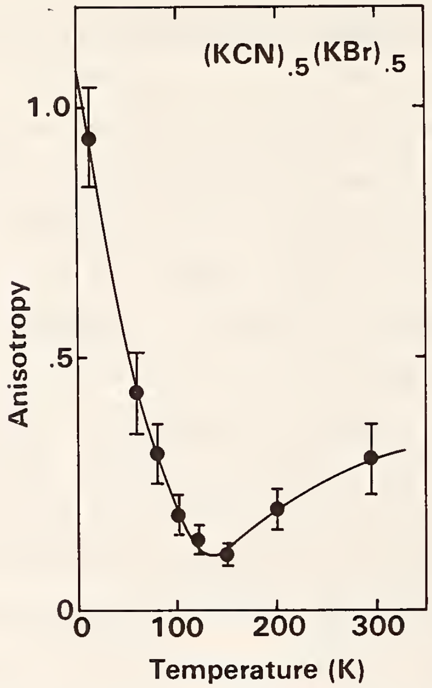

Figure 2. The anisotropy of $(CN)^-$ orientations in $(KCN)_{0.5}(KBr)_{0.5}$, as measured by $1/n\ \Sigma(F_1/F_2 - 1)^2$, where F_1 and F_2 are the structure factors of pairs of reflections with different h, k, l and equal $h^2 + k^2 + l^2$.

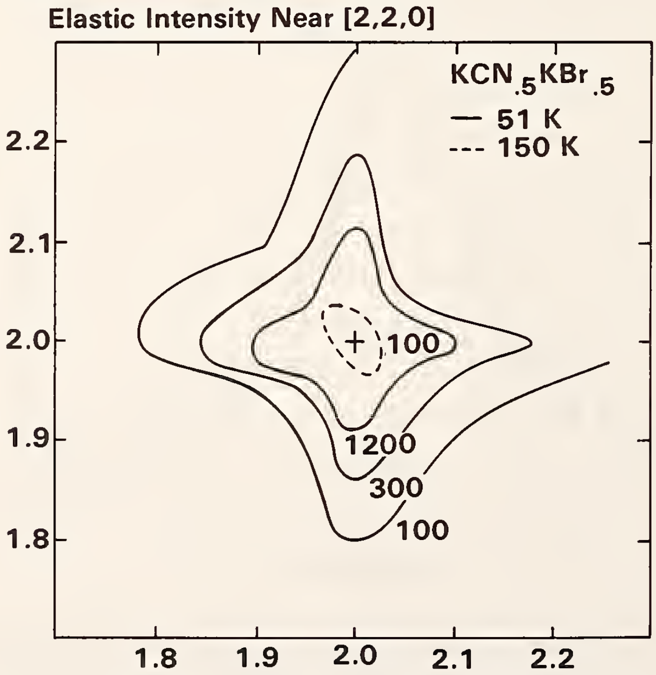

Figure 3. Elastic intensity near the [270] Bragg point in $KCN_{0.5}KBr_{0.5}$ measured at 51 and 150 K.

is reduced. However, since there is no phase transition to a long-range ordered state in this crystal, the trend continues all the way down to 10 K. At 10 K, the orientations are certainly not at all [111] but we cannot say that [100] is strongly preferred over [110]. In addition, the anisotropy of orientation, as measured by reflections of distinct (hkl) but equal $h^2 + k^2 + l^2$ goes through a minimum near 100 K then rises again. This behavior is shown in figure 2. The temperature of the minimum is almost that at which the transverse velocity of sound along [100] directions goes through a minimum and the elastic diffuse intensity starts to increase. The elastic diffuse intensity[2] in this mixed crystal has a characteristic shape around the (220) Bragg point as shown in figure 3. We have calculated this intensity based upon the model of Michel and Rowe[3] for spin-glass behavior, and are able to reproduce these contours exactly. We have also verified that $KCN_{.95}KBr_{.05}$ exhibits similar behavior at low temperatures.

Another recent study has been undertaken of the elastic diffuse scattering in pure KCN and NaCn, in order to look for the effects of the rather different $(CN)^-$ orientations in this crystal. These measurements showed very strong structured diffuse scattering in NaCN at 300 K and almost none in KCN at 300 K or 170 K. We interpret this result as a direct reflection of the predominantly [100] orientations in NaCN as compared to predominantly [111] orientations in KCN. This hypothesis is being checked by molecular dynamics simulation.

Finally, we have undertaken a powder diffraction study of $(KCN)_x(KBr)_{1-x}$ for $x \geq 0.8$. The first results for x = 0.8 showed that the low temperature structure in this mixture (which does undergo a first order phase transition) is not that of KCN, but rather a monoclinic structure. Further, the complete sample does not transform, and part of the sample remains cubic down to 4 K. In light of this unexpected result we are currently measuring samples with x = 0.90 and 0.95.

---

1. J. M. Rowe, J. J. Rush, R. Pynn, A. Heidemann, and K. H. Michel, *J. Chem. Phys.* 74, 5323 (1981).

2. J. M. Rowe, J. J. Rush, D. G. Hinks, and S. Susman, *Phys. Rev. Lett.* 43, 1158 (1979).

3. K. H. Michel and J. M. Rowe, *Phys. Rev.* B22, 1417 (1980).

THEORY OF QUASIELASTIC SCATTERING FROM VANADIUM DEUTERIDES AT LARGE MOMENTUM TRANSFERS

N. F. Berk

Work is continuing on the theory of the direct detection of host relaxation in metal hydrides by quasielastic neutron scattering. The mechanism for such scattering is assumed to be phase incoherence produced by small, random displacements of the host atom equilibrium positions which are caused by the elastic interaction between the host and diffusing impurity nucleii. A preliminary treatment[1] based on the methods of Krivoglaz and Repetskii[2] predicts that the response near $\omega = 0$ is dominated by the long-ranged part of the interaction, which leads to an integrable singularity of the scattering function. Application of the theory has been made to unpublished measurements by Magerl and Wipf[3] on quasielastic scattering from vanadium deuterides at large momentum transfers ($4 \leq Q \leq 10$ Å^{-1}). Impurity and host scatter incoherently with comparable cross sections in this system, and the difference in thermal Debye-Waller factors serves to provide contrast between them at large scattering wavevectors. The results of the study have been inconclusive, however, due mainly to relatively large energy resolution (∿ 8 meV) at the high Q-values. New experiments with tighter resolution are scheduled. Apparently the theory also needs to be extended to develop more systematically than before the regime of large energy transfers and the role of the short range part of the host-impurity interaction, in order to accomodate the constraints of finite instrumental resolution into the description of this subtle effect.

---

1. N. F. Berk and A. Magerl, *Bull. Am. Phys. Soc.* 26, 337 (1981).

2. M. A. Krivoglaz and S. P. Repetskii, *Sov. Phys. Solid State* B, 2325 (1967).

3. A. Magerl and H. Wipf, private communication.

PHONON DISPERSION OF GRAPHITE INTERCALATION COMPOUNDS

A. Magerl
and
H. Zabel
(University of Illinois, Urbana, IL)

The [001]L phonon branch of pyrolytic graphite is well described by a sinusoidal function |1|, indicating that these modes are determined only by nearest neighbor forces. The symmetry, the area mass density, and the forces between the planes change upon intercalation. The [001]L phonons are insensitive to any stacking sequence of graphite and/or intercalated planes. Therefore, there are n graphite planes and one intercalated layer within the repeat distance for a stage n compound. Correspondingly, the [001] dispersion consists of (n + 1) phonon branches.

We measured the [001]L dispersions for stage 1 K and Cs, stage 2 K, Rb and Cs and stage 3 K. The results for the stage 1 compounds together with earlier data on Rb [2] and the stage 2 compounds are shown in figures 1 and 2, respectively.

Calculations of the [001]L dispersion of intercalated graphite by several Born-von Karman models revealed that this formalism is not appropriate to describe the donor compounds. However, extending the model to include an interaction with an electronic layer between alkali and graphite planes results in a shell model, which can consistently describe the measurements for all compounds. The fits are shown as solid lines in figures 1 and 2.

---

1. R. Nicklov, N. Wakabayaski, and H. G. Smith, *Phys. Rev.* B5, 4951 (1972).

2. W. D. Ellenson, D. Semmingsen, D. Guérard, D. G. Onn, and J. Fisher, *Mater. Sci. Eng.* 31, 137 (1977).

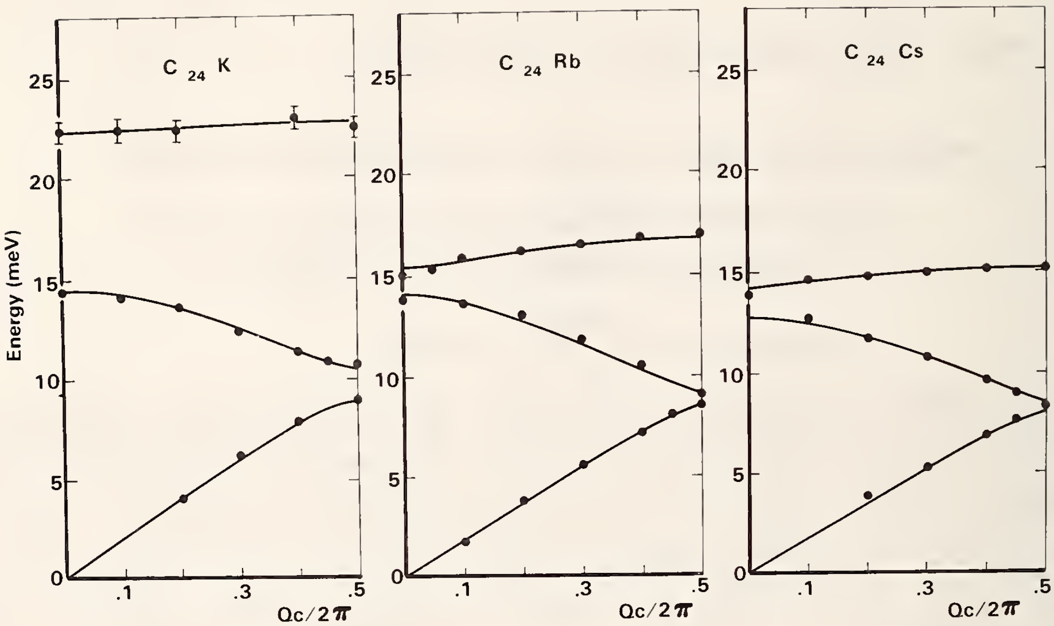

Figure 1. [001]L phonon dispersion for stage 1 intercalated graphite. The solid lines represent fits by a shell model. Data for stage 1 Rb are from reference 2.

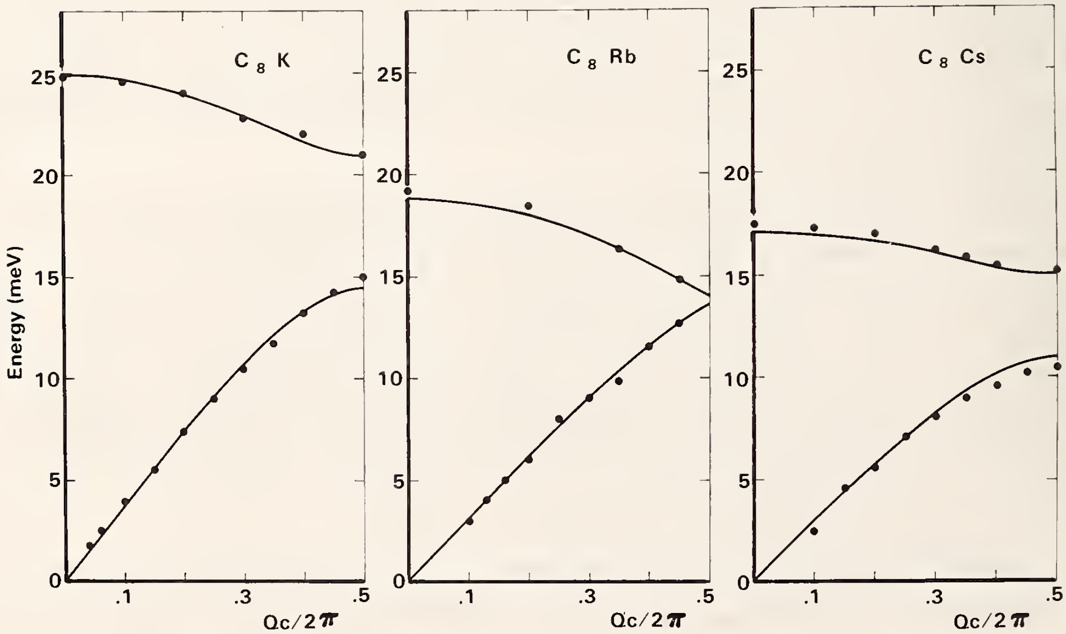

Figure 2. [001]L phonon dispersion for stage 2 intercalated graphite. The solid lines represent fits by a shell model.

UNIFICATION OF THE FUNDAMENTAL FORCES

R. C. Casella

The successes of the Glashow-Weinberg-Salam-Ward model in describing the scattering of electrons, muons, and their neutrinos from hadrons and among themselves,[1] has led to the consensus that a unification of the electromagnetic and weak forces has been achieved, which is comparable in scope to the earlier unification of electricity and magnetism by Maxwell and Faraday. At the heart of this effort lies the notion that both interactions are mediated by the exchange of vector bosons, which, in the presence of an asymmetric vacuum, assume the form of the well-known photon field $A_\mu(x)$ and the fields of the (hopefully) soon-to-be-discovered intermediate vector bosons, $W^\pm$ and Z^o. Formally, the content of the theory is expressed in terms of the gauge invariance of a suitably chosen Yang-Mills Lagrangian. The gauge particles are in fact the materialization of the vector gauge fields (generalizations of $A_\mu(x)$ in elctromagnetism) introduced to implement this invariance under local phase transformations on the fundamental fermion fields, $\psi(x)$:

$$\psi(x) \rightarrow \exp\left\{-iF^a\theta^a(x)\right\}\psi(x). \tag{1}$$

(F^a is the a th generator of the underlying gauge group.) Moreover, the idea, supported by experiment, that the strong forces are also mediated by the exchange of vector particles (gluons) has led to attempts by Pati, Salam, Georgi, Glashow, and others to unify the strong with the electroweak forces. This, in turn, has led to the possibility of proton decay and neutron-antineutron oscillations, the latter potentially observable in reactor experiments.[2] Thus far, attempts to achieve further unification by including the gravitational forces have met with enormous difficulty. I believe that a major reason for this frustration lies in the fact that the classical gravitational field is a (second-rank) tensor field, as first demonstrated by Einstein from the observation that, in the Newtonion limit, it is the energy density which is the source of the gravitational field. Energy density is the component T_{oo} of the general stress-energy tensor $T_{\mu\nu}$ which is the source term in the observationally verified Einstein field equations

$$G_{\mu\nu} = k\ T_{\mu\nu}. \tag{2}$$

This tensor property of the classical Einstein field sets it apart from the vector gauge fields (photons, intermediate bosons, and gluons) in the unified strong-electroweak theory. Within the context of perturbation theory, it has been shown by Weinberg and others that due to the unique sign of the energy density, the assumption of microscopic vector fields mediating the gravitational interaction leads to the result that the classical interaction is repulsive, contrary to observation. Nevertheless, the drive to unify leads to me to look for nonperturbative solutions, in which the underlying microscopic field is of vector character, somehow generating bilinearly the macroscopic tensor field of Einstein. It is anticipated that some progress will eventually come in this direction. At a less ambitious level, I find that the introduction of effective potentials in internal spaces can lead, by analogy with the solid-state work on tunneling, to experimentally accessible relations between the fundamental fermion (i.e., quark and lepton) masses. In a preliminary investigation, I find that the mass of the t guark is predicted to lie in the range 25 GeV to 30 GeV.

---

1. Cf., R. C. Casella, *Il Nuovo Cimento* 42A, 377 (1977).

2. See, e.g., R. C. Casella, *NBS Tech. Note* No. 1142, p. 60, (ed., F. Shorten, 1981).

THEORY OF NEUTRON SCATTERING FROM HYDROGEN IN METALS INCLUDING THE EFFECTS OF TUNNELING

R. C. Casella

The continuing program involving the theory of neutron scattering from systems in which molecular tunneling takes place in solids[1] has been extended to include the case of hydrogen in metals such as niobium, which has recently been investigated experimentally by Magerl, Rush, and Rowe at the NBS Reactor.[2]

At low temperatures, dilute (< 0(1%) concentration) hydrogen atoms in metals such as niobium and tantalum, also doped with 0(1%) concentration oxygen atoms, become trapped at the latter sites in what are believed to be two-well centers. Tunneling of the hydrogen between the two potential minima near the oxygen provides an interesting system in which molecular (atomic) tunneling in solids can be studied. Because of the very large low-energy n-p scattering length it is possible to study the excitations directly via neutron scattering. This has been done both for transitions among the tunnel-split components of the vibronic ground state[3] and also for transitions from them to the first and second vibronically excited states.[2] The picture is complicated by local strains which can produce relative displacements in the energy of the component well minima. This greatly reduces the ratio of inelastic to elastic neutron scattering within the ground doublet according to a model developed in Ref. 3. The reduction is by a factor $\overline{\sin^2 2\theta}$ where θ is a mixing angle between the left and right single-well states, describing their admixture in tight-binding approximate tunneling eigenstates. (The average is over some assumed distribution of the strain induced relative displacements.) In principle, for zero strain (infinite dilution) the elastic and inelastic differential cross sections for scattering within the ground doublet ought to be comparable. It is important to understand theoretically the neutron induced transitions to the tunnel-split excited states in order to confirm the model directly. I have shown that if separated considerably from the ground doublet, the excited doublet can be characterized by a mixing angle ϕ, generally different from θ. Matrix elements for transitions from either component of the ground doublet to either of the tunnel-split excitations depend upon both θ and ϕ. Under suitable experimental conditions, however, the differential cross section for excitations from both components of the ground doublet to either component of the excited doublet can be shown to be independent of θ and of ϕ.[4,5] Thus the ratio Λ of inelastic cross sections,

$$\Lambda = d\sigma/d\Omega)^{\text{excited}}_{\text{inelastic}} \Big/ d\sigma/d\Omega)^{\text{ground}}_{\text{inelastic}}, \tag{1}$$

is enhanced by a (concentration dependent) factor $\overline{1/\sin^2 2\theta)}$. The numerator in the expression for Λ is diminished by the transition form factor $\tilde{F}(\vec{q}\,')$ where $\vec{q}\,'$ is the momentum transfer in the higher energy inelastic neutron scattering experiment involving vibronic excitation. For small $\vec{q}\,'$, $\tilde{F}(\vec{q}\,') \sim (\vec{q}\,'.\vec{D})^2$, where $\vec{D}$ is the dipole transition matrix element. For small momentum transfer $\vec{q}$ in the lower energy experiment involving transitions within the ground doublet, the denominator $\sim (\vec{q}.\vec{r}/2)^2$ where $\vec{r}$ denotes the spatial displacement of the well minima within each two-well complex. Thus, in the limit $\vec{q}\,' \to 0$, $\vec{q} \to 0$ such that ratio ρ of the larger to the smaller remains fixed, Λ remains finite. I find, in this limit,[4]

$$\Lambda = (\rho^2/8)\ (k_F/k_I)\ (\hbar\omega/V_o) \Big/ \overline{(\sin^2 2\theta)}. \tag{2}$$

Here, (k_F/k_I) is the ratio of the final to the initial momenta of the neutron in the higher energy experiment, $\hbar\omega$ is the vibronic excitation energy, and V_o is the barrier height between the potential minima. General expressions have also been derived for Λ and various other cross section ratios when the small $\vec{q}$, $\vec{q}\,'$ expansion is not justified.[5] Because of the disparate conditions under which the higher [0(100 meV)] and lower [0(0.2 meV)] energy neutron scattering experiments are run in Nb:0(1%) H, 0(1%) O, many difficult normalization problems have to be dealt with in order to determine Λ even semiquantitatively.[2] Nevertheless, it would appear worthwhile.

---

1. R. C. Casella, *Phys. Rev.* B20, 5318 (1979).
2. A. Magerl, J. J. Rush, and J. M. Rowe, private communication (unpublished).
3. H. Wipf, A. Magerl, S. M. Shapiro, S. K. Satija, and W. Tomlinson, *Phys. Rev. Lett.* 46, 947 (1981).
4. R. C. Casella, paper to be presented at the International Conference on Phonon Physics, Bloomington, Indiana (1981).
5. R. C. Casella, to appear in *Physical Review*.

COMPUTER SIMULATION OF THE MOLECULAR DISSOCIATION OF A DIATOMIC CRYSTAL

S. F. Trevino
Energetic Materials Division, ARRADCOM, Dover, NJ 07801

and

D. H. Tsai
Thermophysics Division

Computer molecular dynamics has been successfully employed in the study of dense matter under conditions far removed from equilibrium.[1] We have been interested in applying this technique to a molecular system capable of undergoing thermal dissociation and we report here for the first time simulation of systems which exhibit both equilibrium and non-equilibrium chemical kinetics.

Our model consists of 256 particles interacting with each other in a pairwise manner through a compound Morse potential:

$$v(r) = \begin{cases} \varepsilon \left\{ \exp[-2a_1(r-r_1)] - 2\exp[-a_1(r-r_1) \right\}, \quad r \geq r_{dis} & 1(a) \\ \frac{\varepsilon}{2.5} \left\{ \exp[-2a_2(r-r_2)] - 2\exp[-a_2(r-r_2)] \right\} + Q\varepsilon, \quad r < r_{dis} & 1(b) \end{cases}$$

with $r_1 = 1$, $r_2 = .15$, $a_1 = \ln 2/.35$, $a_2 = \ln 2/20$ and Q has two values, viz 4 or 8. r_{dis} is the interparticle separation for which the two expressions for v(r) are equal. Two particles i and j are considered to form a diatomic molecule if their separation r_{ij} is less than r_{dis}, eq. 1(b). If r_{ij} is greater than or equal to r_{dis}, the molecule is dissociated, eq. 1(a). The molecular bond, once formed, is considered to be saturated, and a neighbor k is assumed to interact with i (or j) through eq. 1(a) even if r_{ik} (or r_{jk}) is less than r_{dis}. The interaction is assumed to extend to the 12 nearest molecular neighbors or their dissociated products. Note that an isolated molecule formed through eq. 1(b) is metastable with respect to its dissociated products. The method of Parrinello and Rahman[2] is used to perform the study under constant zero pressure. The sample was prepared by starting with the molecules arranged in the lowest temperature phase of nitrogen (Pa3), heating the crystal slowly through an orientational order-disorder phase transition, quenching the system to a temperature of .05ε, and allowing equilibrium to become re-established in the crystal. The resulting sample exhibited disorder among the molecular orientations as reflected in a broad angular correlation function. In this and subsequent experiments, the equations of motion were solved[3] in time steps of $\Delta t = .01\tau$ where $\tau = (mr_1^2/\varepsilon)^{1/2}$ and m is the mass of the particle.

In the first dissociation experiment with Q = 4, the enthalpy of the system was raised initally by .72ε and thereafter by .25ε four more times. At each enthalpy level, the system was allowed to evolve for 3500 time steps. The kinetic energy, pressure, volume, and distribution of molecules and free particles were monitored. Figure 1 shows the kinetic energy and the number of free particles for this run. During the latter part of each of the five constant enthalpy steps, indicated by the boxed intervals in figure 1, the system attained a constant temperature and a constant number of free particles on average. For the chemical reaction

$$A_2 \rightleftharpoons 2A$$

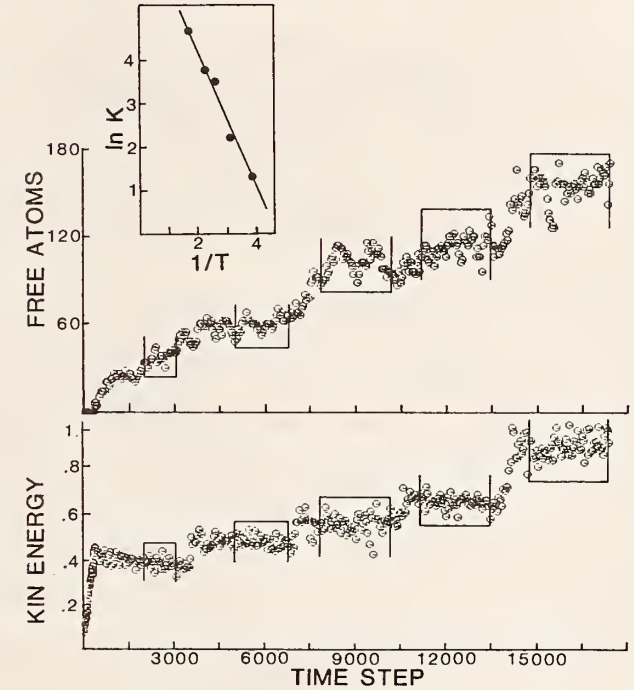

Figure 1. The lower figure is the kinetic energy per particle and the upper the concentration of free particles as a function of time for Q = 4. The boxed intervals indicate the regions over which equilibrium averages are obtained. The insert is a plot of ln K (the equilibrium reaction rate) vs. 1/T and the straight line the least squares fit.

in which the forward rate constant is k_1 and the reverse rate constant is k_{-1}, the quantity

$$K = k_1/k_{-1}$$

can be obtained[4] at each temperature from the number of free particles at that temperature. Its temperature dependence can be written[4] as

$$K = f \exp\left\{-(H_1-H_{-1})/kT\right\}$$

The insert in figure 1 shows lnK vs 1/T. The least squares fit of the data with a straight line gives $H_1 - H_{-1} = 1.57\varepsilon$. This implies that the barrier H_1 for the forward reaction is greater than the barrier H_{-1} for the reverse reaction, despite the metastability of the isolated molecule, eq. 1. This is a reflection of the many-body effect experienced by the molecules in the field of their neighbors.

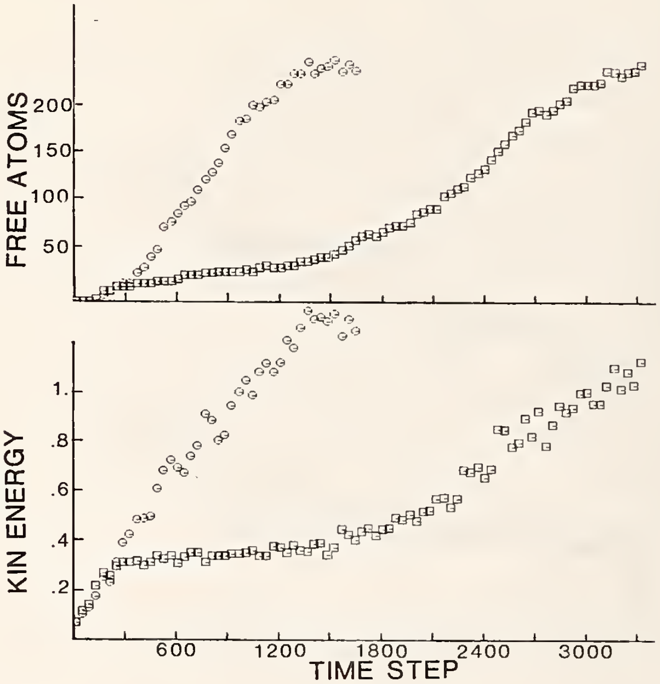

Figure 2. The lower figures are the kinetic energy per particle and the upper the concentration of free particles for Q = 8. The squares correspond to the enthalpy increment of .4ε and the circles to .8ε.

In the second dissociation experiment with Q = 8, the system was allowed to evolve after the enthalpy of the original sample was raised by each of three values, .15ε, .4ε and .8ε. In the case of .15ε, the temperature reached .16ε, one molecule decomposed and the system remained in this condition for 6000 time steps. The results for the other two runs are shown in figure 2. For .4ε, slow and partial decomposition persisted for the first 2000 time steps after which more rapid decompositon occurred until all the molecules were reacted. For .8ε, rapid decompostion occurred almost immediately until all the molecules were reacted.

These results show that with Q = 4, the system undergoes well-behaved endothermic reactions when it is heated, and exhibits equilibrium chemistry. With Q = 8, the system undergoes an explosive exothermic reaction when it is heated, and the reaction rate as well as the induction time depend on the temperature of the system.

We thank N. Berk, R. D. Mountain, and W. Braun for their discussions and interest in this work. This work was supported in part by the Army Research Office under contract MIPR No. ARO 2-79.

---

1. A. Paskin and G. J. Dienes, *J. Appl. Phys.* 43, 1605 (1972); W. T. Ashurst and W. G. Hoover, *Phys. Rev.* *A*11, 658 (1975); D. H. Tsai and R. A. MacDonald, *Phys. Rev.* *B*14, 4714 (1976); D. H. Tsai and R. A. MacDonald, *High Tempuratures-High Pressures*, 8, 403 (1976); V. Y. Klimenko and A. N. Dremin, Detonatsiya, Chernogolovka, eds. O. N. Breusov et al. (Akad Nauk., USSR, 1978) p. 79; B. L. Holian, W. G. Hoover, B. Moran and G. K. Straub, *Phys. Rev.* *A*22, 2798 (1980).

2. M. Parrinello and A. Rahman, *Phys. Rev. Lett.* 45, 1196 (1980).

3. D. H. Tsai, in Accurate Characterization of the High Pressure Environment, ed. E. C. Lloyd (*Natl. Bur. Stds. Spec. Publ.* 326, Washington, DC 1971) pp. 105-123.

4. Walter J. Moore, *Physical Chemistry*, second edition (Prentice-Hall Inc, 1956) Chapter 17.

SPIN WAVE EXCITATIONS IN DILUTE Pd(Fe)

J. W. Lynn
(University of Maryland, College Park, MD)
and
(National Bureau of Standards, Washington, D.C.)
and
J. J. Rhyne
and
J. I. Budnick
(University of Connecticut, Storrs, CT)

The properties of magnetic impurities, such as Fe, Co, or Ni in Pd, have attracted considerable interest because of the formation of "giant moments" in this system. In the range of impurity concentrations where these giant-moment clusters are isolated from each other, the system is thought to form a spin-glass state at low temperatures, whereas at high concentrations a transition to a conventional ferromagnetic state is observed. In the intermediate concentration range, a crossover from ferromagnetic to spin-glass behavior should be observed.

The critical concentration for ferromagnetism to occur is ∿0.12 percent Fe, and a relatively uniform ferromagnetic state is achieved for Fe concentrations exceeding ∿3 percent. To study the dynamics of this system in the dilute ferromagnetic region, we have carried out triple-axis measurements on a 9.1 gm powder sample of Pd(1.5 percent Fe). The incident energy was fixed at 4.87 meV, and a cold Be filter was placed in the incident beam to suppress the transmission of higher energy neutrons and reduce the ambient background. Figure 1 shows the observed magnetic scattering (after subtraction of nonmagnetic background scattering) at 40 K and 50 K (T_c = 67 K). Relatively well-defined spin-wave excitations are observed, which are seen to shift to lower energy as T_c is approached. The dispersion of these excitations is consistent with a

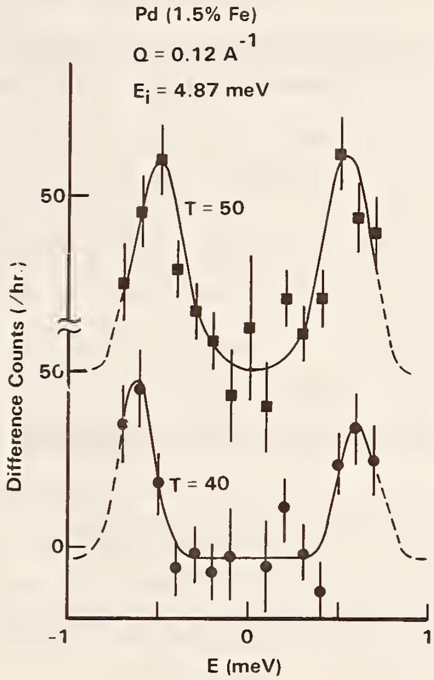

Figure 1. Observed spin-wave scattering at two temperatures below T_c (67 K), showing that the scattering shifts to smaller energies with increasing temperature. At this momentum transfer, the energy transfer is restricted by conservation of momentum and energy to 0.6 meV.

quadratic dispersion relation with $D \simeq 40$ meV-$\mathring{A}^2$ at 40 K. Further work as a function of temperature and concentration is in progress.

MAGNETIC PROPERTIES OF THE SUPERCONDUCTOR $(Ce_{1-x}Tb_x)$ Ru_2

J. A. Fernandez-Baca and J. W. Lynn
(University of Maryland, College Park, MD)

and

(National Bureau of Standards, Washington, DC)

Neutron scattering measurements have been carried out on polycrystalline specimens of $(Ce_{1-x}Tb_x)Ru_2$, for x=0.07, 0.18 and 0.44, in order to study the inelastic magnetic scattering as well as the development of magnetic correlations at low temperatures.

High resolution neutron inelastic scattering on the lowest Tb concentration sample shows the existence of an excitation at ∿0.75 meV at He temperature. At T=15K this excitation decreases in intensity while another excitation at ∿0.35 meV appears. These two peaks are consistent with the energy levels scheme predicted from the experimental values of the Lea, Leask, and Wolf parameters x and W found for the $(Ce_{1-x}Ho_x)Ru_2$ system.[1] According to this prediction the ground state is a Γ_1 singlet and the two first excited states are a Γ_4 and a Γ_5[1] triplets respectively.

Further inelastic scattering shows the existence of an excitation at ∿3.3 meV[2] in all the samples. The relative intensity of this excitation increases with increasing Tb concentration and this is attributed to Tb-Tb exchange interaction. A very weak peak appearing at ∿6.6 meV is also consistent with the predicted energy levels scheme. As the Tb exchange appears to be larger than the Ho exchange in the related Ho system,[3] further measurements at a lower concentration of Tb will be necessary to establish the single ion crystal field level diagram unambigously.

Small angle neutron scattering measurements have been carried out on the x=0.18 sample in order to study the spatial and temperature dependence of the magnetic correlations in this system. Momentum transfer values between 0.04 and $0.15 Å^{-1}$ were measured and the data were found to be well represented by an Ornstein-Zernike correlation function. The correlation range increased from $\xi=8Å$ at 5K to $\xi=16Å$ at T=1.17K with no sign of saturation. This behavior is similar to that found in the related Ho system.[1]

---

1. J. W. Lynn, D. E. Moncton, L. Passell, and W. Thomlinson, *Phys. Rev.* B21, 1, 70 (1980).

2. J. A. Fernandez-Baca and J. W. Lynn, *NBS Technical Note* 1142, F. Shorten Ed. 77 (1981).

3. J. A. Fernandez-Baca and J. W. Lynn, *J. Appl. Physics* 52, 3, 2183 (1981).

MEAN FIELD BEHAVIOR OF FERROMAGNETIC $HoRh_4B_4$

J. W. Lynn
(University of Maryland, College Park, MD)

and

(National Bureau of Standards, Washington, DC)

and

R. N. Shelton
(Iowa State University, Ames, IA)

The pseudoternary alloy $(Er_{1-x}Ho_x)Rh_4B_4$ exhibits both magnetic and superconducting properties. Pure $ErRh_4B_4$ becomes superconducting at T_{c1} = 8.6 K, then reenters the normal conducting state at T_{c2} = 0.9 K[1] as it becomes ferromagnetic.[2] With the substitution of Ho for Er, all three phase transitions (T_{c1}, T_{c2} and T_M) decrease in temperature. Around $x \sim 0.3$ T_{c2} and T_M reverse direction and increase with x, and the three phase boundaries meet at a multicritical point[3] at $x = 0.89$, $T_M = 6.0$ K. Our susceptibility and neutron scattering studies on an alloy in this concentration region showed[4] the magnetic phase transition was mean-field like in that we obtained a critical exponent $\beta = 1/2$ for the order parameter, and we found very little critical scattering at small wavevectors. To further characterize the magnetic transition, we have carried out neutron scattering experiments on pure $HoRh_4B_4$, which shows no superconducting phase transition. Figure 1 shows the {101} Bragg peak intensity, which is proportional to the square of the magnetization. The diffraction data

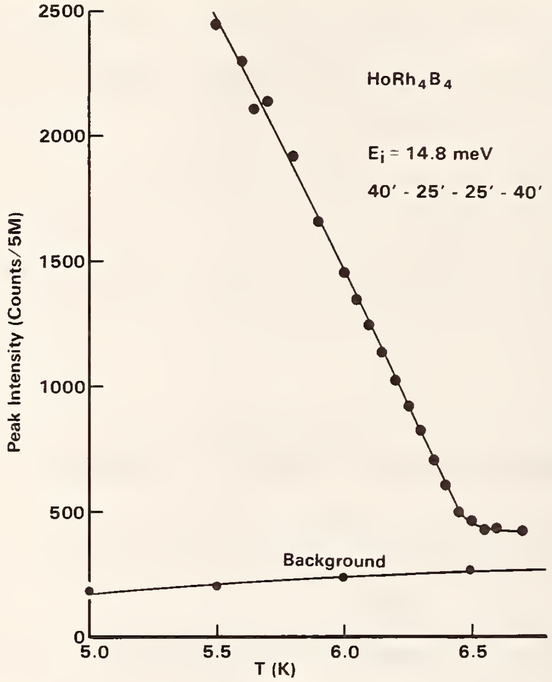

Figure 1. Intensity of the {101} Bragg peak as a function of temperature.

established the Ho moment is directed along the unique tetrogonal axis, with a low temperature saturated moment $\mu_Z = (8.34 \pm 0.3)\mu_B$. The solid curve is the mean-field result for S = 1/2, which is seen to agree well with the experimental results over the entire temperature range. Mean-field behavior has already been observed in the specific heat data.[3]

Our inelastic scattering data show that the crystal-field ground state is a doublet, with the first excited state at 4.3 meV. Therefore, S = 1/2 is to be expected. If the spins are locked along the c-axis, then the system would correspond to a three-dimensional Ising ferromagnet. Mean-field behavior (with logarithmic corrections) would then be expected if the coupling is dipolar in nature since the marginal dimensionality d^* is three in this case. However, the observed T_c of 6.5 K is too large to be due to dipolar coupling alone. The only other way to have (apparent) mean-field behavior is if the range of the exchange interaction is very long. We suspect this is the case since the magnetization is strongly coupled to the conduction electron system at lower Ho concentrations, producing the reentrant superconducting phase transition. The range of the coupling in this case is of the order of the London penetration depth λ, which is typically of the order the hundreds of angstroms. For pure $HoRh_4B_4$ the superconductivity does not appear since $T_M > T_{c1}$($\sim$5 K), but the propensity to be a superconductor is still present, leading to the apparent mean-field behavior of the magnetization.

---

1. W. A. Fertig, D. C. Johnston, L. E. deLong, R. W. McCallum, M. B. Maple, and B. T. Matthias, *Phys. Rev. Lett.* 38, 987 (1977).
2. D. E. Moncton, D. B. McWhan, J. Eckert, G. Shirane, and W. Thomlinson, *Phys. Rev. Lett.* 39, 1164 (1977).
3. H. B. Mackay, L. D. Woolf, M. B. Maple, and D. C. Johnston, *Phys. Rev. Lett.* 42, 918 (1979). Errata; 43, 89 (1979).
4. J. W. Lynn and R. N. Shelton (to be published). J. W. Lynn, in Ternary Superconductors, ed. by Shenoy, Dunlap, and Fradin, (North-Holland, 1981) p. 57.

MAGNETIC PROPERTIES OF CUBIC AND HEXAGONAL $HoMn_2$

J. Rhyne

and

K. Hardman
(Chemical Stability and Corrosion Division)

and

S. Malik and W. Wallace
(University of Pittsburgh, Pittsburgh, PA)

$HoMn_2$ crystallizes in the cubic Laves phase C-15 (Fd3m) structure which has two inequivalent sites, one for the Ho (a) and one for the Mn (d). The structure can be transformed to the hexagonal Laves phase C-14 ($P6_3$/mmc) structure by a careful annealing procedure. In this structure, the Mn occupies two sites (a and h), and the Ho occupies an f site.

High resolution neutron magnetic profile refinement studies have been performed on both the cubic and hexagonal phases at 295 K and 4 K. Bulk magnetization measurements gave a Curie temperature of 26 K for both phases and essentially equal saturation magnetizations, the latter values being affected by the large crystal field anisotropy of the Ho, particularly in the hexagonal structure.

The neutron refinement method calculated 4 K sublattice magnetization values for both the Ho and the Mn sites as given in table 1. R-factors for the profile fits are also given and indicate excellent agreement between the experimental data and the nuclear and magnetic model. Ho and Mn spins are oriented antiparallel resulting in a ferrimagnetic structure. The spins are aligned in the basal plane of the hexagonal $HoMn_2$ as expected from the symmetry of the Ho 4f electron charge distribution.

Table 1. Cubic and hexagonal $HoMn_2$ structural and magnetic parameters obtained from neutron profile refinement (Neu) and magnetization (Mag) data.

	Latt. Param. (A)	$\mu^{4K}_{Ho}(\mu_B)$	$\mu^{4K}_{Mn}(\mu_B)$	$^{4K}_{HoMn_2}$	T_c (Mag)
CUBIC	7.518	8.12	-0.84	6.45 (Neu) 6.4 (Mag)	26 K
HEX	5.282 (a) 8.622 (c)	9.40	-0.64 (a) -1.03 (h)	7.5 (Neu) 6.4 (Mag)	26 K

R factors of fit above and below Curie temperature ($R_{w.p.}$ = weighted profile R factor, $R_{expd.}$ = calculated statistical "perfect fit" R factor, $R_{mag.}$ = magnetic model R factor only):

	Cubic	Hexagonal
$R_{w.p.}/R_{expd.}$ (295 K)	8.66/4.76	5.01/3.32
$R_{w.p.}/R_{expd.}$ (4 K)	7.73/3.05	6.31/3.08
$R_{mag.}$ (4 K)	4.3	3.55

MAGNETIC AND STRUCTURAL PROPERTIES OF $Th_6Mn_{23}D_x$ AND $Y_6Mn_{23}D_x$

K. Hardman
(Chemical Stability and Corrosion Division)

and

J. J. Rhyne and E. Prince

and

H. K. Smith, S. K. Malik, and W. E. Wallace
(University of Pittsburgh, Pittsburgh, PA)

The magnetic behavior of the isostructural compounds Y_6Mn_{23} and Th_6Mn_{23} is drastically altered on hydrogenation (or deuteration). Y_6Mn_{23} is a ferrimagnetic compound with T_c = 486 K and a bulk magnetization value of 13 μ_B/f.u. (formula unit). The long-range magnetic order vanishes on hydrogen absorption. In contrast, Th_6Mn_{23} is a Pauli paramagnet, while $Th_6Mn_{23}H_{30}$ exhibits long-range magnetic ordering with T_c = 329 K and a bulk magnetization value of 18.5 μ_B/f.u.

Th_6Mn_{23} and Y_6Mn_{23} are f.c.c. (space group Fm3m) with 116 atoms per unit cell and four formula units per unit cell. There is one thorium or yttrium site and four manganese sites (b, d, f_1, and f_2). The magnetic structure of Y_6Mn_{23} is collinear with spins along the <111> direction with the b and d sites coupled antiparallel to the two f sites. All magnetically ordered spins within each of the sites are coupled in the same direction. At liquid helium temperatures, the magnetization of the manganese moments is 1.8 μ_B/Mn atom at the f sites and greater than d 2 μ_B/Mn atom at the b and d sites.

The compounds $Th_6Mn_{23}D_{16}$ and $Y_6Mn_{23}D_{22}$ were studied at 295 and 4 K by neutron diffraction profile refinement methods. The pressure isotherms of $Th_6Mn_{23}D_x$ and $Y_6Mn_{23}D_x$ were measured at 295 K. $Th_6Mn_{23}D_x$ exhibits a pressure plateau between 17 and 24 atoms of deuterium, while $Y_6Mn_{23}D_x$ has no plateau from 13 to 24 atoms of deuterium.

The site occupancies and atomic positions of the deuterium atoms were determined for both compounds. At 295 K there are 5.67 and 8 deuterium atoms in the tetrahedral f sites of $Y_6Mn_{23}D_{22}$ and $Th_6Mn_{23}D_{16}$ respectively

Table 1. $Th_6Mn_{23}D_{16}$-4 K-$P4_2mnm$ structural parameters.

	x	y	z	N
Th e	0	0	0.213 (0.214)	2
f	0.224 (0.214)	0.224 (0.214)	0	2
g	0.207 (0.214)	0.793 (0.786)	0	2
Mn b	0	0	0.5	1
Mn c	0	0.5	0	2
j_1	0.25 (0.25)	0.25 (0.25)	0.75 (0.75)	4
Mn k_1	0.005 (0)	0.359 (0.358)	0.182 (0.179)	8
Mn k_2	0.017 (0)	0.259 (0.264)	0.363 (0.368)	8
D k_3	0.005 (0)	0.204 (0.204)	0.097 (0.102)	8
D i	0.249 (0.22)	0.500 (0.5)	0	4
j_3	0.353 (0.36)	0.350 (0.36)	0.146 (0.14)	4

(space group Fm3m). However, the octahedral a site (one atom), which is fully occupied in the yttrium compound, is virtually empty in the thorium compound. The trigonal i site (8 atoms) in $Th_6Mn_{23}D_{16}$ is two-thirds full, while the tetrahedral j site (9) was occupied in $Y_6Mn_{23}D_{22}$. The remaining deuterium atoms in $Y_6Mn_{23}D_{22}$ occupied the tetrahedral k site (6.13 atoms).

$Y_6Mn_{23}D_{22}$ becomes primitive tetragonal ($P4_2$/mnm) and undergoes a magnetic phase change around 160 K corresponding to a transition in the magnetic susceptibility. Neutron diffraction data suggest this change to be from the paramagnetic phase to a short range magnetic cluster phase, in that antiferromagnetic peaks as well as magnetic contribution to nuclear peaks are present.

A structural and magnetic phase change occurs in $Th_6Mn_{23}D_{16}$ below 80 K. At 4 K, $Th_6Mn_{23}D_{16}$ has a tetragonal structure ($P4_2$/mnm). The atom positions and occupancy are given in table 1. The values in parenthesis are the face-centered cubic equivalent atomic positions. The lattice has been slightly stretched along the c axis and contracted along the a axis from that of FCC structure with a = 9.077 Å and c = 12.961 Å.

$Th_6Mn_{23}D_{16}$ becomes ferrimagnetic below the ordering temperature. Its magnetic coupling structure is similar to that of Y_6Mn_{23} except that the d site has broken down into two sites which are c and j. The magnetic moment spins on the b and c sites are coupled antiparallel to the j and two k sites. Although the bulk magnetization values (12.32 μ_B/f.u. in $Th_6Mn_{23}D_{16}$ and 13.23 μ_B/f.u. in Y_6Mn_{23}) are similar, the magnetic moments are generally less than in Y_6Mn_{23}. The magnitude of the moments in $Th_6Mn_{23}D_{16}$ at 4 K are 0.56, 2.62, 1.67, 0.99, and 0.44 μ_B/f.u. for b, c, j, k_1, and k_2 sites respectively. The striking differences in these compounds suggest that electronic and steric effects are dominant in determining the magnetic and structure order.

PREFERENTIAL ATOMIC ORDERING AND MAGNETIC STRUCTURES IN $Y_6(Fe_{1-x}Mn_x)_{23}$

K. Hardman
(Chemical Stability and Corrosion Division)

and

J. J. Rhyne

and

W. James
(University of Missouri, Rolla, MO)

The ternary system $Y_6(Fe_{1-x}Mn_x)_{23}$ exhibits unusual magnetic behavior. The end numbers, Y_6Mn_{23} and Y_6Fe_{23}, magnetically order around 485K and have magnetic moments with magnitudes of 2 to $3\mu_B$/atom. However, the Curie temperatures and bulk magnetization values of the intermediate composition ternary compounds are drastically reduced. In the compositional region, x=0.4 to 0.75, there exists no long range magnetic ordering.

The crystal structure of $Y_6(Fe_{1-x}Mn_x)_{23}$ is face-centered cubic (Fm3m), isotypical with Th_6Mn_{23}. There are four nonequivalent lattice sites occupied by Mn and/or Fe atoms and one lattice site (e), occupied by the six Y atoms. The four transition metal crystallographic sites are as follows: b (one atom), d (six atoms), and f_1 and f_2 (eight atoms each).

Neutron diffraction studies of eleven compounds across the compositional range of the $Y_6(Fe_{1-x}Mn_x)_{23}$ system reveal the presence of substantial preferential atomic ordering of Fe and Mn atoms on the four transition metal crystallographic sites. As shown in figure 1, the most striking result of the atomic ordering is the preference of Fe atoms for the f_1 site and the preference of Mn atoms for the f_2 site. The Mn atoms exhibit a preference for the b site, especially if the f_2 site is occupied with a majority of Mn atoms. The d site appears to be stoichiometrically occupied in the Mn-rich compounds but shows a preference for Fe atoms in the Fe-rich compounds. Since the b site contributes only 1 atom/f.u. and little ordering occurs on the d site, the atomic ordering of the ternary system is largely dependent on the two f sites.

The neutron results show that both Y_6Fe_{23} and Y_6Mn_{23} are magnetically ordered with different magnetic moments on the four transition metal crystallographic sites. The Fe moments in Y_6Fe_{23} are ferromagnetically coupled while the Mn moments on the b and d sites are coupled antiparallel to those on the two f sites in Y_6Mn_{23}. The magnitude and coupling of the Mn moments is very similar to those found in the polarized neutron diffraction study of a single crystal of Y_6Mn_{23}.[1]

The sublattice magnetizations of the Mn rich compounds (x=0.8, 0.9, 1.0) are given in figure 2a. In all three cases the Mn moments on the b and d sites remain coupled antiparallel to the two f sites. The introduction of Fe into Y_6Mn_{23} sharply weakens the Mn-Mn interactions and leads to the sharply reduced curie temperatures and magnetizations of figure 2a. Figure 2b illustrates the sublattice magnetization on the iron-rich ternary compounds which shows a corresponding drop on the introduction of Mn atoms favoring antiferromagnetic exchange onto the iron sites. The $Y_6(Fe_{0.73}Mn_{0.27})_{23}$

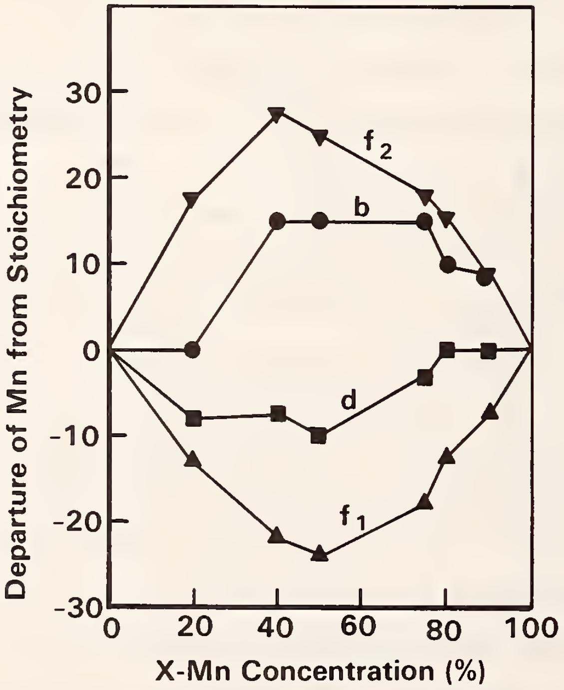

Figure 1. Preferential site ordering on Mn atoms expressed as a percentage departure from a stoichiometric distribution.

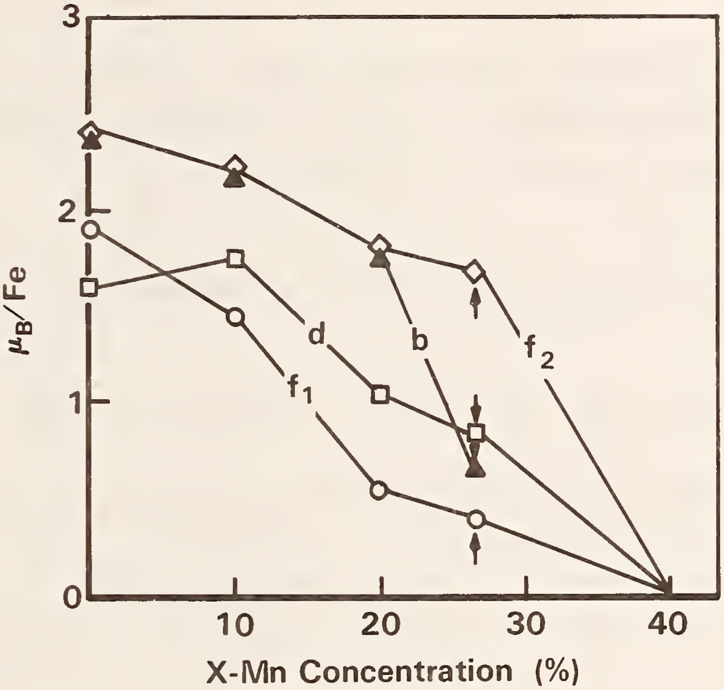

Figure 2a. Mn magnetic moments on the four independent sublattices as a function of Mn composition. The Fe atoms are not ordered in the composition range. The arrows indicate the relative spin direction on each site.

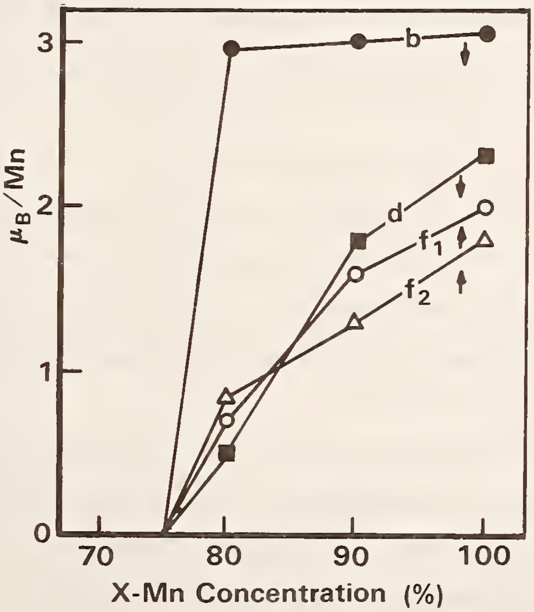

Figure 2b. Fe sublattice magnetic moments as a function of Mn composition. The Mn atoms are not ordered. All iron moments are coupled parallel except for x=0.27 which has the antiparallel configuration shown.

compound, which is close to composition for the breakdown of long range order, exhibits antiferromagnetic coupling between the Fe spins as opposed to the ferro order of the other Fe rich compounds.

---

1. A. Delapalme, J. Deportes, R. Lemaire, K. Hardman, and W. J. James, *J. Appl. Phys.* 50, 1987 (1979).

AMORPHOUS STRUCTURE OF $TbFe_2$ AND YFe_2

P. D'Antonio and J. Konnert
(Naval Research Laboratory, Washington, DC)

and

J. J. Rhyne

and

C. R. Hubbard
(Ceramics, Glass, and Solid State Science Division)

A high precision structural refinement was performed on neutron and x-ray diffraction data taken on $TbFe_2$ and neutron data on YFe_2 using the RADILS technique.[1]

The procedure allowed the calculation of radial distribution functions form from spacious scaling, background, and termination errors and the determination of the atomic coordination numbers, average inter-atomic distances, and disorder parameters. The latter are due to a combination of thermal disorder (Debye-Waller) and positional disorder peculiar to the amorphous structure.

Figure 1 shows the reduced atomic radial distribution function for YFe_2 and calculated Gaussian components arising from first through third Fe-Fe coordination spheres, first and second Y-Fe spheres and, first Y-Y coordination. The corresponding coordination numbers (N), atomic separation distances (r) and thermal plus positional disorder parameters (σ) are given in table 1 for amorphous YFe_2 and $TbFe_2$ (neutron--N and x-ray--X). The table also lists equivalent values for crystalline laves phase

Table 1. Coordination numbers, N, interatomic distances, r, and disorder parameters, σ, for amorphous YFe_2, $TbFe_2$ and compared to crystalline YFe_2.

	YFe_2			$TbFe_2$-N			$TbFe_2$-X			YFe_2-C		
Distance	N	r,A	σ,A	N	r,A	σ,A	N	r,A	σ,A	N	r,A	σ,A
Fe-Fe	12.0	2.49	0.17	12.0	2.52	0.18	12.0	2.50	0.13	12.0	2.60	0.10
R-Fe	15.2	3.03	0.21	15.2	3.06	0.19	15.0	3.02	0.19	24.0	3.05	0.20
				14.8	3.07	0.28						
				20.5	3.2							
R-R	9.3	3.50	0.21	9.2	3.49	0.20	7.2	3.43	0.21	4.0	3.19	0.22
				7.2	3.50	0.25						
				6.3	3.42							
Fe-Fe	24.5	4.20	0.30	23.3	4.24	0.30	29.4	4.18	0.21	24.0	4.51	0.29
				21.0	4.36	0.37						
R-Fe	28.5	4.80	0.32	28.5	4.83	0.27	28.8	4.79	0.22	32.0	4.78	0.29
				22.0	4.88	0.36						
Fe-Fe	24.0	5.12	0.29	24.0	5.21	0.27	18.0	5.13	0.19	24.0	5.20	0.30
				19.0	5.15	0.43						

phase YFe_2 (YFe_2-C) for comparison. It is noted that Fe-Fe coordination values are largely exchanged in the amorphous structure which the R-Fe (rare earth-ion) and R-R values differ considerably between the amorphous and crystalline structures.

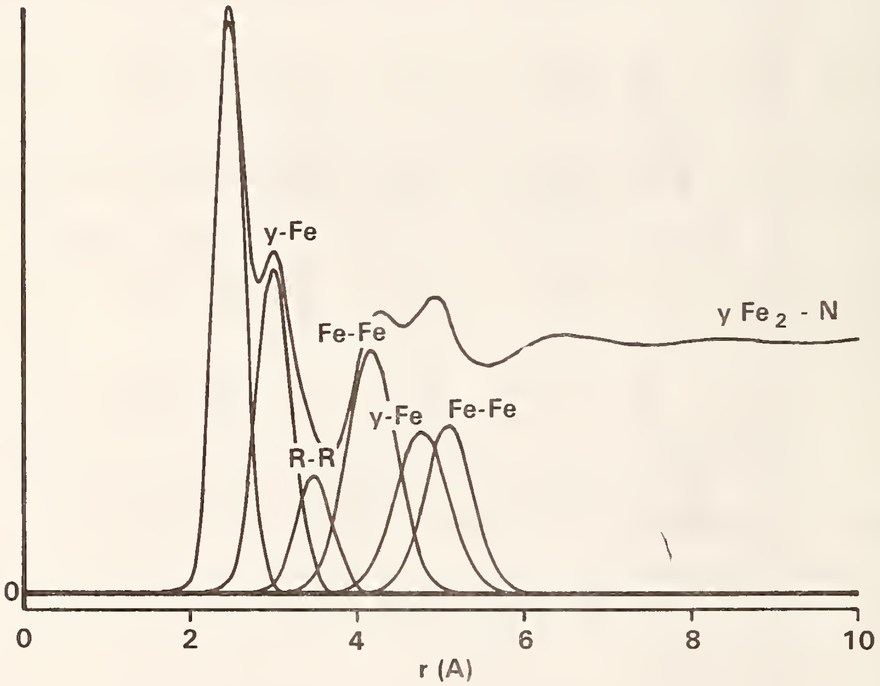

Figure 1. Reduced radial distribution function $4\pi p(r)$ for amorphous YFe_2 showing individual Gaussian coordinator components and corresponding average interatomic distances.

---

1. P. D'Antonio and J. H. Konnert, *J. Appl. Cryst.* 12, 634 (1979).

COMPARISON OF THE FITS OF TWO MODELS TO THE SAME SET OF POWDER DIFFRACTION DATA

E. Prince

It frequently happens that it is necessary to compare two models that both appear to give reasonably good fits to a powder diffraction pattern when refined by the Rietveld[1] method. Hamilton's R-factor ratio test,[2] can only be used if it is possible to define independent statistics both of which have χ^2 distributions. This condition can be met if the parameters of one model form a subset of the parameters of the other, but it may not be possible otherwise. A statistical test that can be used in more general cases was introduced by Williams and Kloot.[3] This test involves looking for correlations between the differences in the predictions of the models and the differences between the observed data and the arithmetic means of the model predictions. Let $Z_i = Y_{oi} - (1/2)(Y_{1ci} + Y_{2ci})$, and $X_i = (Y_{ici} - Y_{2ci})$, where Y_{oi} is the observed intensity at point i and Y_{1ci} and Y_{2ci} are the intensities predicted by model 1 and model 2, respectively. We want to determine the slope, λ, of the regression line $Z = \lambda X$. This is the value of λ which minimized the function

$$f(\lambda) = \sum_{i=1}^{N} (Z_i - \lambda X_i)^2,$$

which is $\hat{\lambda} = \sum_{i-1}^{N} Z_i X_i \Big/ \sum_{i=1}^{N} X_i^{\,2}$.

The estimated variance of $\hat{\lambda}$ is given by

$$\hat{\sigma}_\lambda^{\,2} = \left\langle (\lambda - \hat{\lambda})^2 \right\rangle = \left[\sum_{i=1}^{N} Z_i^2 - \hat{\lambda}^2 \sum_{i=1}^{N} X_i^2\right] \Big/ \left[(N - 1) \sum_{i=1}^{N} X_i^2\right].$$

The $(1 - \alpha)\%$ confidence interval for λ is $\hat{\lambda} \pm \hat{\sigma}_\lambda T_{1-\alpha}$, where $T_{1-\alpha/2}$ is the

$$\int_{-\infty}^{T} \phi(t,\nu)dt = 1 - \alpha/2,$$

and $\phi(t, \nu)$ is the density function for student's t distribution with $\nu = (N-1)$ degrees of freedom.

The comparison of two proposed models for a lithium defficient lithium tantalate[4] gave a slope for the regression line of -0.01877 ± 0.01069 with 95% confidence, showing that model 2 was a significantly better fit to the data than model 1.

---

1. H. M. Rietveld, *J. Appl. Cryst.* 2, 65 (1969).
2. W. C. Hamilton, *Acta Cryst.* 18, 502 (1965).
3. E. J. Williams and N. H. Kloot, *Aust. J. Appl. Sci.* 4, 1 (1953).
4. A. Santoro, R. S. Roth, and M. Austin (this report, page 46).

PRECISE WAVELENGTH DETERMINATION FOR THE MULTIDETECTOR POWDER DIFFRACTOMETER

E. Prince

The maximum utility of the high-resolution powder diffractometer depends partly on as precise as possible determination of the wavelength. In order to calibrate the instrument, we calculated a diffraction pattern from yttrium iron garnet (YIG), $Y_3Fe_5O_{12}$. This compound was known because it is cubic with a relatively large unit cell, giving many well-resolved diffraction peaks. The lattice constant of a sample of was determined by Ms. E. Evans, of the International Center for Powder Diffraction Standards, to be 12.3779(3) Å. Using this value and a Rietveld refinement of the neutron powder pattern, the wavelength is YIG 1.5423(1) Å.

USE OF THE PEARSON TYPE VII DISTRIBUTION IN THE NEUTRON PROFILE REFINEMENT OF THE STRUCTURES OF $LiReO_3$ AND Li_2ReO_3

A. Santoro and R. S. Roth
and
R. J. Cava and D. W. Murphy
(Bell Laboratories, Murray Hill, NJ)

In the course of a powder neutron diffraction study of $LiReO_3$ and Li_2ReO_3, it became apparent that the peaks produced by samples of the two compounds had tails too broad to conform to a Gaussian distribution. In fact, an attempt to fit some isolated reflections with Gaussians gave unreasonably high values of the goodness of fit χ (figure 1). The agreement between observed and calculated values, however, improved dramatically when the Pearson type VII function[2,3] was used to fit the same experimental data (figure 2). This function was taken into consideration because it can be varied gradually from a Lorentzian to a Gaussian by changing the value of one of its parameters. On the basis of these preliminary results, it was decided to use the Pearson distribution in an attempt to refine the structures of $LiReO_3$ and Li_2ReO_3 with the profile analysis method.

1. Pearson Type VII Distribution

The Pearson function is represented by the equation

$$y_i = 2I\left(\frac{2^{1/m} - 1}{\pi}\right)^{1/2} \frac{\Gamma(m)}{\Gamma(m - 1/2)} \frac{I}{H}\left[1 + 4\left(\frac{2\theta_i - 2\theta_o}{H}\right)^2 (2^{1/m} - 1)\right]^{-m} \quad (1)$$

where I is the integrated intensity; H, the full width at half maximum; $2\theta_o$, the Bragg angle of the reflection; and m, a parameter defining the peak shape. For m = 1, Eq. (1) becomes:

$$y_i = (4I)/(H\pi)[1 + 4(2\theta_i - 2\theta_o)^2/H^2]^{-1} \quad (2)$$

which is a Lorentzian. For m = 2, we obtain:

$$y_i = [4I(2^{1/2} - 1)^{1/2}/(H\pi)][1 + \{4(2\theta_i - 2\theta_o)^2/H^2\}(2^{1/2} - 1)]^{-2} \quad (3)$$

which is the so called "modified Lorentzian."[4,5,6] Finally it can be shown that, for $m \to \infty$, Eq. (1) becomes a Gaussian:

$$y_i = 2I[(\ell n2)/\pi]^{1/2}(1/H)\ \exp[-(4\ell n2)(2\theta_i - 2\theta_o)^2/H^2] \qquad (4)$$

For values of m as low as 20 or 25, the Pearson function is practically undistinguishable from a Gaussian.

2. Experimental

Neutron diffraction data were collected with a five-detector diffractometer at the National Bureau of Standards Reactor using a wavelength $\lambda = 1.5416(3)$ Å produced by the reflection 220 of a Cu monochromator. The horizontal divergences of the first, second, and third collimator were 10', 20', 10' arc, respectively. The neutron data were anlyzed with the Rietveld method,[1] modified by Prince[7] to include the Pearson function. In the calculations, the value of m was assumed to be 2θ-independent. The background was assumed to be a straight line with finite slope and was refined together with the profile and structural parameters. Both structures were refined with different values of the Pearson parameter m. The final results for the refined structures are given in tables 1 and 2.

3. Discussion

It has been noted previously that the value of m was considered to be 2θ-independent. This is almost certainly an approximation which was adopted for both rhenium compounds, because line overlapping prevented the experimental determination of the variation of m with the diffraction angle. In those cases in which well separated peaks are available over the entire angular range, the value of m, in general, decreases as 2θ increases. For example, in the case of a sample of Fe_3O_4, the peaks have the shape of a modified Lorentzian at low diffraction angles and become close to a Lorentzian at high angles (figure 3). It is difficult to find a unique explanation for the departure of the powder diffraction lines from Gaussian shape. Instrumental factors can be excluded by the fact that the diffractometer, used with identical experimental conditions, gives Gaussian peaks with standard materials such as Al_2O_3 (χ between 1.1 and 1.2).

Table 1. Results of the profile refinement of the structure of $LiReO_3$.

Atom	Position	x	y	z	B
Re	6a	0	0	0	0.18(6)
O	18b	0.3801(7)	-0.012(1)	0.2540(9)	0.27(6)
Li	6a	0	0	0.227(1)	1.6(3)

$m = 1.5$, $R = 5.66$, $R_p = 5.55$, $R_w = 7.04$, $R_E = 5.00$
Space group: R3c, Z = 6; Number of observations: 2464
Number of independent Bragg reflections: 49

Table 2. Results of the profile refinement of the structure of Li_2ReO_3.

Atom	Position	x	y	z	$B^{(*)}$
Re	6a	0	0	0	0.21
O	18b	0.3580(9)	0.008(2)	0.2449(8)	0.21
Li(1)	6a	0	0	0.188(1)	1.4
Li(2)	6a	0	0	0.831(1)	1.4

(*) Thermal parameters were not refined for this compound.

$m = 3$, $R = 8.05$, $R_p = 7.58$, $R_w = 9.77$, $R_E = 7.71$
Space group: R3c, Z = 6; Number of observations: 2505
Number of independent Bragg reflections: 65

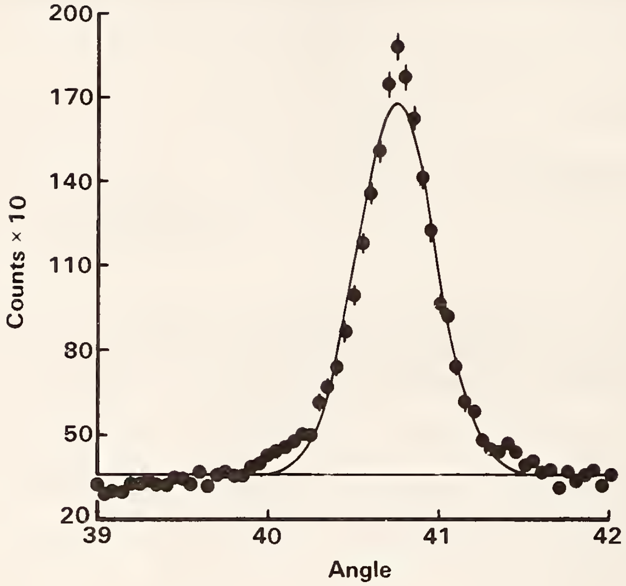

Figure 1. Least-squares fit of a Gaussian to the intensity data of a single peak of $LiReO_3$. (χ = 2.21).

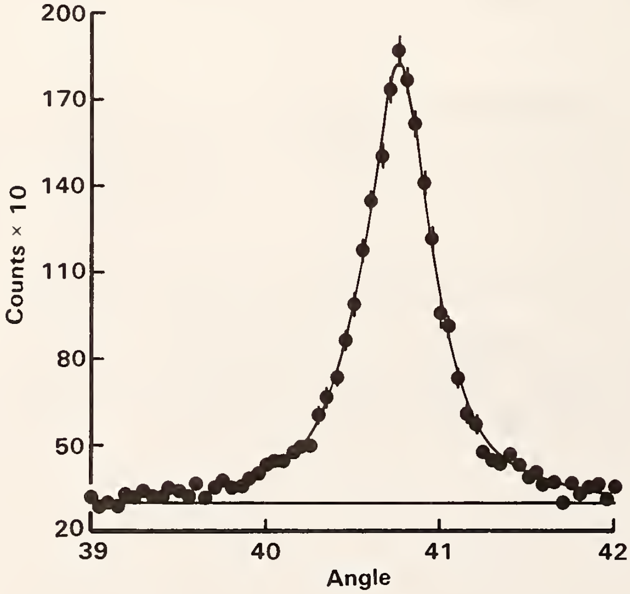

Figure 2. Least-squares fit of a Pearson distribution to the same data of figure 1 (m = 1.2, χ = 1.16).

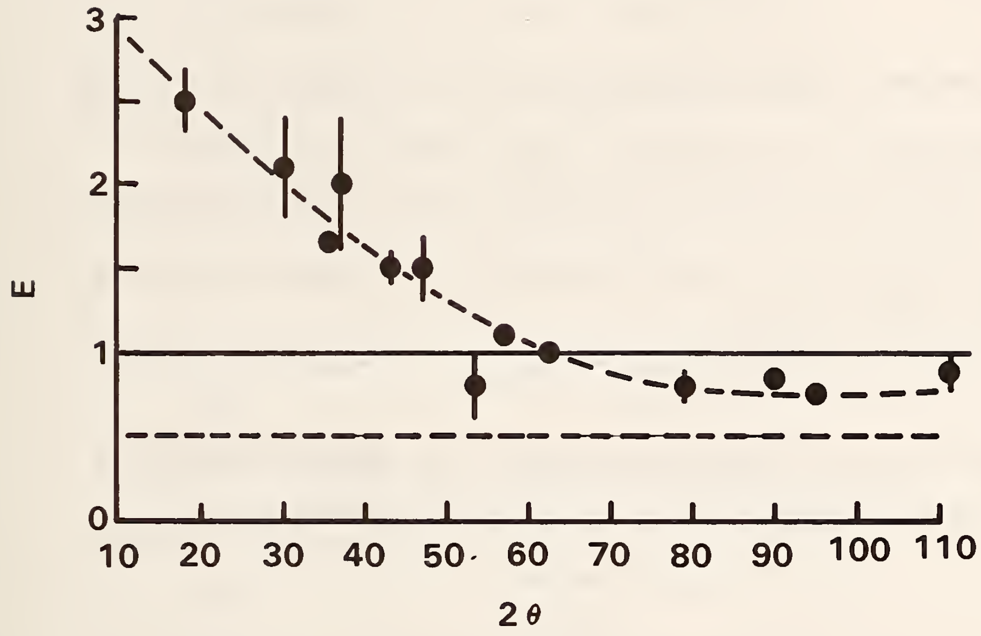

Figure 3. Plot of m versus 2θ for a sample of Fe_3O_4.

Broadening caused by particular distributions of crystallite sizes may be a possible reason for the observed shapes. However, other factors, such as structural distortions or thermal diffuse scattering, could play an important role in determining the observed intensity distributions.

The results obtained for the two rhenium compounds show conclusively that the Pearson function can be applied successfully to neutron profile refinements. However, a detailed understanding of the factors which may cause departures from the Gaussian shape is still needed, especially to predict the variation of m with 2θ.

---

1. H. M. Rietveld, *J. Appl. Cryst.* 2, 65-71 (1969).

2. W. D. Elderton and N. L. Johnson, *Systems of Frequency Curves* (Cambridge Press, NY, 1969), pp. 77-78.

3. M. M. Hall, V. G. Veeraraghavan, H. Rubin, and P. G. Winchell, *J. Appl. Cryst.* 10, 66-68 (1977).

4. E. G. Sonneveld and J. W. Visser, *J. Appl. Cryst.* 8, 1-7 (1975).
5. G. Malmros and J. O. Thomas, *J. Appl. Cryst.* 10, 7-11 (1977).
6. C. P. Khattak and D. E. Cox, *J. Appl. Cryst.* 10, 405-411 (1977).
7. E. Prince, *Natl. Bur. Stand. U.S. Tech. Note* 1117 (edited by F. J. Shorten, 1980), pp. 8-9.

POWDER NEUTRON DIFFRACTION STUDY OF THE NONSTOICHIOMETRIC SOLID SOLUTION OF LITHIUM TANTALATE $9LiTaO_3:Ta_2O_5$

A. Santoro
and
R. S. Roth and M. Austin
(Ceramic, Glass, and Solid State Science Division)

Lithium tantalate, $LiTaO_3$, exists over a fairly large nonstoichometric solid solution range. Some of the most important properties of the compound depend on the Li/Ta ratio, and for this reason possible mechanisms of nonstoichiometry have received considerable attention in the past. The most important models proposed so far for the defective structure of $LiTaO_3$ are those of: (i) Lerner, Legras, and Dumas [J. of Crystal Growth, 3, 231, (1968)], schematically represented in figure 1; (ii) Nassau and Lines [J. Appl. Phys, 41, 533, (1970)], represented in figure 2; and (iii) Raeuber [Current Topics in Materials Science, Vol. I, edited by E. Kaldis, North Holland Publishing Co. (1977)], represented in figure 3. Figure 4 shows the structure of stoichiometric $LiTaO_3$ and explains the symbols used in the previous illustrations. Due to lack of experimental data it has not been decided which of these models is present in the structure of nonstoichiometric $LiTaO_3$. We have, therefore, attempted to solve the defective structure of the compound by dualizing with the Rietveld method the neutron intensities collected at the NBSR with the high resolution powder diffractometer.

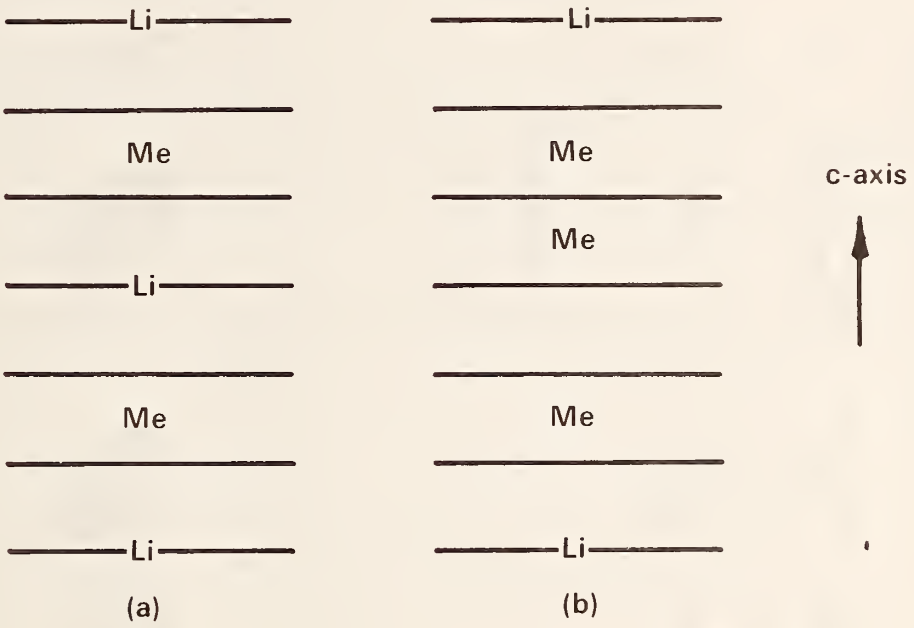

Figure 1. (a) Stacking sequence of cations in the nondefective structure of $LiMeO_3$. The horizontal lines indicate the oxygen layers. (b) The defective structure proposed by Lerner et al. (1968). The Me ion which substitutes the lithium ion is shifted along the c-axis so that it occupies an octahedral site rather than the triangular environment of oxygen ions of the original Li^+.

The nonstoichiometric lithium tantalate was prepared by mixing commercially available $LiTaO_3$ and Ta_2O_5 (99.9% purity) in the molar ratio 9:1 and by heating the mixture in a platinum crucible for 19 hours at 1000°C. The product of this treatment was ground and reheated at 1550°C for 18 hours. Intensity data were collected with the same conditions used for other compounds (see, e. g., NBS Technical Note 1142, May 1981, edited by F. Shorten, p. 104). The models refined with the profile fitting method [Rietveld, H. M., J. Appl. Cryst., 2, 65, (1969)] are illustrated in figure 5 and the results of all the refinements are given in table 1.

In order to choose between the models, we have to test the hypothesis that they give equally good descriptions of the structure. The hypothesis is analyzed in a different part of this report (E. Prince, "Comparison of the Fits of Two Models to the Same Data Set) where it is shown that the model of Nassau and Lines gives a fit to the data better than those given by the other two models.

Table 1. Results of the refinements of nonstoichiometric and stoichiometric $LiTaO_3$ - numbers in parenthesis are standard deviations on the last decimal figure. The letter C indicates that the corresponding parameter was constrained during refinement. The first three models were refined in space group R3, the others in space group R3c.

		Model of Lerner et. al. (1968)		Model of Nassau & Lines (1970)		Model of Raeuber (1977)		Defects Ignored	Stoichiometric $LiTaO_3$	Abrahams, Hamilton, & Sequeira (1967)	Δ/σ
Ta1	x	0		0		0		0	0	0	
	y	0		0		0		0	0	0	
	z	0		0		0		0	0	0	
	B	0.53(3)		0.54(3)		0.53(3)		0.43(3)	0.16(3)	0.32(7)	2.1
	n	0.33		0.33		0.33		0.33	0.33		
Ta2	x	0		0		0					
	y	0		0		0					
	z	1/2		1/2		1/2					
	B	0.53	C	0.54	C	0.53	C				
	n	0.33		0.33		0.33					
Ta3	x	0		0		0					
	y	0		0		0					
	z	0.280(4)		0.273(5)		1/3					
	B	0.53	C	0.54	C	0.53	C				
	n	0.02		0.01		0.01					
Ta4	x			0		0					
	y			0		0					
	z			0.773	C	2/3					
	B			0.54	C	0.53	C				
	n			0.01		0.01					
Ox1	x	0.0494(2)		0.0498(2)		0.0496(3)		0.0493(3)	0.0492(3)	0.0498(6)	0.9
	y	0.3401(4)		0.3407(4)		0.3403(4)		0.3403(4)	0.3430(4)	0.3436(4)	1.1
	z	0.0720(2)		0.0720(2)		0.0721(2)		0.0724(2)	0.0693(2)	0.0688(4)	1.1
	B	0.44(2)		0.45(2)		0.48(2)		0.38(2)	0.22(2)	0.52(6)	4.7
	n	1.0		1.0		1.0		1.0	1.0		
Ox2	x	0.6599	C	0.6593	C	0.6597	C				
	y	0.9506	C	0.9502	C	0.9504	C				
	z	0.5720	C	0.5720	C	0.5721	C				
	B	0.44	C	0.45	C	0.48	C				
	n	1.0		1.0		1.0					

Li1	x	0		0		0		0	0	0	
	y	0		0		0		0	0	0	
	z	0.2783(6)		0.2765(5)		0.2808(5)		0.2799(4)	0.2803(3)	0.278(2)	1.1
	B	2.3(2)		2.0(2)		3.3(2)		5.2(2)	1.9(1)	1.2(2)	3.1
	n	0.27		0.2756		0.28		0.33	0.33		
Li2	x	0		0		0					
	y	0		0		0					
	z	0.7783	C	0.7765	C	0.7808	C				
	B	2.3	C	2.0	C	3.3	C				
	n	0.29		0.2756		0.28					
Li3	x			0							
	y			0							
	z			0.62(1)							
	B			2.0	C						
	n			0.01							
Rn		4.88		4.37		5.09		5.59	3.64	3.88 based on F	
Rp		7.03		6.91		7.10		7.26	6.97	6.04 based on F^2	
Rw		9.50		9.34		9.61		9.75	9.70		
Re		5.58		5.58		5.58		5.58	5.63		
χ		1.70		1.67		1.72		1.75	1.72		

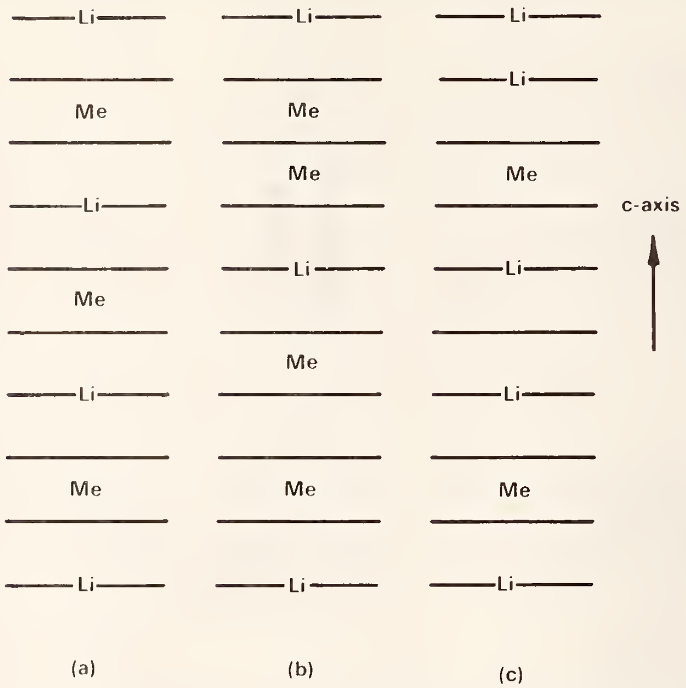

Figure 2. The stacking-fault model proposed by Nassau and Lines (1970) showing the three-cation fault. (b) Me^{5+}-rich compositions. (c) Li^{+}-rich compositions. The reference nondefective structure is shown in (a).

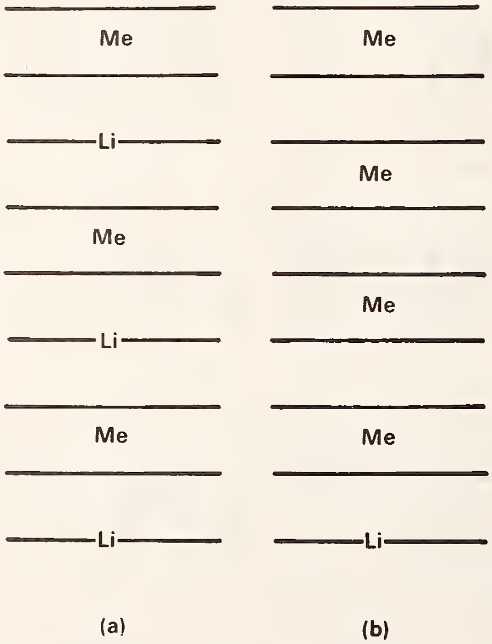

Figure 3. (a) Nondefective reference structure of $LiMeO_3$. (b) Symmetric nonpolar stacking disorder proposed by Raeuber (1977).

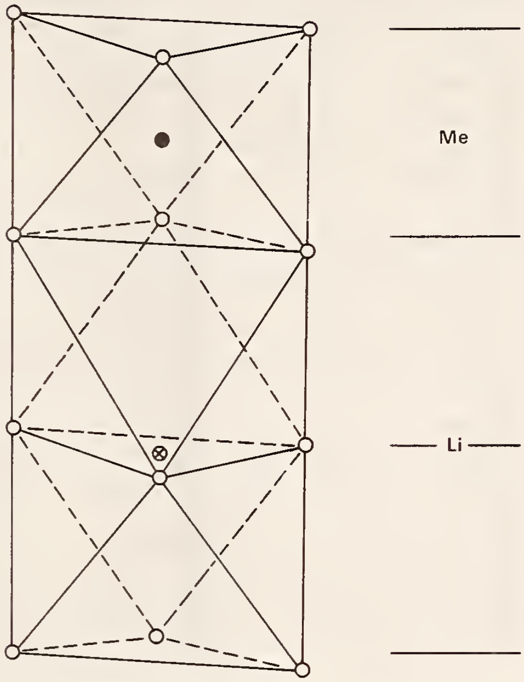

Figure 4. The structure of $LiTaO_3$ in space group R$\bar{3}$c. On the right of the figure is the schematic representation of the structure used in all the other illustrations.

The changes introduced in the structure of $LiTaO_3$ by the presence of defects indicate that $9LiTaO_3:Ta_2O_5$ approximates a centrosymmetric configuration more closely than stoichiometric $LiTaO_3$ does. Since at the Curie point the symmetry of $LiTaO_3$ is R$\bar{3}$c, this result implies that the Curie temperature of the nonstoichiometric compound should be lower than that of the stoichiometric material. This conclusion is in full agreement with experimental observations.

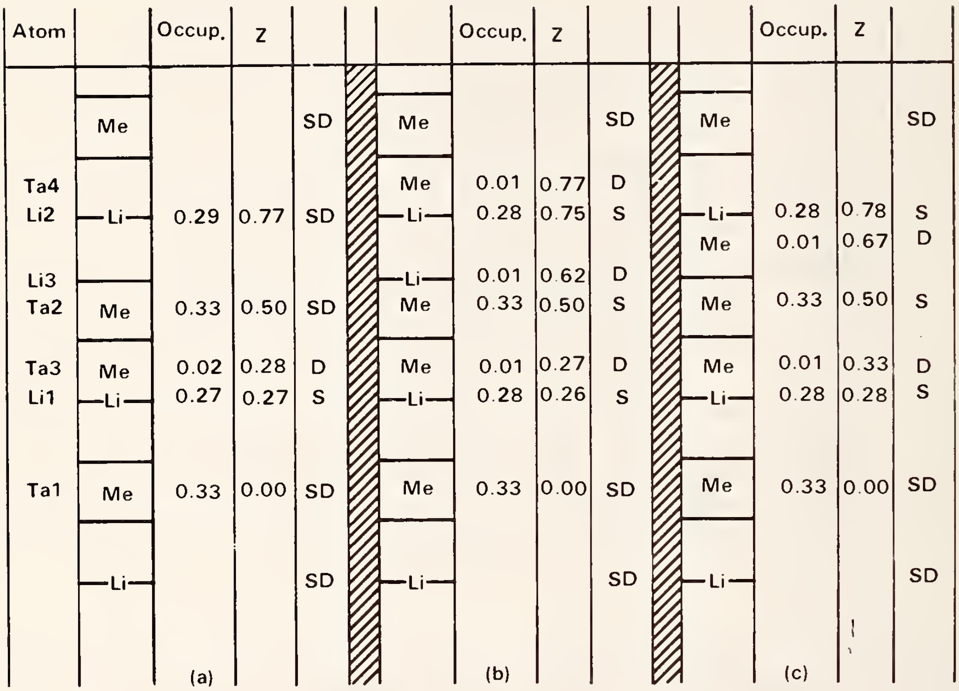

Figure 5. The "average" defective structures analyzed in the present study: (a) Model proposed by Lerner et al. (1968); (b) Model proposed by Nassau and Lines (1970); (c) Model proposed by Raueber (1977). The letters S and D indicate whether the corresponding atom is present in the stoichiometric or in the defective structure. The approximate values of the occupancies and of the z-coordinates of each metal atom are also indicated. As in the previous figures, the heavy horizontal lines indicate the layers formed by the oxygen atoms. The labeling of the atoms is the same as that given in table 1.

STRUCTURE REFINEMENT OF $LiI \cdot D_2O$ BY NEUTRON DIFFRACTION

P. M. Skarstad
(Medtronic Energy Technology, Brooklyn Center, MN)

and

E. Prince and J. J. Rush

Lithium iodide is widely used as a solid electrolyte in long-lived low-drain batteries with high energy density.[1] A dispersed-phase solid electrolyte containing lithium iodide monohydrate as one phase also has been used effectively in low-rate solid state cells.[2,3] The monohydrate of lithium iodide has been shown to be one to two orders of magnitude more conductive than lithium iodide itself by several investigators.[4,5,6] A higher conductivity for the monohydrate might well be expected on the basis of a formal similarity to the α-AgI family of solid electrolytes.[6]

The basic antiperovskite-like arrangement of the iodide and oxygen atoms in the small cubic unit cell (a = 4.30 Å) of $LiI \cdot H_2O$ was determined from x-ray powder diffraction data by Weiss.[7] Likely positions for the lithium and hydrogen atoms can be inferred from the iodide-oxygen arrangement. However, these cannot be determined from the x-ray data.

We have investigated the structure of $LiI \cdot D_2O$ by neutron diffraction. Both single-crystal and powder techniques were employed for structure refinements over the temperature range 14 K to 300 K. At room temperature the diffraction data are adequately modeled by independent harmonically vibrating atoms. The single lithium atom in the unit cell is disordered over the face-center sites of space group Pm3m, and the two deuterons are disordered over an eightfold siteset along the cell diagonals.

No unit cell in this structure can be cubic if the time of observation is fast with respect to the reorientation rate of water molecules. No splitting or significant broadening of peaks is observed that would indicate a differentiation of the unit cell axes down to 14 K, the lowest temperature of the investigation. Table 1 shows the cubic cell constants at the various temperatures.

The simple structural model used at room temperature is not adequate below 128 K. Although refinement based on observed reflections gave a weighted R index, R_w, below 0.05 at both 128 K and 80 K, several of the unobserved reflections had calculated structure amplitudes very substantially above the threshold for observable intensity. Accordingly, in spite of the very small degree of overdetermination, fourth cumulant coefficients for the oxygen atoms were incorporated in the model. This results in significant reductions in R_w, from 0.046 to 0.040 at 128 K and from 0.039 to 0.030 at 80 K. More importantly the calculated intensities of the unobserved reflections, even though these reflections had no influence on the refinement, were no longer above the threshold for observability. The refined structure parameters are listed in table 2.

The actual distribution of scattering density may be expressed in terms of the fourth cumulant coefficients by means of an Edgeworth expansion. For a cubic site, the Edgeworth series is

$$\phi(x,y,z) = \exp\left[-(1/2)r^2\right]\Big(1 + [1/24]\Big\{{}^4K_{1111}\left[H_4(x) + H_4(y) + H_4(z)\right]$$

$$+ 6\,{}^4K_{1122}\left[H_2(x)H_2(y) + H_2(x)H_2(z) + H_2(y)H_2(z)\right]\Big\}\Big).$$

In this expression $x = u_x/\langle u^2\rangle^{1/2}$, $y = u_y/\langle u^2\rangle^{1/2}$, and $z = u_z/\langle u^2\rangle^{1/2}$,

where u_x, u_y, u_z are displacements from the equilibrium position in the x, y, and z direction, respectively, and $\langle u^2\rangle$ denotes the second moment of the density distribution about its mean. If the distribution were due to thermal displacements only, this would correspond to a mean-square displacement of a nucleus from its equilibrium position. In this formula $r^2 = x^2 + y^2 + z^2$, and H_2 and H_4 denote Hermite polynomials. They are

$$H_2(x) = x^2 - 1,$$

$$H_4(x) = x^4 - 6x^2 + 3.$$

Using these, the density function becomes

$$\phi(x,y,z) = \exp\left[-(1/2)r^2\right]\left\{1 + (1/24)\left[{}^4K_{1111}(x^4 + y^4 + z^4 - 6r^2 + 9) + 6\,{}^4K_{1122}(x^2y^2 + x^2z^2 + y^2z^2 - 2r^2 + 3)\right]\right\}$$

All constant and quadratic terms in the expressions multiplied by the fourth cumulants are isotropic. The quartic terms divide into a function with lobes pointing in <100> directions multiplied by ${}^4K_{1111}$ and a function with lobes pointing in <111> directions multiplied by ${}^4K_{1122}$. However, if ${}^4K_{1111} = 3\,{}^4K_{1122}$ the quartic terms reduce to ${}^4K_{1111}(r^2)^2$, so they are also isotropic. Because this condition is satisfied within one standard deviation in $LiI \cdot H_2O$, the density distribution for the oxygen is essentially spherical, but with a radial variation that has positive kurtosis, i.e., it has more area in the tails than a Gaussian curve with the same variance.

An attempt was made to determine if the observed density distribution for the oxygen could be approximated by the sum of six spherical harmonic distributions each displaced from the body center of the unit cell along a different <100> axis. A calculation of the ${}^4K_{1111}$ coefficient for such a distribution gave the somewhat surprising result that it is identically zero, independent of the magnitude of the displacement. In other words, the sum of three Gaussian curves with the same width, evenly spaced but with the middle one four times as high as the others, has the same fourth moment as a single Gaussian curve with the same second moment. It follows from the result that a six spheres model cannot account for the observed data. The distribution must be approximated rather by a set of prolate ellipsoids pointing along the <100> directions.

Table 1. The cubic cell edge of $LiI \cdot H_2O$ at various temperatures as determined by neutron powder diffraction.

T	a_o
14 K	4.2434(1) Å
80 K	4.2487(1) Å
130 K	4.2565(2) Å
298 K	4.2955(2) Å

Table 2. Structure parameters for lithium iodide monohydrate. Note: $\delta_{ijkl} = (2\pi^4/3)^4 K_{ijkl}$. Space Graphics Space Graphics Pm3m.

Atom	x	y	z	occupancy	B or β_{11}	β_{33}	β_{12}	δ_{1111}	δ_{1122}
128 K									
Li	.5	.5	0	.3333	.052(14)	.032(16)	0	0	0
I	0	0	0	1.0	1.64(32)				
O	.5	.5	.5	1.0	.060(9)	.060(9)	0	.00147(29)	.00057(16)
D	.3905(27)	.3905(27)	.3905(27)	.25	.113(12)	.113(12)	-.038(4)		
80 K									
Li	.5	.5	0	.3333	.033(11)	.043(18)	0		
I	0	0	0	1.0	0.99(22)				
O	.5	.5	.5	1.0	0.049(11)	0.049(11)	0	.00151(32)	.00050(22)
D	.3930(24)	.3930(24)	.3930(24)	.25	0.097(13)	0.097(13)	-.016(5)		

---

1. C. C. Liang and C. F. Holmes in Proceedings of the Symposia on Biomedical Implantable Applications and Ambient Temperature Lithium Batteries, N. Margalit and B. B. Owens, eds., Proceedings Vol. 80-4 (The Electrochemical Society, Princeton, NJ, 1980) pp. 27-33.

2. B. B. Owens and H. J. Hanson, *U. S. Patent* 4,007,122.

3. B. B. Owens, K. Fester and T. Kuder, *Extended Abstracts* 77-2, #25, The Electrochemical Society, (1977).

4. S. Pack, B. B. Owens, and J. B. Wagner, *J. Electrochem. Soc.* 127, 2177-2179, (1980).

5. P. Hartwig and W. Weppner, Abstract C210, Third International Meeting on Solid Electrolytes, Tokyo, (1980).

6. P. M. Skarstad, D. R. Merritt, and B. B. Owens, Abstract C217, Third International Meeting on Solid Electrolytes, Tokyo, (1980).

7. E. Weiss, *Z. anorg. allgem. Chem.* 340, 203-206 (1965).

NEUTRON POWDER DIFFRACTION STUDY OF THE FAST-ION CONDUCTOR CuAgS BETWEEN 20° AND 115°C

C. Skarda and B. J. Wuensch
(Massachusetts Institute of Technology,
Cambridge, MA)

and

E. Prince

The compound CuAgS, which exists in nature as the mineral stromeyerite, occurs on the binary join midway between two fast-ion conductors, Cu_2S and Ag_2S. The structures of the high temperature phases of both end members have been determined in single-crystal neutron diffraction studies [Cava, R. J. (June, 1978). Ph.D. thesis, Department of Materials Science and Engineering, Massachusetts Institute of Technology]. But their low temperature forms are complex and invariably twinned, unlike the simpler, untwinned CuAgS. A single crystal of CuAgS, however, does not appear to survive the transition to its fast-ion phase, which offers the interesting possibility of two cation species becomming mobile. For these reasons, powder profile analysis by the Rietveld method was undertaken in an attempt to describe the structure of CuAgS in both its low and high temperature and high temperature modifications.

An x-ray diffraction study [Skinner, B. J. (1966). Econ. Geol., 61, 1-26] indicated that stromeyerite encompasses the narrow composition range $Cu_{1+6}Ag_{1-x}S$, where $0 \leq x \leq 0.07$, with Cu substituting in part for Ag. Orthorhombic at room temperature, the stoichiometric compound undergoes a transition at 93.3°C to a hexagonal phase, in which the S atoms retain their hcp configuration but the cations disorder. A third phase, appearing at 127.5°C and characterized by fcc packing of sulfur, is not considered in the present investigation.

Although the structure of orthorhombic stromeyerite had been solved [Frueh, A. J. (1955). Z. Krist., 106, 299-307], it was poorly determined with R = 30%, and required refining. The unit cell contains 4 CuAgS. Displaying the symmetry of space group Cmcm, the structure consists of

Table 1. Experimental conditions for powder diffraction study of CuAgS.

Monochromatic beam: reflection 220 of a Cu crystal
Neutron wavelength: 1.5423 A
Mosaic spread of monochromator: 15 min. of arc
Horizontal divergences:
- a) in-pile collimator: 10 min. of arc
- b) monochromatic beam collimator: 20 min. of arc
- c) diffracted beam collimator: 10 min. of arc

Region from $2\theta = 20°$ to $122°$ scanned in $0.05°$ steps
Detectors: 20-42°, 40-62°, 60-82°, 80-102°, 100-122°
Sample container: V can of 1 cm diameter
Scattering lengths: $Cu = 0.76 \times 10^{-12}$ cm
$Ag = 0.597 \times 10^{-12}$ cm
$S = 0.285 \times 10^{-12}$ cm

zigzagging chains of silver and sulfur atoms paralleling the c axis. Trigonal Cu-S layers (as in Cu_2S) alternate with layers of loosely packed face-centered silver atoms parallel to the (001) face.

Above the phase transition, CuAgS enters a region of solid solution with hexagonal Cu_2S [Skinner, Loc. cit.], suggesting that the two compounds are structurally related. Single-crystal neutron diffraction [Cava, Loc. cit.] showed that Cu_2S exhibits symmetry of space group $P6_3/mmc$, with close-packed S atoms in site 2(d). The cations are statistically divided between two sites: I) 0.7068 Cu in the 3-coordinated site 2(b) within close-packed S layers; and II) 0.2156 Cu in the 12(k) site x 2x z, with x = 0.2573 and z = 0.4339 at 120°C. This distribution of atoms was considered a possible model for hexagonal CuAgS, for which no structural work had previously been done.

The large sample of CuAgS required for the neutron powder diffraction study was prepared by heating a 1:1 $Cu_2S{:}Ag_2S$ 35-g mixture in an evacuated, sealed Vycor tube at 250°C for five days, followed by a five-day annealing at 90°C. X-ray analysis of the specimen revealed that a trace of free silver existed as a second phase, probably the result of some sulfur loss at high temperature. The powder was packed into a thin-walled vanadium can 1 cm in diameter and mounted in a top-heated furnace which could be placed directly in the neutron beam. To facilitate thermal conduction along the V can and through the sample, the furnace chamber was evacuated. The temperature of the sample was not directly measured, but that of the furnace was precalibrated as a function of current flow through the heating unit. Diffracition data were collected with the experimental conditions given in table 1.

Initially four sets of intensities were measured, with the furnace at room temperature, at 100°C, at 115°C, and at 250°C. The diffraction patterns indicated, however, that the compound remained in its orthorhombic phase through the 115°C setting. It was concluded that poor heat transfer through the dense ceramic CuAgS prevented the sample from reaching the temperature of the furnace. To enhance thermal conductivity, a strip of

Table 2. Results of structure refinement for CuAgS: room temperature phase

$R_{Bragg} = 9.47$ $u = 5309.16$ scale factor = 0.110(1)

$R_{WP} = 7.77$ $v = 2023.73$

$R_E = 6.35$ $w = 1490.93$ space group = Cmcm

$N\text{-}P = 2064$ $z = 1.095$

$a = 4.0638(4)$ Å $b = 6.6337(6)$ Å $c = 7.9724(7)$ Å $v = 214.92(4)$ Å^3

	x	y	z	B	B_{11}	B_{22}	B_{33}	B_{23}
Cu (4cmm)	0.0	0.4311(5)	0.25	2.15(10)	0.97(19)	3.29(17)	2.20(19)	
Ag (4 a 2/m)	0.0	0.0	0.0	5.59(16)	2.73(28)	10.84(65)	3.21(31)	4.74(32)
S (4cmm)	0.0	0.7837(11)	0.25	1.48(24)	0.69(49)	2.13(44)	1.61(49)	

Table 3. Results of structure refinement for CuAgS: 50°C phase

R_{Bragg} = 10.03
R_{WP} = 7.58
R_E = 5.89
N-P = 2144

u = 4225.03
v = 982.54
w = 1139.94
z = 0.975

scale factor = 0.082(1)

space group: cmcm

a = 4.0672(3) Å   b = 6.6392(5) Å   c = 7.9681(6) Å   v = 215.16(3) $Å^3$

	x	y	z	B	B_{11}	B_{22}	B_{33}	B_{23}
Cu (4cmm)	0.0	0.4324(4)	0.25	2.56(8)	1.12(16)	3.43(14)	3.13(17)	
Ag (4 a 2/m)	0.0	0.0	0.0	6.48(15)	3.71(28)	12.96(50)	2.77(25)	4.89(21)
S (4cmm)	0.0	0.7861(9)	0.25	1.99(17)	0.81(43)	1.96(37)	3.20(44)	

silver foil with lateral branches was inserted in the V can; silver shot was placed at both ends of the CuAgS powder to a depth of 0.5 cm, insuring thermal contact between the foil and vanadium. With this arrangement, another set of intensity data was collected at a furnace setting of 115°C, at which point the sample had transformed completely to the hexagonal phase. For future high-temperature neutron powder diffraction studies of ceramic materials, a container should be constructed which would permit better thermal conductivity, perhaps by running one or more thin vanadium rods through the interior of the cylinder.

Results of the refinement of the room temperature phase are given in table 2. Although the formation of free silver during the original calcining suggested that the sample was somewhat Cu-rich, the fit obtained assuming perfect stoichiometry was so good that adjustment of the Cu:Ag ratio would provide no basis for comparing models. Thus all refinement was carried out as though for stoichiometric CuAgS.

Analysis of the data collected at the nominal temperature of 100°C yielded an isotropic thermal parameter for sulfur of 1.99. Assuming that this value varies linearly with temperature for the S atoms, the actual temperature of the sample was estimated to be 50°C. Table 3 gives the parameters refined for this data.

The highly disordered hexagonal phase gave a weak diffraction pattern at 115°C. Profile analysis was performed over the narrow range 33.80° $33.80° \leq 2\theta \leq 62.00°$, which included the six or seven Bragg reflections present. To reduce the number of parameters, the half-width values U, V, and W were held fixed at estimates obtained from the room-temperature phase refinement, and the zero-point was not refined. Initial calculations were carried out for a structure consisting only of sulfur. Atoms were placed in the 2(d) sites of space group $P6_3/mmc$ occupied by the sulfur atoms in hexagonal Cu_2S. This partial model yielded an R_B of 36.22%. A difference Fourier showed residual densities in sites corresponding to the Cu sites in Cu_2S. Close lattice match (within about 4%) between Cu_2S and CuAgS gave further indication that the two compounds are isostructural. Therefore, various models were tested using the occupation

Table 4. Results of structure refinement for CuAgS: 115°C phase.

$R_{Bragg} = 22.85$ (unrefined): scale factor = 0.083(1)

$R_{WP} = 9.30$ u = 5238.0

$R_E = 7.84$ v = 2001.0

N-P = 556 w = 1491.0

z = 0.0

a = 4.1389(10) c = 7.0817(27) v = 105.06(5)

	x	y	z	B	n	occupancy
S 2(d) $\bar{6}m2$	0.3333	0.6667	0.7500	3.26(1.28)	0.0833	1.0
Cu1 2(b) $\bar{6}m2$	0.2573	0.5146	0.4339	8.61(1.39)	0.0244	0.04887
Cu2 12(k) m	0.0	0.0	0.25	12.03(1.61)	0.0589	0.7068
Ag 12(k) m	0.2573	0.5146	0.4339	8.61(1.39)	0.0833	0.1667

numbers and atomic positions proposed by Cava for Cu_2S. A best fit of R_B = 22.85% was obtained for the model described in table 4. Ag and Cu are not completely disordered, but the partial site 2(b) is populated solely by Cu, so that most of the Cu atoms remain coplanar with S as in the low temperature phase. The remainder of the cations partially fill the 12(k) positions. Lack of data prevented refinement of atomic coordinates and occupancies. However, the value of R_B, when taken in conjunction with the evidence for correlation between CuAgS and Cu_2S, seems to indicate that the model is a viable one, until successful growth of a single crystal of hexagonal CuAgS makes further analysis possible.

THE STRUCTURE OF THE RHOMBOHEDRAL PHASE OF $Na_3Sc_2(PO_4)_3$

E. Prince
and
T. Brun and S. Sussman
(Argonne National Laboratory)

The compound $Na_3Si_2(PO_4)_3$ is a fast ion conductor at elevated temperatures. Studies of resistivity as a function of temperature indicate that there is a phase transition at about 60°C which is associated with an abrupt increase in conductivity. Above the transition the conductivity increases steadily, with an activation energy of 0.49 eV, up to a temperature of about 180°C. Above 180°C the activation energy drops to 0.20 eV. The crystal structure at room temperature has been reported[1] to be monoclinic, space group Cc, with cell constants a = 16.10 Å, b = 8.928 Å, c = 9.109 Å, β = 127.15°. This unit cell doesn't differ very much from a rhombohedral cell, and it is unclear how strong the evidence is for the lack of a center of symmetry. The crystal structure above the phase transition was previously unknown, although it was believed to be rhombohedral.

In an effort to elucidate the nature of the phase transition and the mechanism of conductivity, neutron powder patters were collected, on the multidetector powder diffractometer, at 25°C, 100°C, and 225°C. The room temperature structure with space group Cc has too many parameters to refine with powder data. An attempt was made to refine the structure in space group C2/c, but the fit was only fair (R_{wp} = 9.86%, R_e = 4.89%, so the fit is not consistent with the statistical precision of the data). This refinement did, however, yield a satisfactory set of refined lattice parameters: a = 16.0679(15) Å, b = 8.9234(6) Å, c = 9.0894(8) Å, β = 126.994(4)°. Analysis of these constants and of the shapes of a few critical peaks establishes that the true symmetry of this phase is monoclinic or lower.

At the higher temperatures the powder pattern sharpens up in a manner that is consistent with a transition to a rhombohedral structure. At both 100 °C and 225 °C models based on space group $R\bar{3}c$ gave reasonably

Table 1. Refined parameters for rhombohedral phases of $Na_3Sc_2(PO_4)_3$

Atom	x	y	z	Occupancy	β_{11}	β_{22}	β_{33}	β_{12}	β_{13}	β_{23}
100°C										
Na1	0	0	0	1	.1096(86)	.1096(86)	.0009(5)	.0548(43)	0	0
Na2	.6399(9)	0	.25	.6667	.0043(13)	.0055(16)	.0062(5)	.0027(8)	.0020(3)	.0040(6)
Sc	0	0	.1490(1)	1	.0030(2)	.0030(2)	.0007(1)	.0015(1)	0	0
P	.2928(3)	0	.25	1	.0034(5)	.0022(6)	.0008(1)	.0011(3)	-.0003(3)	-.0001(1)
01	.1857(3)	-.0250(3)	.1948(1)	1	.0082(5)	.0086(5)	.0019(1)	.0054(5)	-.0022(2)	.0009(1)
02	.3139(3)	-.1595(2)	.1561(1)	1	.0057(5)	.0019(4)	.0012(1)	.0025(4)	-.0006(1)	.0006(1)
225°C										
Na1	0	0	0	.799(25)	.1701(83)	.1701(83)	-.0001(4)	.0851(41)	0	0
Na2	.6356(8)	0	.25	.734(8)	.0034(11)	.0045(15)	.0101(5)	.0022(8)	.0044(3)	.0088(6)
Sc	0	0	.1494(1)	1	.0047(2)	.0047(2)	.0007(1)	.0023(1)	0	0
P	.2919(3)	0	.25	1	.0019(4)	.0051(5)	.0006(1)	.0026(3)	-.0002(1)	-.0003(1)
01	.1827(3)	-.0306(3)	.1955(1)	1	.0107(5)	.0079(5)	.0015(1)	.0063(4)	-.0021(2)	-.0003(1)
02	.3118(3)	-.1594(2)	.2575(1)	1	.0066(4)	.0020(3)	.0012(1)	.0018(3)	-.0008(1)	.0005(1)

satisfactory fits to the data. (R_{wp} = 6.28%, R_e = 3.83% at 100 °C; R_{wp} = 5.81%, R_e = 3.87% at 225 °C.) At 100 °C the cell constants are a = 8.9273(2) Å, c = 22.3668(6) Å. At 225 °C they are a = 8.9274(1) Å, c = 22.5493(6) Å. It is interesting to note that all of the thermal expansion is along the c axis. The refined parameters are listed in table 1.

The most notable feature of the structure is that three sodium atoms occupy four sites in two crystallographically non-equivalent sets, set 6b with point symmetry $\bar{3}$ and set 18e with point symmetry 2. At both temperatures the occupancies of these sites were refined, with a constraint applied to force the total number to remain at three. At 100°C this refinement resulted in an entirely insignificant change from a model in which the b site was entirely full and the e site was only two thirds full. At 225°C there is a significant shift toward a model with vacancies on both sites. At both temperatures the thermal motions of both sites are extremely anisotropic, with the b site having a very large amplitude perpendicular to the c axis and the e site having a large amplitude parallel to the c axis. This is entirely consistent with a model for the electrical conductivity in which the sodium ions are free to move through channels perpendicular to the c axis in the vicinity of the b sites and through channels parallel to the c axis in the vicinity of the e sites. The two types of channels are connected to each other, but neither is connected to others of its own type. Thus, the difference in activation energy may be associated with the appearance of vacancies on both types of site.

---

1. V. A. Ehemov and V. B. Kalinia, *Sov. Phys. Crystallogr.* 393 (1978).

SEARCH FOR A LOW TEMPERATURE PHASE TRANSITION IN LiH

Q. Johnson
(Lawrence Livermore Laboratory, Livermore, CA)

and

E. Prince

Some years ago Yates, Westenholm, and Bingharn[1] reported a specific heat anomaly in LiH at about 20 K. They speculated that this might represent a phase transition from an NaCl type structure to a CsCl type structure. A transition of this type is a possible mechanism for a volume change at high pressure observed by the high pressure crystallography group at Livermore. Although it seemed that a more likely explanation of the low temperature specific heat was the condensation of bubbles of hydrogen trapped in the crystal, it was desirable to make a direct check for a CsCl type phase. Accordingly, a high-resolution powder pattern was obtained at 4.2 K on the multidetector powder diffractometer at NBS from a sample of Li^6D. There was no evidence in this powder pattern of any phase other than the NaCl type phase.

---

[1] B. Yates, G. H. Westenholm, and K. Bingharn, *J. Phys. C: Solid State Phys.* 7, 1769 (1974).

CRYSTAL STRUCTURE OF AMMONIUM NITRATE PHASE III

C. S. Choi and H. J. Prask
(Energetic Materials Division, LCWSL, ARRADCOM, Dover, NJ)

and

(National Bureau of Standards, Washington, DC)

Two recent powder neutron diffraction studies[1,2] of the structure of AN phase III have reported two different orientations for the ammonium group. The present study was undertaken to resolve the controversy. Using a single crystal of AN containing 5 wt. % KNO_3 in solid solution form, three-

Table 1. Comparison of thermal motions of the ammonium ions in the structure of phase 2 and 3.

ion	phase	Temperature(K)	disorder	principal axes	
			(angle)	$T_{ii}(A^{o2})$	$L_{ii}(^{o})$
ND_4	2	357-398	90°	.058	14.4
				.058	14.4
				.065	10.3
NH_4	3	305-357	∿42°	.055	22.4
				.034	19.1
				.015	16.0

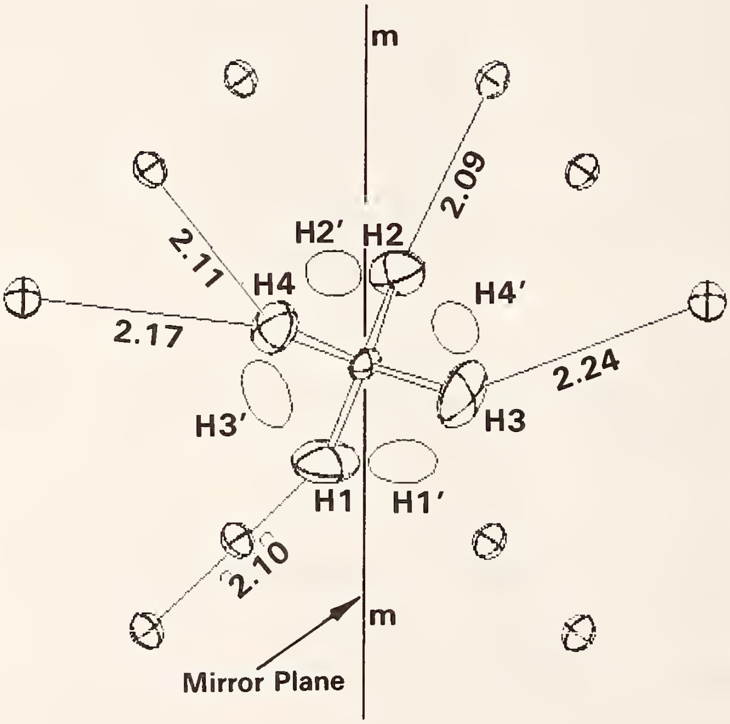

Figure 1. The ammonium group of AN phase III viewed along the z-axis. The ammonium groups are orientationally disordered by an angle of 42° about an axis parallel to the z-axis. The two alternate molecular sites are related by mirror symmetry.

dimensional neutron diffraction data were collected. The structure of the ammonium group was determined by a Difference Fourier synthesis and was refined with a tetrahedral rigid body constraint for the ammonium group. The final residual indices were $R_w = 0.043$ and $R = 0.042$. The ammonium groups are disordered orientationally with two alternate sites which are related by mirror symmetry and have one of their $\bar{4}$-axes directed approximately parallel to the c-axis direction. Figure 1 is the c-axis view of the ammonium ion and its alternate sites marked with the envelopes of the thermal ellipsoids. Several interesting features were found in the strucuture:

1. The ammonium group which possesses a mm symmetry in free form does not have the mirror symmetry in the crystal despite the m symmetry of the molecular site. Instead, the two disordered molecular sites are related to each other with the m symmetry.

2. One-dimensional rotational reorientations of 42^o about the c-axis direction appear likely for the NH_4 groups.

3. The observed reorientation angle, 42^o, is not fixed by the molecular or crystal symmetry, and hence, may be temperature dependent.

4. As shown in figure 1, H(3) and H(4) are not structurally equivalent; the H(3) involves with a weak H-bond, whereas H(4) involves two stronger H-bonds. Rotational reorientations of 42° entail $H(4) \rightarrow H(3)'$ and $H(3) \rightarrow H(4)'$ so that each hydrogen alternates sites of relatively weak and strong bonding. The large librational components of the rigid ammonium ion--compared with Phase II in table 1--may possibly arise from the disturbance due to the sudden change of interaction at the two dissimilar sites.

---

1. B. W. Lucas, M. Ahtee, and A. W. Hewat, *Acta Cryst.* B36, 2005-2008 (1980).

2. C. S. Choi, H. J. Prask, and E. Prince, *J. Appl. Cryst.* 13, 403-409 (1980).

REFINEMENT OF 2-NITROGUANIDINE BY NEUTRON POWDER DIFFRACTION

C. S. Choi
(Energetic Materials Division, LCWSL, ARRADCOM, Dover, NJ)
and
(National Bureau of Standards, Washington, DC)

The crystal structure of 2-nitroguanidine was studied earlier by Bryden, Burkardt, Huges, and Donahue (1956), but did not report the H positions. This study was undertaken to determine the H positions by using neutron powder diffraction method. A powder diffraction intensity profile was measured up to 118° in scattering angle by using the five detector neutron diffractometer with collimation of 10', 20', and 10'. The refinement was carried out by means of the modified Rietveld method with isotropic temperature factors for all atoms and obtained the final R indices, $R_i = 0.057$ and $R_w = 0.020$. The molecules are linked together by a three-dimensional network of hydrogen bonds. The bond lengths are given in figure 1.

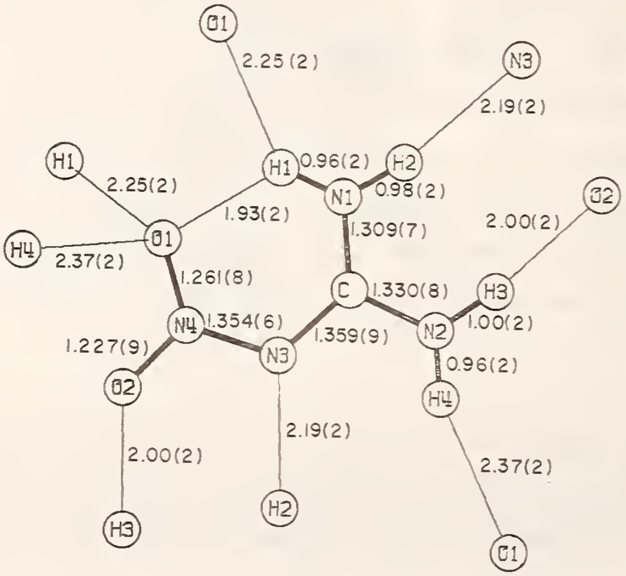

Figure 1. ORTEP drawing of nitroguanidine molecule.

STUDIES OF RIBONUCLEASE A
BY X-RAY AND NEUTRON DIFFRACTION

A. Wlodawer
and
L. Sjölin
(Laboratory of Molecular Biology, National Institutes of Health,
NIADDK, Bethesda, MD)
and
(National Bureau of Standards, Washington, DC)

The structure of ribonuclease A has been refined with the X-ray and neutron data at 2.0 Å resolution. The refinement proceeded in several steps. Initially only the x-ray data were used and the structure was refined by a restrained-parameter least-squares procedure at 2.0 Å resolution and rebuilt using computer graphics. The final agreement factor $R = \Sigma(||F_o| - |F_c||)/\Sigma|F_o|$ was 0.159. The positions of the 951 main-chain atoms have been determined with an estimated accuracy of 0.17 Å. In addition, the model included a phosphate group in the active site and 176 waters, many of them with partial occupancy. The bond lengths in the refined structure of RNase A differ from the ideal values by an overall root-mean-square deviation of 0.022 Å; the corresponding value for angle distances is 0.06 Å. The r.m.s. deviation of planar atoms from ideality is 0.017 Å, and the r.m.s. deviation of the peptide torsion angles from 180° is 3.4°. The model is in good agreement with the final difference Fourier maps.

Two active site histidines, His 12 and His 119, form hydrogen bonds to the phosphate molecule. His 119 is also hydrogen bonded to the carboxyl of Asp 121 (figure 1) and His 12 to the carbonyl of Thr 45. The observed sequence of hydrogen bonds is in good agreement with the postulated mechanism of change transfer involving His 119, Asp 121, His 12, and the phosphate. The structure of the RNase A is very similar to that of RNase S, particularly in the active site region. The r.m.s. discrepancy

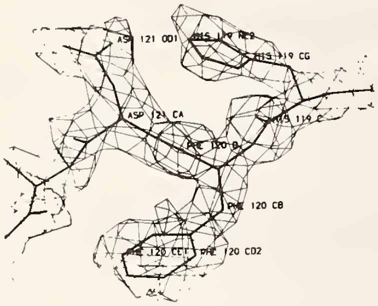

Figure 1. The electron density superimposed on the model of residues 119-121. The distance between NE2 of His 119 and OD1 of Asp 121 is 2.59 Å. The quality of the map for His 119 is comparable to that for the two neighboring side chains, as well as for most of the remaining parts of the molecule.

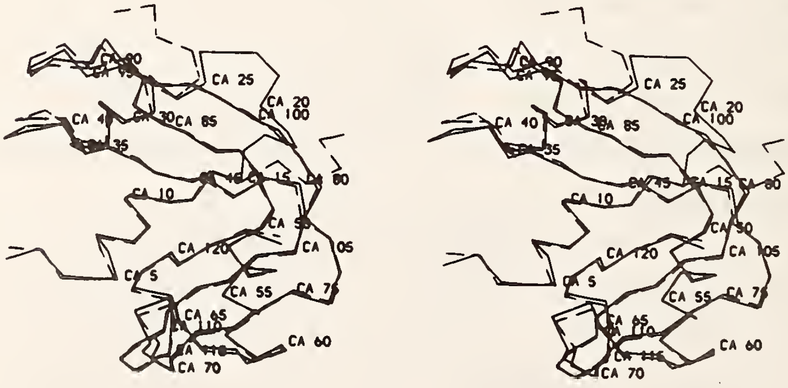

Figure 2. Superimposed C_{α} coordinates for the final model of RNase A and for the refined structure of RNase S. RNase A solid, RNase S dashed.

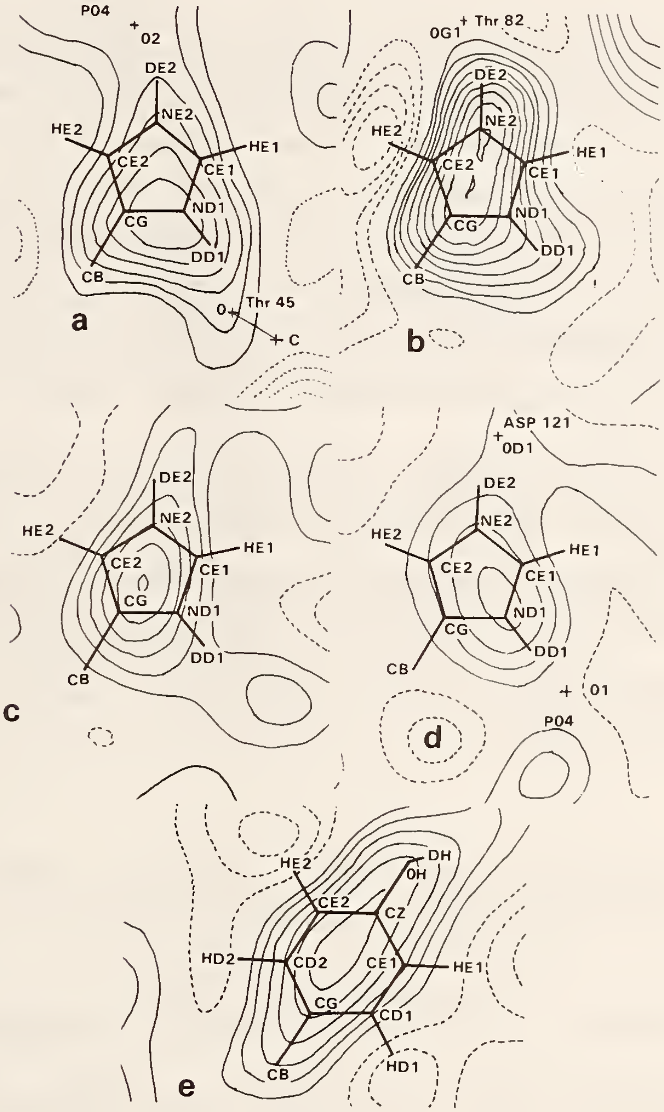

Figure 3. Sections through difference Fourier maps for five side chains of RNase A. The maps were calculated at 2.8-Å resolution, with coefficients $(F_o - F_c)\alpha_c$. The atoms belonging to these side chains, as well as a phosphate molecule, were removed from the structure factor calculation. All maps were contoured at the same arbitrary level. Solid lines, positive density; dashed lines, negative density; zero contour is omitted. The low density around the CB atoms is caused by the negative scattering of the attached hydrogens not resolved at this resolution. (a) Histidine-12; (b) histidine-48; (c) histidine-105; (d) histidine-119; (e) tyrosine-25 (note that deuterium DH lies below the contoured plane).

of all atoms for residues 1-16 and 24-123 is 1.06 Å, and the r.m.s. discrepancy for the active site region is 0.6 Å. The comparison of the C_α positions in the two models is shown in figure 2.

In the next step of analysis, x-ray data to 2.0 Å and neutron data to 2.8 Å respectively were used in a joint refinement. This procedure converged with the crystallographic R factors of 0.162 (x-ray) and 0.258 (neutron). Refined neutron data enabled unambiguous assignment of the orientation of all four histidines, including the active site His 12 and His 119 (figure 3).

Recently joint refinement has been extended to include neutron data to 2.0 Å resolution. The R factors are currently at 0.159 (x-ray) and 0.190 (neutron), and the refinement and rebuilding is being continued. New data include a more detailed description of the network of hydrogen bonds, especially those involving solvent and an analysis of the pattern of amid hydrogen exchange.

REFINEMENT OF THE CRYSTAL ORIENTATION MATRIX FOR THE FLAT-CONE DIFFRACTOMETER

A. Wlodawer and L. Sjölin
(National Institutes of Health, Bethesda, MD)
and
(National Bureau of Standards, Washington, DC)
and
A. Santoro

A procedure for refining a crystal orientation matrix for the flat-cone diffractometer has been developed. The positions of the centers of gravity of reflections obtained during routine data collection are transformed in such a way that they can be used as input to the least-squares procedures of Busing and Levy (1967) or Shoemaker and Bassi (1970). The orientation matrix can be refined on the basis of the positions of all observed reflections, and not only of a selected sample, thus increasing its reliability. The procedure is particularly suited for protein crystallographic studies, as it makes it possible to compensate for crystal movements and electronic drifts encountered during data collection.

Let us assume that the position of each reflection has been accurately determined by finding its center of gravity in the (d, ψ) space, where d represents the position of a point along the counter and ψ the rotation angle. This can be used to obtain better estimates of the orientation matrix and the lattice parameters of the crystal with a method similar to that proposed by Busing and Levy (1967) or with the procedure given by Shoemaker and Bassi (1970) and Shoemaker (1970). If we adopt the first method, we may assume that the Bragg condition is satisfied for the center of gravity of a reflection, and we may take as an observation the value ψ_d(*) corresponding to this point.

The only requirement here is that the scattering vector u make an angle of $90^{\circ} + \theta$ with the primary beam direction, i.e.,

$$u_{\ell 2} = - \sin \theta \qquad (1)$$

where

$$\underset{\sim}{u}_{\ell} = \underset{\sim}{M}_{d} \, \underset{\sim}{\Psi}_{c} \, \underset{\sim}{u}_{\phi} \qquad (2)$$

From Equations (1) and (2), we obtain

$$(u_{\phi 3} \cos \mu_d) \sin \psi_c + (u_{\phi 2} \cos \psi_c = (u_{\phi 1} \sin \mu_d - \sin \theta) \qquad (3)$$

and the calculated value ψ_c corresponding to the observation ψ_d can be obtained since

---

(*) Here and in what follows we will adhere to the procedure of Busing and Levy (1967) of indicating with the subscript d the instrumental dial readings and their matrices, with the subscript c the calculated angles and their matrices, and without subscripts the quantities evaluated from the trial parameters. All other symbols, as well as the reference systems used here, are defined in Busing and Levy (1967) and/or Prince et al. (1978).

$$\mathbf{u}_{\phi} = \mathbf{U}\,\mathbf{B}\,\mathbf{h}\,/q \qquad (4)$$

From the above considerations it is clear that the observations most easily obtainable with a linear detector operated in flat-cone geometry are analogous to the type 5 observations analyzed by Busing and Levy (1967).

On the other hand, the input required by the procedure of Shoemaker and Bassi (1970) and Shoemaker (1970) requires precise values of the setting angles of reflections analyzed with the geometry of a four-circle diffractometer. From these the coordinates $\mathbf{h}_{\phi}$ of the corresponding reciprocal lattice points can be evaluated, and the observational equations are

$$\mathbf{V}_{o}^{-1}\,\mathbf{h}_{\phi} = \mathbf{V}_{o}^{-1}\,\mathbf{V}\,\mathbf{h} = \mathbf{h}' \qquad (5)$$

where all the symbols have the same meaning as those defined by Shoemaker and Bassi (1970). This procedure can be extended to flat-cone geometry in the following way. From the settings ϕ, χ, ω, μ, and T, which center a reflection on the linear detector, we may calculate the vector $\mathbf{h}_{\phi}$ in the Cartesian system attached to the Φ-circle with the equations

$$\mathbf{h}_{\phi} = \mathbf{P}\,\mathbf{h}_{\ell} \qquad (6)$$

where

$$\mathbf{P} = \mathbf{M}\,\mathbf{\Omega}\,\boldsymbol{\chi}\,\mathbf{\Phi} \qquad (7)$$

and

$$\begin{aligned} h_{\ell 1} &= \cos T \sin \mu \\ h_{\ell 2} &= \cos T \cos \mu - 1 \qquad (8) \\ h_{\ell 3} &= \sin T \end{aligned}$$

The coordinates $\mathbf{h}_{\phi}$ (Equation 6) are sufficient as input to Shoemaker's procedure, but their use requires some modification. If one desires to use the unmodified procedure, the required input consists of the setting angles of reflections in four-circle geometry which are given by

$$\begin{aligned} \phi_o &= \tan^{-1}(h_{2\phi}/h_{1\phi}) \\ \chi_o &= \tan^{-1}[h_{3\phi}/(h_{1\phi}^2 + h_{2\phi}^2)^{1/2}] \\ 2\Theta_o &= \cos^{-1}(\cos T \cos \mu) \\ \omega_o &\equiv 0 \end{aligned} \qquad (9)$$

The procedure was tested on a crystal which was deliberately misset and was shown to perform successfully. Even when the maximum misalignment for individual reflections was as large as .5° in ψ, the recalculated matrix properly centered all reflections. The limits of convergence were reached when the reflections were becoming only partially recorded in their boxes, since under these conditions the apparent centers of gravity would no longer correspond to the true position of each reflection. Since incompletely recorded reflections can be recognized as such and properly marked, it is possible to extrapolate the positions of their centers of gravity and to use them in the recalculation of the orientation matrix. Under these conditions the intensity data are not useful anyway, and the level has to be recollected. We have found that, as long as the centers of gravity of the reflections did not fall outside of their predicted boxes, the procedure was powerful enough to ensure that during a subsequent scan they would be completely enclosed within their boxes, even though they would not necessarily be very well centered.

---

1. W. R. Busing and H. A. Levy, *Acta Cryst.* 22, 457-464 (1967).

2. E. Prince, A. Wlodawer, and A. Santoro, *J. Appl. Cryst.* 11, 173-178 (1978).

3. D. P. Shoemaker, *J. Appl. Cryst.* 3, 179-180 (1970).

4. D. P. Shoemaker and G. Bassi, *Acta Cryst.* A26, 97-101 (1970).

ADVANCED NEUTRON METHODS

J. M. Rowe, C. J. Glinka, N. Berk, J. LaRock,
R. H. Williams, and D. Fravel

1. Small Angle Neutron Scattering (SANS)

a. The Small-Angle Scattering Spectrometer

During the past year, construction and installation of all of the major components of the new small-angle scattering (SANS) spectrometer described in previous reports[1,2] have been completed. A photograph of the instrument is shown in figure 1. By May 1981, construction had progressed to the point that the 25 x 25 cm position-sensitive detector, the smaller of two such detectors purchased[3] for the facility, could be installed at the end of the instrument's 8 m evacuated flight path. Since then calibration measurements and operational testing of the entire instrument and its data acquisition system[2] have been underway. Some of the highlights of the assembly and testing phases are summarized below.

Flux: Following the installation of the beam port shutter and the liquid-nitrogen-cooled beam filter, consisting of 25 cm of beryllium and 15 cm of single crystal bismuth, the neutron flux was measured at the entrance to the 4.5 m pre-sample flight tube. The instrument's mechanical velocity selector had not been installed at this time and, therefore, all neutrons with wavelengths greater than 4 Å were included in the measurement. The measurements were made by G. Lamaze and D. Gilliam of the Nuclear Radiation Division using a precisely calibrated double fission chamber. The measured flux was 1.1×10^7 n/cm^2-sec. From this value we have calculated the flux at the sample position taking into account the transmission of the velocity selector and the collimation along the flight tube. For a wavelength of 6 Å ($\Delta\lambda/\lambda = 0.25$) and a reactor power of 10 MW, the flux at the sample for the tightest collimation available is 2×10^4 n/cm^2-sec, and for the coarsest collimation, 3×10^5 n/cm^2-sec. The latter number has now been verified by direct measurements with the velocity selector installed. The cadmium ratio for the beam is > 1,000 indicating an extremely low fast neutron component.

High Resolution Collimation System: Along the 4.5 m evacuated flight tube preceeding the sample position, a series of twelve cadmium-plated masks, with nine apertures each, have been precisely aligned in order to define nine independent beams which converge to a point at the center of the detector.[1] The positions and profiles of the beams on the detector were measured individually and found to coincide thus verifying the focussing effect of the collimation system.

Post-Sample Flight Path: The evacuated post-sample flight path consists of three shielded cylindrical sections which mount on a frame that can be rotated about the sample position. In addition, the section which houses the detector rolls along rails in the frame so that the sample-to-detector distance can be changed from 3.5 m to 2.0 m by removing the middle flight path section. This arrangement provides considerable flexibility in positioning the detector as needed for a particular experiment.

Beam Stop: Incorporated in the detector shield is an external positioning device for manipulating a thin aluminum tube which holds a beam stop in front of the detector. With this device, the beam stop can be quickly and accurately adjusted to any possible beam position on the detector while the flight path is under vacuum. Initially we used cadmium for the beam stop, however, the detector has a non-negligible sensitivity to the capture gamma rays from cadmium. We are now trying alternative materials, which produce fewer capture gammas, in seeking a more suitable beam stop.

Sample Chamber: An evacuated sample chamber has been installed which is coupled to the two flight paths by steel bellows to avoid having windows along the beam line. The chamber can be isolated from the rest of the flight path by closing gate valves on either side of the chamber. A sample can then be changed and the chamber reevacuated in about ten minutes. An automatic sample changer will be added to the chamber in the near future so that up to four samples can be changed without intervention.

Detector: Earlier calibration measurements[2] of the 25 x 25 cm detector showed that this detector has a resolution of 4 mm in both directions and a linear position versus pixel relationships. Recent measurements have been aimed at determining the efficiency of the detector over its entire active area. Incoherent scattering measurements have shown that the efficiency is constant over a 24 x 24 cm area except along the two narrow vertical strips (∿ 4 mm wide each) where the efficiency drops by about 10%. Data in these regions (which comprise only ∿3% of the active area) must either be disregarded or normalized pixel by pixel for the dip in the detector's response.

The 65 x 65 cm detector for the SANS facility was received from the manufacturer[3] in June 1981 and was installed in July. When testing and calibration of this detector is completed, the SANS facility will then be fully operational. Based on our experience thus far, and the expected performance of the larger detector, the operating characteristics of the facility are given in table 1. As of September 15, 1981, data are being collected using the 65 x 65 cm detector.

Figure 1. Photograph of the new SANS spectrometer.

Table 1. Operating parameters of the NBS SANS facility.

Wavelength:	variable from 4 to 10 Å ($\Delta\lambda/\lambda \approx 0.25$)
Collimation:	single pair of irises or 9 channel converging collimation
Minimum Q:	0.003 Å^{-1} at 6 Å, 0.002 Å^{-1} at 9 Å
Q range:	0.002 Å^{-1} to 0.5 Å^{-1}
Sample size:	0.4 to 2.5 cm diameter
Flux at sample: (at 10 MW)	10^4 to 3×10^5 n/cm^2-sec depending on slit sizes and wavelength (These fluxes will be doubled at
Detector:	65 x 65 cm^2 position-sensitive counter with 5 x 5 mm resolution

b. Data Display and Analysis

SANS data are examined at the instrument with the aid of interactive computer graphics. Running totals of neutron counts recorded along individual rows and columns of the area detector are graphically monitored on line with automatic scaling and update. The entire detector field is inspected at the end of a data collection run using displays of constant intensity contour maps and three-dimensional perspective plots, each of which offers a variety of viewing options. Immediate hard copy is provided. Data from completed sets of runs are transferred to a minicomputer for further study using a color imaging graphics unit and for general processing. The color display unit effectively maps the area detector data field onto a user selected color field for detailed interactive examination. A computer terminal command environment provides access to a system of image analysis procedures that have been especially developed here for application to SANS. Computer software utilities have also been installed for use with standard data processing schemes. Among these are means for producing background corrected and calibrated data, and for averaging data over annular rings and ring segmented with respect to an arbitrary center. The data reduction facilities provide for the logical masking of arbitrary detector elements using computer mask files created with the color graphics system as part of the image processing analysis.

2. Neutron Time-of-Flight Facility (TOF)

The new neutron time-of-flight facility is designed to allow studies of neutron inelastic scattering by means of time-of-flight techniques over a wide range of incident energies and energy transfer resolution. A monochromatic beam is obtained by Bragg reflection from two parallel single crystals of pyrolytee graphite. This beam is then chopped by a compact Fermi chopper into short bursts (∿ 5-20 μsec) every 3000-5000 μsec, thus yielding a duty cycle of from .1 to 1%. These bursts of neutrons are scattered by the sample, and their time of arrival at the detectors, some 2.4 m away, is used to measure the energy transferred in the scattering process. The inherent low-duty cycle is compensated by two factors--first, "all" scattered energies are measured simultaneously (and hence all energy transfers) and second, by the use of multiple (up to 64 in the present case) detectors at various angles, allowing coverage of a wide range of momentum transfers simultaneously. While the latter technique is also applicable in principle to 3-axis instruments, it is of limited utility in such cases. The instrument is best adapted to isotropic samples, although diffuse scattering from single crystals is also of interest.

The facility at NBS is presently being completed at the CTW beam port. The crystal monochromators have been installed and many of the detectors have been installed and tested. Two of the choppers have been built and tested. The data acquisition system has been assembled and installation and testing are in progress. The facility will be operational before January 1, 1982. When completed, it will offer excellent intensity and better resolution than any current NBS facility, with a maximum resolution of 25 μeV. It will be at the forefront of such instruments in the USA.

---

1. C. J. Glinka, et al., *NBS Tech. Note* 1117, F. Shorten, Ed., 66 (1980).
2. C. J. Glinka, et al., *NBS Tech. Note* 1142, F. Shorten, Ed., 66 (1981).
3. Product of the Technology for Energy Corp., Knoxville, TN.

PHASE DECOMPOSITION IN THE Ni RICH SIDE OF Ni|Ni_3Al MISCIBILITY GAP: A SMALL-ANGLE NEUTRON SCATTERING STUDY

Satish P. Singhal
(State University of New York, Stony Brook, N.Y.)
and
Harvey A. Alperin
(Naval Surface Weapon Center, White Oak, MD)
and
F. Biancanello
(Metallurgy Division)
and
H. Herman
(State University of New York, Stony Brook, N.Y.)

The solid state thermomechanical processing of recent high performance superalloy components[1] essentially involves the precipitation of a variety of metastable phases either by nucleation and growth (NG) or spinodal decomposition (SD). The existing theories[2] describing these phenomena however, have been used only as a coarse guide-line by alloy designers. The advancement of predictive capabilities of the more promising recent theories[3] for alloy design applications needs a careful comparison between the theory and the experimental data. The present small angle neutron scattering (SANS) study on the Ni-Al alloy system has been carried out with these objectives in mind.

Approximately 1 mm thick samples of Ni - 14.4 at. % Al alloy were homogenized and quenched from 1200°C. The phase diagram (fig. 1) shows

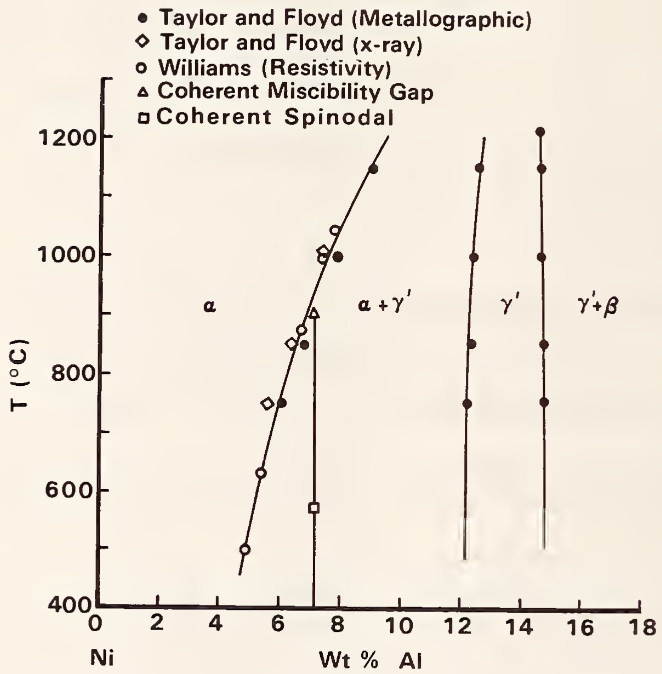

Figure 1. Ni(α) and Ni$_3$Al(γ') side of Ni-Al phase diagram.
△ ≡ A, coherent miscibility gap limit for Ni-14.4 at % Al alloy.
□ ≡ B, coherent spinodal point for the above composition.

the γ(Ni)|γ'(Ni$_3$Al) solvus line. The theoretically calculated[4] locations of the coherent miscibility gap and spinodal are also shown by points A(900°C) and B(572°C) for our alloy. Isothermal aging on the as-quenched samples was carried out at the temperatures of 540, 600 and 629°C. Other experimental details have been described elsewhere.[5]

In general, following Cahn and Hilliard[6] in a binary miscibility gap (MG), two regions of phase separation are defined; one comprising NG and the other SD. At the spinodal this and other classical theories[7] predict a singularity in various measurable quantities. A gradual transition from NG to SD is, therefore, not describable by these theories. This problem has been avoided by a recent phenomenological theory of nucleation, based on "cluster dynamics" by Binder and Stauffer (BS).[3a & 3b] A further advantage of this theory is that it does not make any assumptions about the criticality of nucleus size or require any steady state approximations. Although the existence of the spinodal is ignored by the BS theory, presently it is valid up to the maximum concentration bounded by the percolation threshold for a particular lattice type*. Numerical computations and phenomenological approximations[9, 3a] based on the BS theory suggest that the peak intensity (I_m) and peak position (Q_m) in the SAS spectra of an isothermally decomposing alloy exhibit a power law dependence** on the aging time (t) according to the equations

$$I_m = 1 + at^{\phi} \tag{1}$$

$$Q_m = b \cdot t^{-\phi'} \tag{2}$$

For the Ni - 14.4 at. % Al alloy figure 2 and 3 show the time dependence of I_m and Q_m derived from the SANS spectra at three aging temperatures. We see that, except in the early stages, where measurement errors are large, the behavior described by equations (1) and (2) is adequately obeyed.

---

* For fcc crystals this is about 20 at. % solute; so Ni - 14.4 at. % Al alloy is in this limit. [See ref. (8) for other lattices.]

** It must be pointed out here that a similar prediction has also been made by Langer, Bar-On, and Miller (LBM)[10] theory. The LBM theory, though most successful in the spinodal region, has been shown to give results in disagreement with experimental data in that region of the phase diagram, which is of interest in this experiment.

Phenomenologically, however, the time, temperature relationship for the transformation kinetics in an alloy follows a 'C' curve behavior. This is because the kinetics are limited by the driving force near the MG boundry, but at the lower temperatures, it is limited by the diffusion coefficient[11]. Therefore, if the kinetics of phase decomposition are to be studied closely, based on equations (1) and (2), a very important issue arises as to the temperature and composition dependence of the exponents ϕ and ϕ'. The theoretical predictions about such dependences are only qualitative[3a] but for a quantitative understanding a small body of SANS and computer simulation results are now available. These, and the results of the present study, have been summarized in table 1. Some of the conclusions based on this table will now be discussed. At first sight, we observe that in contrast to ϕ, the value of ϕ' is less sensitive to (i) alloy system, (ii) method of experimentation and computation, and (iii) alloy concentration. The value of ϕ' seems to be in the range 0.1 to 0.3. However, one must remember that the number of particles per unit volume (Nv) is $\sim [(Q_m/2\Pi)^3]$;[12] therefore even minor systematic variations in the value of ϕ' have a great bearing*** on Nv.

In the present study we have found an apparent linear dependence of ϕ' on the reduced temperature (T/T_{MG}^{Coh}). The fact that this dependence was not displayed by the computer simulation results[13a & 13b] points either to the inherent limitation of these methods or to the alloy model chosen for these studies.

For Ni-Al and Au-Pt systems ϕ increases linearily with T/T_{MG}^{Coh}; but in the temperature range of study, the increase is faster for Ni-Al.

*** It must be pointed out here that in the limit $t \to o$, Nv give the nucleation rate predicted by classical theories.[14]

TABLE 1
POWER LAW EXPONENTS: THEORETICAL AND "EXPERIMENTAL" RESULTS

Alloy Model and "Experimental" Technique	C_B/C_B^{crit}	T/T_{MG} or T/T_{MG}^{Coh}	ϕ'	ϕ	Reference
3-d S·C Ising Model Numerical Computations	0.2	0.8	0.16	0.70	9
3-d S·C Ising Model Computer Simulation	1.0	0.6	0.21	0.69	13(a)
		0.8	0.25	0.74	
		0.9	0.25	0.65	
3-d S·C Ising Model Computer Simulation	0.4	0.63	0.20	0.70	13(b)
		0.95	0.16	0.41	
Al-Zn SANS Study	0.17	0.92	0.10	0.8	12
		0.97	0.3	3	
Au-Pt SANS Study	1.0	0.39	-	0.03	15
		0.51	-	0.184	
		0.58	-	0.260	
		0.59	-	0.261	
		0.62	-	0.355	
Ni-Al SANS Study	0.59	0.69	0.15	0.52	This Study
		0.75	0.22	0.71	
		0.77	0.26	0.83	

C_B = Solute concentration in the alloy, C_B^{crit} = C_B at the critical point.

T_{MG} = Miscibility gap temperature, T_{MG}^{Coh} = Coherent miscibility gap temperature for alloys involving strain energy.

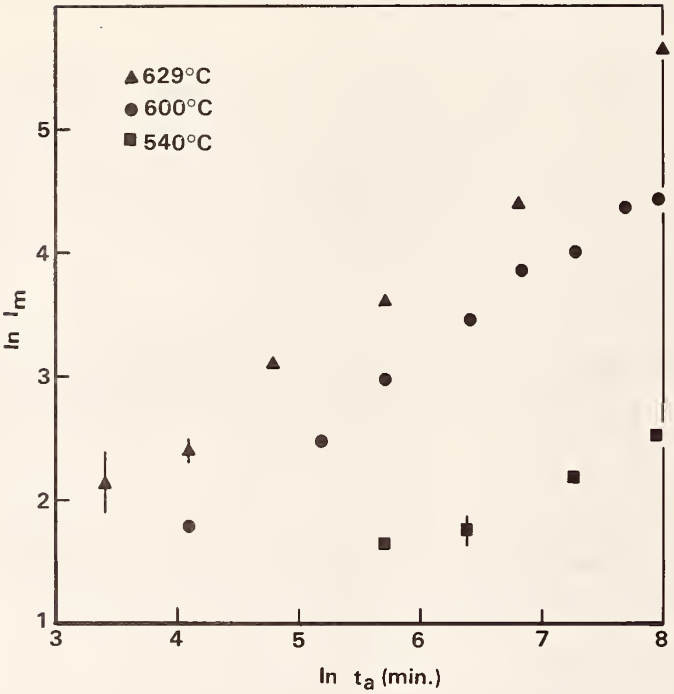

Figure 2. Variation of normalized peak intensity (I_m) as a function of aging time (ta).

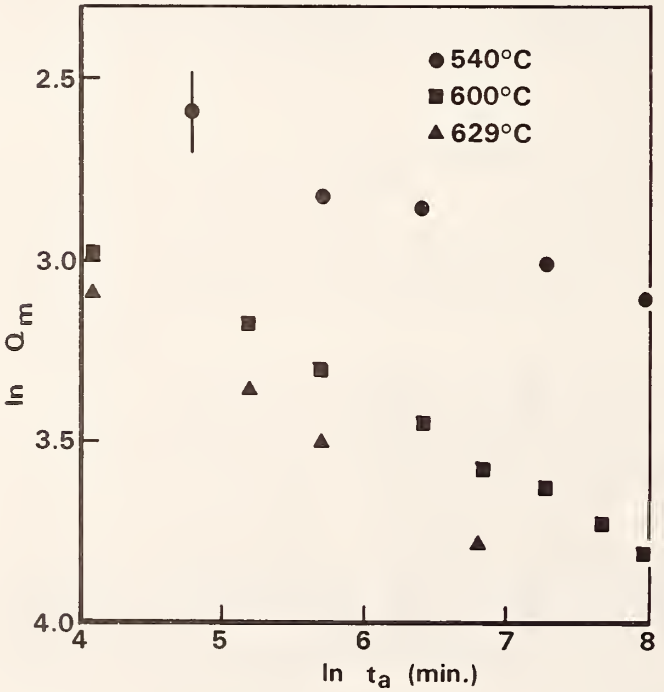

Figure 3. Variation of peak position (Q_m) as a function of aging time (ta).

The Al-Zn data compared to the Ni-Al data extrapolated to $T/T_{MG}^{Coh} \sim 0.92$ is low for both ϕ and ϕ'. On the other hand, it is much higher for ϕ at $T_{MG}^{Coh} \sim 0.97$. We must point out here, that in the Al-Zn study[12] at $T/T_{MG}^{Coh} \sim 0.97$; complications were seen due to incoherent precipitation at the grain boundary.

In conclusion, we can say that the SANS data on the isothermal phase decomposition kinetics in Ni-Al system is in qualitative agreement with a recent nucleation theory based on cluster dynamics. Additionally it exhibits an apparent linear temperature dependence of the power law exponents for the peak intensity and peak position, in clear disagreement with the computer simulation results. For a rigorous comparison of the Ni-Al data with the BS theory, it is necessary to obtain the complete scattering function (I vs. Q) from the theory. Such numerical computations based on non-linear equations are in progress[16].

---

1. R. Mehrabian, B. H. Kear, and M. Cohen, Rapid Solidification Processing, *Principles and Technologies, II: Second International Conference on Rapid Solidification Processing,* Reston, VA (1980).

2. J. W. Christian, *The Theory of Transformations in Metals and Alloys I,* Pergammon Press (1975). For example see Chapter 10.

3. a. K. Binder and D. Stauffer, "Theory for the Slowing Down of the Relaxation and Spinodal Decomposition of Binary Mixtures," *Phy. Rev. Lett.* 33, 1006-1009, (1974).

   b. K. Binder and D. Stauffer, "Statistical Theory of Nucleation, Condensation, and Coagulation," *Advances in Physics,* 25(4), 343-396 (1976).

   c. K. Binder, "Theory for the Dynamics of 'Clusters' II. Critical Diffusion in Binary Systems and Kinetics of Phase Separation," *Phys. Rev. B,* 15, 4425-4447, (1977).

4. For the procedure for such calculations see C. M. F. Jantzen and H. Herman in *Phase Diagrams in Materials Science and Technology*, Vol. 5 (1978), Ed. by A. M. Alper, New York: Academic Press.

5. S. P. Singhal, H. A. Alperin, H. Herman, and F. Biancanello, *NBS Technical Note,* 1142, 118-123, (1979-80).

6. J. W. Cahn and J. E. Hilliard, "Free-Energy of a Non-Uniform System III: Nucleation in a Two Component Incompoversible Fluid," *J. Chem. Phys.* 1959, 30, 688-699.

7. a. R. Becker, "Die Keimbildung bei der Ausscheidung in Metallischen Mischkristallen," *Ann. Physik,* 32, 128 (1938).

   b. G. Borelius, "Zur Theorie der Unwandlungen von Metallischen Mischphasen IV. Die Ausscheidung Ungeordneter Misgohphasen," *Ann. Physik,* 28, 507 (1937).

   c. J. N. Hobstetter, "Stable Transformation Nuclei in Solids," *Trans AIME,* 1949 180 121-130.

8. D. Stauffer, "Scaling Theory of Percolation Clusters," *Physics Reports,* 54(1), 1-74 (1979).

9. K. Binder, C. Billotet, and P. Mirold, "On the Theory of Spinodal Decomposition in Solid and Liquid Binary Mixtures," *Z. Physik,* B30, 183-195 (1978).

10. J. S. Langer, M. Bar-On, and H. Miller, "New Computational Methods in the Theory of Spinodal Decomposition," *Phys. Rev.* A11, 1417-1429 (1975).

11. See Chapter 15 in Reference 2.

12. G. Laslaz, P. Guyot, and G. Kostorz, "Decomposition Kinetics in Al-6.8 at % Zn," *J. de Physique*, Colloque C7, 406-410 (1977).

13. a. J. Marro, A. B. Bortz, M. H. Kalos, and J. L. Lebowitz, "Time Evolution of a Quenched Binary Alloy II Computer Simulation of a Three-Dimensional Model System," *Phys. Rev.* B12, 2000-2011 (1975).

    b. A. Sur, J. L. Lebowitz, J. Marro, and M. H. Kalos, "Time Evolution of a Quenced Binary Alloy IV. Computer Simulation of a Three-Dimensional Model System," *Phys. Rev.* B15, 3014-3026 (1977).

14. T. Hirata and D. H. Kirkwood, "The Prediction and Measurement of Precipitate Number Densities in a Nickel-6.05 wt.% Aluminum Alloy," *Acta. Met.* 25, 1425-1433 (1977).

15. S. P. Singhal, H. Herman, and G. Kostorz, paper presented in the International Conference on Solid-Solid Phase Transformations, Aug. 10-14, 1981, Carnegie Mellon University , Pittsburgh, PA.

16. N. Berk, S. P. Singhal, and H. A. Alperin, work in progress.

COMPOSITIONAL AND MAGNETIC INHOMOGENIETIES IN $Fe_{.67}Co_{.18}B_{.14}Si_{.01}$ AMORPHOUS RIBBON

H. A. Alperin
(Naval Surface Weapons Center, White Oak, MD)
and
(National Bureau of Standards, Washington, DC)
and
S. P. Singhal
(State University of New York, Stony Brook, NY)
and
(National Bureau of Standards, Washington, DC)

Iron-boron ribbons with ∿18% cobalt, prepared by rapid quenching exhibit an amorphous structure. Upon low-temperature annealing in a magnetic field, the magnetostrictive properties are greatly enhanced. In this preliminary study, neutron scattering was employed to investigate the compositional and magnetic microstructures induced by the field annealings. Both wide angle and small angle neutron scattering (SANS) were used. A saturating magnetic field (H) applied parallel to the scattering vector was used to eliminate the magnetic scattering and hence give the non-magnetic scattering component. Since the same measurement repeated with H=0 gives the sum of the magnetic and nuclear scattering, the difference of the two measurements gives the magnetic scattering (for H=0).

Thirty sheets of (2μm thick x 1.27 cm wide x 3 cm long) ribbon annealed at 370 c for 10 minutes in a magnetic field (in the ribbon plane and perpendicular to its length) were used for conventional wide angle scattering at a neutron wavelength of 0.973A and were compared to a similar as-quenched sample. The resulting amorphous diffraction patterns (taken with an external magnetic field of 1000G along the scattering vector which is sufficient to eliminate all magnetic intensity) were practically identical. This indicates that i) the field annealing treatment did not cause any crystallization of the ribbon and ii) there is at most, only very small changes in atomic rearrangement in the bulk of the sample upon field annealing.

SANS measurements were made with the NBS linear detector instrument on samples, each having 8 sheets, at a neutron wavelength of 6.5 A with (and without) an external field of 10KG applied along the scattering vector (i.e. in the plane of the ribbon) and for two 90° orientations of the sample (rotated about the normal to the ribbon face) to look for anisotropies in the scattering. In contrast to the as-quenched sample which shows no (compositional) inhomogenieties (i.e. no small angle scattering was observed), upon field annealing there is a great increase in the SANS showing that the compositional microstructure has changed significantly and in addition, exhibits a small but measurable anisotropy. A very large anisotropy is seen in the magnetic microstructure (at $H=0$) the details of which can be explained by assuming that these inhomogenieties are located in domain walls.

Figure 1 shows the angular dependence of the scattered intensity (according to the Guinier Law) for the field annealed sample measured in the two orientations "vertical" and "horizontal" which designate the orientation of a direction transverse to the ribbon length (i.e. the direction of the magnetic field during annealing). The Guinier Law $q - 4\pi \sin\theta/\lambda$ and 2θ is the scattering angle) then a straight line will result with slope equal to $-R_g^2$ where R_g is the radius of gyration of the scattering entities. The "vertical" and "horizontal" measurements for the nuclear (compositional) scattering are immediately fit with R_g's of ∿135A. Note the small spatial asymmetry of this scattering as indicated by the different intensities. It is clear, however, that a single R_g will not fit the magnetic scattering; so we have analyzed the data in terms of two R_g's. The high-q points are fit by $R_g = 135$A (which is the same as for the nuclear scattering) and after subtracting this contribution from the measured values we are left with another straight line (labeled "corrected" in the figure) which yields an R_g of ∿272A which is the same for both "vertical" and "horizontal" orientations even though the intensities are very different for these two cases.

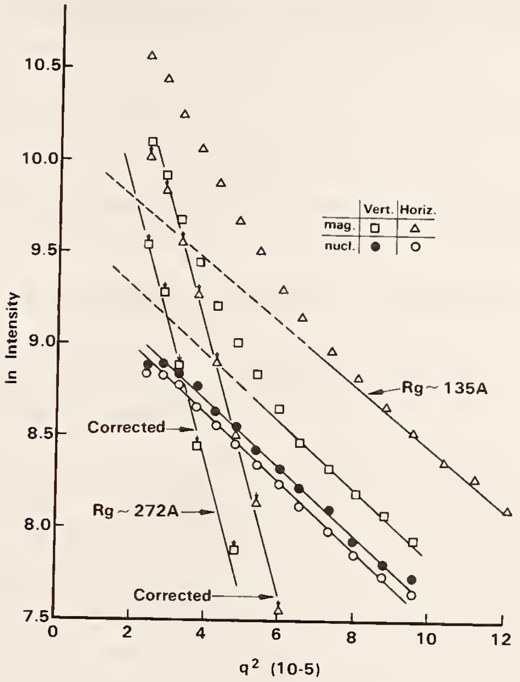

Figure 1. ln intensity vs. q^2 $(q = 4\pi\sin\theta/\lambda)$ for field-annealed amorphous ribbon analyzed according to a Guinier Law.
Δ - magnetic scattering for "horizontal" sample orientation.
□ - magnetic scattering for "veritcal" sample orientation.
● - nuclear scattering for "vertical" sample orientation,
O - nuclear scattering for "horizontal" sample orientation,
The meaning of the orientations are explained in the text. The points with attached arrows are replotted from the data after subtracting the straight lines fitted at large q^2 and result in the new straight lines labeled "corrected".

The results suggest that the compositional microstructure sets the basic scale (135A) for the magnetic microstructure (probably domain walls) but it is also possible for a magnetic inhomogeniety to be twice as large by jumping over to the next compositional inhomogeniety.

COMPUTATIONAL METHODS IN THE NON-LINEAR THEORY OF SPINODAL DECOMPOSITION

N. F. Berk
and
S. P. Singhal
(State University of New York, Stony Brook, NY)
and
(National Bureau of Standards, Washington, DC)

In 1975 Langer, Bar-On, and Miller[1] (LBM) gave the first general non-linear treatment of the kinetics of spinodal decomposition of binary systems with conserved order parameter and thus moved beyond the classical theories of Cahn-Hilliard[2] and Cook[3], which are known to fail even in the early stages of decomposition. In its full generality the LBM theory is not amenable to practical application, requiring as it does a knowledge of a hierarchy of correlation functions defined over a mesh of coarse grain cells. Therefore, LBM suggested a decoupling scheme which simplifies the theory while maintaining its essential non-linearity. In this approximation the small angle scattering (SAS) intensity S(k,t) is determined from the equation of motion

$$\partial_t S = - 2Mk^2(Kk^2 + A(t))S + 2Mk_BTk^2 \tag{1}$$

where k is the scattering wavevector, M is the atomic mobility, and K is the gradient energy coefficient introduced by Cahn and Hilliard.[2] In this equation

$$A(t) = \langle u\partial_u f(c_o + u)\rangle / \langle u^2\rangle, \tag{2}$$

where $u = c - c_o$ is the compositional deviation of a coarse grain cell and f is the Helmholtz free energy density of the cell whose composition is assumed to remain spatially uniform during the phase separation. The average in (2) is taken over the single cell compositional distribution $\rho_1(u)$ which itself satisfies a complicated non-linear diffusion-like equation within the approximation. This set of three equations formally provides a means of computing S(k,t) for a given form of f, which incorporates the specific system attributes. Even the simplified theory is difficult to treat numerically. To date, published treatments typically assume that $\rho_1(u)$ has the form of a double gaussian whose evolution is approximately determined by truncation of the set of equations for its moments. Moreover, the main interest has focused on the theory near the critical point, $1 - T/T_c \lesssim 10^{-2}$, where f may be well approximated by the convenient Landau form ($f = Au^2 + Bu^4$) or its extensions to finite higher order. However, these functional forms predict unphysical miscibility gaps at lower temperatures and so are unsuited to application to real SAS data from systems quenched deep into the spinodal region. As a result, the LBM theory has yet to be systematically tested against a wide range of laboratory experiments.

We have undertaken a research program to extend the LBM approximate theory to realistic free energy functions and to further simplify the still considerable numerical effort required to extract results for comparison with experiment or metallic solid solutions. As a first step, we are considering the subregular and regular solution models[4], which are known to predict realistic miscibility gaps. We have also developed a new set of equations for S(k,t) and A(t) based on the adoption of a double δ-function ansutz for $\rho_1(u)$. Seemingly a severe approximation this form actually interpolates between the physically expected limits of a single sharp peak at the quench and a pair of sharp peaks at the miscibility gap in the steady state. Moreover, as the temperature is lowered the average in (2) becomes increasing insensitive to the value of the width parameter of the double gaussian model, suggesting that this parameter is not the physically crucial one.

---

1. J. S. Langer, M. Bar-on, and H. Miller, *Phys. Rev. A* 11, 1417 (1957).

2. J. W. Cahn and J. E. Hilliard, *J. Chem. Phys.* 28, 258 (1958);
J. W. Cahn, *Acta Met.* 9, 795 (1961).

3. H. E. Cook, *Acta Met.* 18, 297 (1970).

4. H. K. Hardy, *Acta Met.* 1, 202 (1953); B. E. Sundquist, *Trans. AIME*, 236 (1966).

RELAXATION BEHAVIOR OF SiC FIBERS IN SiC/Al COMPOSITE MATERIAL UNDER STRESS

H. A. Alperin
(Naval Surface Weapons Center, White Oak, MD)
and
(National Bureau of Standards, Washington, DC)
and
S. P. Singhal
(State University of New York, Stony Brook, NY)
and
(National Bureau of Standards, Washington, DC)

We have utilized the penetrating power of neutrons to measure the elastic response of SiC fibers within an aluminum matrix composite material. A cylindrical sample (1 cm diameter) formed by extrusion was placed on the neutron diffractometer in a special fixture and subjected to compressive loads of up to a maximum of 317 MPa while changes in the Bragg peak positions were observed separately for the βSiC (111) and the Al (111) reflections. Several runs of d-spacing as a function of applied stress were taken and the following results obtained:

1. For the Al (111) reflection, within experimental error all points fell on a straight line whose reciprocal slope is equal to E/ν, the ratio of Young's modulus of elasticity to the Poisson ratio. Taking $\nu = .31$ we find $E = 17.8 \times 10^6$ psi (1.2×10^5 MPa) which is to be compared to $\sim 15 \times 10^6$ psi obtained from mechanical measurements on these samples. This value is considerably greater than the value 10.5×10^6 psi for an alluminum alloy, indicating that the composite material has been considerably stiffened by the SiC fibers.

2. In contrast to the Al (111) reflection for which no relaxation was observed, the βSiC (111) reflection exhibited a relaxation in the d-spacing under constant stress for periods of 6 hours and also when the external stress was returned to zero.

A tentative explanation for the above observations is that under compression the yield stress for the aluminum matrix is exceeded at the tips of the SiC fibers (which have been aligned along the cylindrical axis by the extrusion process) so that plastic flow in the matrix relieves the stress on the fibers but leaves the stress on the bulk of the aluminum matrix unchanged. Further experiments are planned to verify the explanation.

NUCLEAR SAFEGUARDS STANDARDS FOR DETECTOR CALIBRATION TOMOGRAPHY

W. M. Parker and Y. T. Cheng

The purpose of this project was to measure the transmission by U-235 and U-238 of the complete neutron spectrum coming from the NBS Research Reactor. From these measurements it should then be possible to calibrate the NBS double fission chamber detectors used in the Nuclear Safeguard project.

The uranium was available as uranium oxide in a finely powdered form which had to be encapsulated to form samples of a known thickness which could then be used for the transmission measurements. The containers consisted of an outer shell which had a well to contain the sample and a plug to compress the powder. The plug was 0.002 to 0.003 inch oversize and after loading was pressed into the container using an arbor press which exerted a force of several tons. The mass of the specimen was measured with an accuracy of 0.1 of a milligram.

In order to get other information on the thickness of the specimen, transmission measurements were made using gamma rays from a cobalt-60 source. A well collimated beam, 1/4 inch in diameter, was used, and measurements were made for the lower peak (1.10 to 1.25 meV), the upper peak (1.25 to 1.40 meV), and the two combined. The average of the three measurements was used as the value for the gamma ray transmission.

Radiographs were taken of the samples using a 250 kvp x-ray system. It is apparent from the radiographs that, for some of the samples, leakage of the powder from the well had occurred and that in others the distribution of the powder was not uniform. Finally, it is apparent that the density of the powder varies from sample to sample. For nine of the samples the radiographs indicate that the data should be reliable. For these samples the gamma ray transmission values were fitted by linear regression to the equation

$$I = I_o \exp (-\alpha m_s) \tag{1}$$

where m_s is the mass of a cylinder of U_3O_8 6.4 mm in diameter. Figure 1 shows the data used and the fitted line. The equation was then used to calculate m_s for the other samples. Three methods were used to calculate the total mass of the samples used for the neutron transmission measurements. They were as follows:

Method I is the one just described--a combination of the values of m_s obtained from measurements made on the radiographs and the known masses of the reliable samples with the values of m_s for the other samples calculated from the gamma ray transmission using equation (1).

Method II smooths the data by using equation (1) to calculate all of the values of m_s from the gamma ray transmission.

Method III was suggested by the fact that when the neutron transmission is plotted against the design values of the thickness, the resulting curve appears to be as good as the one obtained from Methods I or II which are based on the gamma ray transmission. Method III, in effect, assumes that all of the sample is effective in absorbing the neutrons.

As shown in previous reports, a plot of the neutron transmission versus the thickness of the absorber is expected to follow the equation

$$I = I_o (a_o + a_1x + a_2x^2) \tag{2}$$

with the expected value of a_o being 1.

The neutron transmission was measured using a two compartment fission chamber with one foil being U-235 and the other Pu-239. The

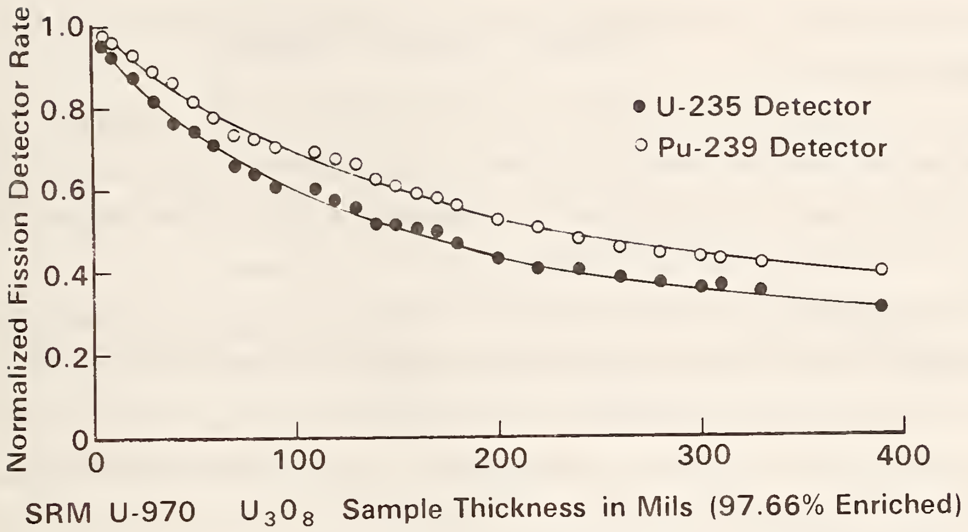

Figure 1. Gamma ray transmission for 6.4 mm diam. U_3O_8 sample.

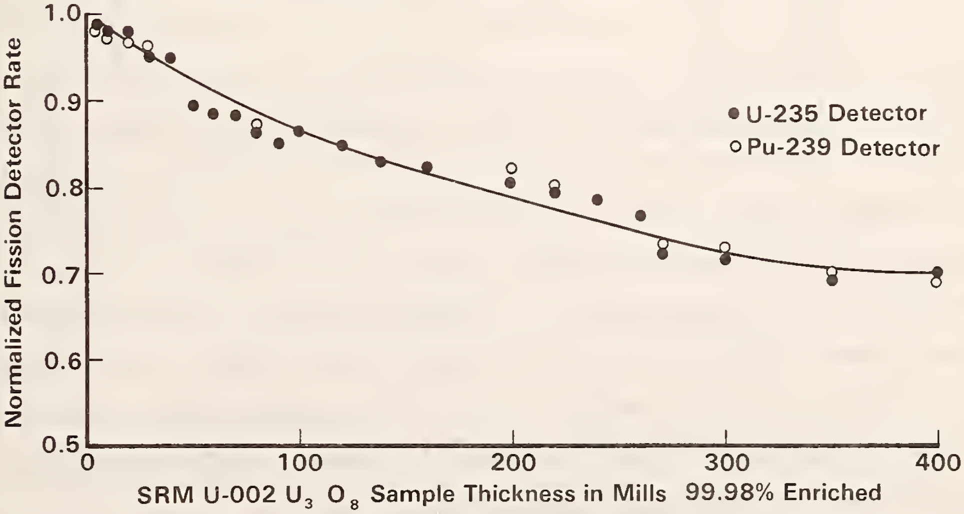

Figure 2. Data points for U-235 sample and a U-235 detector and curves using a_1 and a_2. The average values found using method II and III.

absorbers were 97% enriched U-235 (NBS SRM U 970) and fully depleted U-238 (NBS SRM U0002).

When the data are fitted to equation (2) by a least squares calculation, a_o is found to be 0.9 for U-235, U-235 sample detector combination, about 0.95 for U-235, Pu-239 pair and about 0.97 for U-238 with either detector. No reasonable explanation for this is known.

It was decided to do two things. One is set $a_o = 1$ in equation (2) and to weight the data so that larger values of x are given more weight. The 26 data points were divided into groups of 9, 9, and 8 which were given weights of 1, 2, and 3, respectively. The results for Methods II and III agree quite well and are considered to be the best available from the present data. Figure 2 shows the data points for a U-235 sample and a U-235 detector, where m_s is used as a measure of the thickness, together with the curve obtained by taking a_1 and a_2 as the average of the values found using Methods II and III. Table I gives the values of a_1 and a_2 obtained by this method for all four combinations of sample and detector, expressed in cm^{-1} and cm^{-2}. These are the numbers that would apply if the sample is a solid metal foil.

Table 1. Calculated values of a_1 and a_2.

		Absorber	
		U^{235}	U^{238}
Absorber	U^{238}	$a_1 = 4.941\ cm^{-1}$ $a_2 = 9.534\ cm^{-2}$	$a_1 = 1.518\ cm^{-1}$ $a_2 = 1.467\ cm^{-2}$
	U^{235}	$a_1 = 3.776\ cm^{-1}$ $a_2 = 6.233\ cm^{-2}$	$a_1 = 1.440\ cm^{-1}$ $a_2 = 1.321\ cm^{-2}$

It would be very difficult to estimate what the probable error is. If the program is continued, it would be most desirable to repeat the experiment using solid metal foils.

RESONANCE NEUTRON TOMOGRAPHY

Y. T. Cheng and D. A. Garrett

The effort on the resonance neutron tomography project during last year was devoted to (1) the continuing development of software programming and the library data set; (2) the construction of the reactor-based resonance neutron safeguards experimental system and the making of provisions for its use, (3) an experiment to verify the resonance neutron self-indication effect with the NBSR, and (4) the initial tomographic construction of a nuclear waste container.

In the first area, a mathematical analysis has been conducted and a computer code written for solving multiple non-linear equations relating fission detector response to fissile sample thickness. The cross section data library has been further upgraded; this has helped to improve the sensitivity for the self-indication effect.

The detail design of the reactor-based resonance neutron safeguard experimental system was completed in April 1980 and has been approved by the NBS Reactor Hazards Evaluation Committee. The NBS Shops Division was responsible for the construction of the system and the letting of bids to private contractors.

In addition, glovebox provisions were made to the SRM Shop to permit the handling of SRM U_3O_8 powders of various enrichments for the fabrication of transmission cells.

In order to verify the resonance neutron self-indication effect with the NBS reactor facility, an experiment was conducted to quantitatively determine the U-235 and U-238 contents in three nuclear fuel pellets supplied by General Electric Wilmington Manufacturing Department. The known information is in table 1.

A horizontal neutron beam of 1/4 in. (0.635 cm)-diameter was extracted from the NBSR core on port BT-7. The thermal neutron portion of the beam was removed by using a 0.04 in. (0.102 cm)-thick Cd sheet as filter. The filtered beam was then transmitted through the fuel pellet and detected by NBS double fission ionization chamber detectors.

The experimental setup and fuel pellet holder are shown in figure 1. The holder was made with a lucite block approximately 15 cm long, 5 cm wide, and 1 cm thick. Four holes were drilled to accommodate the three fuel pellets and a blank reference hole. The three fuel pellets, along with the blank hole, were scanned by the neutron beam and detected with U-235, Pu-239 double fission chamber detectors and then with U-235, U-233 detectors. The reason for using Pu-239 and U-233 detectors was that the fission cross section for U-238 was very small. A count rate of $\gtrsim$ 1000 cps was obtained using very thin fission foil in all detectors, thus no corrections were made for detector dead-time, self-absorptions, and background noise. A total count of $\gtrsim$ 50,000 was accumulated for each data point.

Table 2 lists the measured U-235 and U-238 contents in grams in the third pellet as compared to the known quantities.

The measured U-235 content in the third pellet is about 11 percent of the known U-235 quantity when the U-233 and U-235 detectors set are used, and about 15 percent with the U-235, Pu-239 set. The accuracies for the measured U-238 content in the third pellet are 4 percent and 6 percent, respectively, for the two sets of detectors. The fact that all neutrons with energies below 0.5 eV were filtered out in the beam caused the Pu-239 detector to perform less satisfactorily relative to U-233 and U-235 detectors, since 60 percent of the resonance strength for Pu-239 lies in the 0.3 eV region. Nevertheless, the results indicate that a reasonably accurate estimation of U-235 and U-238 contents can be obtained in a very short time ($\lesssim$ 1 min.) with the self-indication method with counting statistics of 0.1 percent.

The tomographic reconstruction of a point object using the filtered back projection technique has been carried out before. In an effort to further study the reconstruction technique as applied to those actual fuel pellets within a gallon-sized container. A second experiment was conducted on the BT-7 beam port of the NBSR.

The experiment consisted of three parts: 1) the production of reference calibrations, 2) the scanning of the waste container by the resonance neutron beam, and 3) the mathematical reconstruction of the

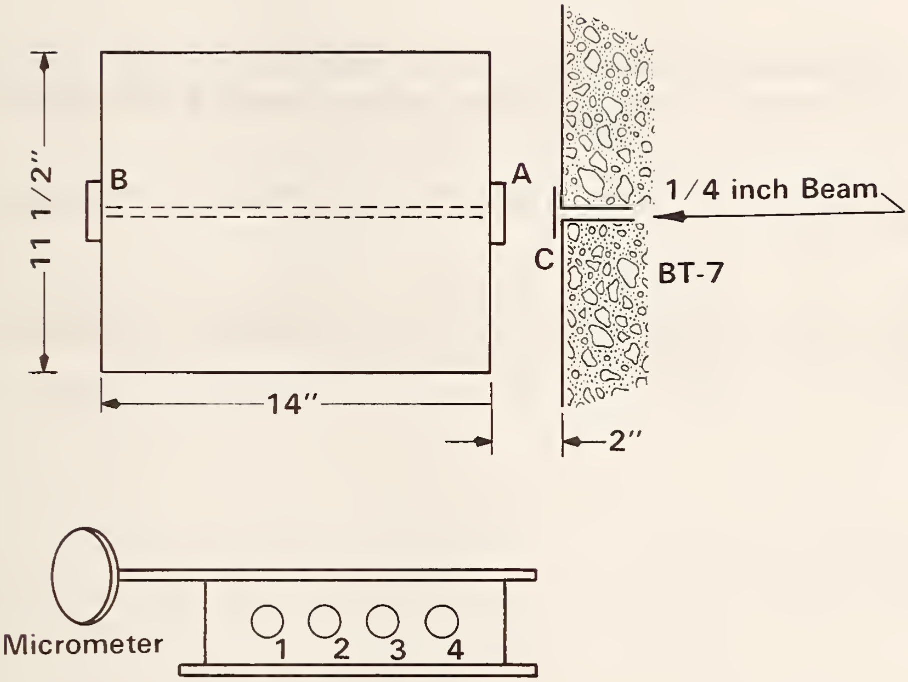

Figure 1. Neutron telescope and fuel pellet holder.

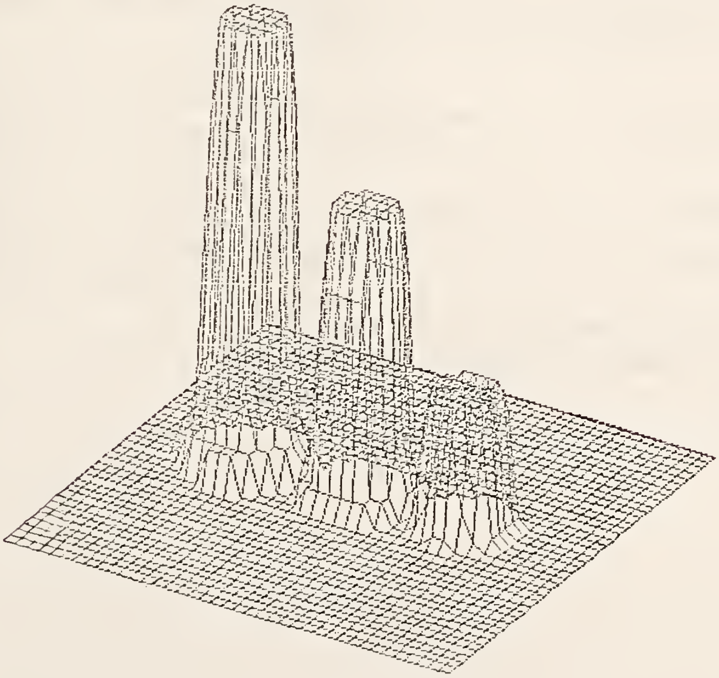

Figure 2. Tomographic construction of U-235 contents in the fuel pellets.

Table 1. Known characteristics of three nuclear fuel pellets supplied by General Electric Wilmington Manufacturing Department.

Isotopic U-235 enrichment %	% U	Density	Length	Diameter
3.9572	88.15	95.9243	0.432"	0.410"
2.5174	88.168	96.56	0.4395"	0.410"
1.194	88.14	95.52	0.434"	0.410"

Table 2. Measured U-235 and U-238 Contents, in grams, in the third pellet as compared to the known quantities.

	Known quantities*	Measured with U-235, Pu-239 detectors**	Measured with U-233, U-235 detectors**
U-235	0.2174	0.185 ± 0.03	0.193 ± 0.03
U-238	5.2764	5.581 ± 0.05	5.476 ± 0.49

*Corrected for 1/4" neutron beam size.
**Errors were estimated second order effects.

container based on the results of 1 and 2. The reference calibrations were necessary to interpret the responses of the fission detectors. The responses were functions of particular neutron beam characteristics, detector system efficiencies and the effect of neutron beam softening in the object to be studied.

U-235 and U-238 reference discs were made from SRM U-097 and U-002 materials, respectively. The U-235/U-238 reference discs were then placed in the resonance neutron beam and the transmitted beam recorded by both U-235 and Pu-239 foils in the NBS double fission detectors. The self-indication effort is clearly demonstrated in the case of U-235 detector, while the responses of Pu-239 detector to both U-235 and U-238 materials are very similar due to the fact that Pu-239 resonant cross sections do not match the total cross sections of either materials.

The waste container was first moved horizontally with respect to the neutron beam at 1.6 mm intervals, the total width covered was 6.4 cm. At the end of each horizontal scan, the container was rotated 3^{o}. Sixty such rotations were acquired for each slice of the container to be reconstructed. A total count of > 10,000 was recorded for each point scanned on both U-235 and Pu-239 detectors. Dwell times on each point varied from 15 sec. to 25 sec.

The preliminary tomographic reconstruction of the slice of the container that passes through the centers of all three pellets is shown in figure 2. The heights of the three columns indicate the relative U-235 contents. The errors are mainly introduced by the calibration process. To minimize the errors, one has to use metallic reference discs instead of the ones made from powder SRM's so the effective thickness of each disc can be measured more accurately.

DESIGN STUDY OF A FACILITY FOR NEUTRON-ACTIVATION AUTORADIOGRAPHY OF PAINTINGS AT THE NATIONAL BUREAU OF STANDARDS REACTOR

Y. T. Cheng and D. A. Garrett

Art conservation laboratories regularly employ techniques such as x-ray radiography and microscopic examination of pigment layer cross sections in the study of paintings. X-ray radiographs, however, show only the distribution of dense pigments such as lead white and thus provide only part of the analysis. Relatively recently neutron-activation autoradiography has been used. It extends the range of information that can be obtained by being able to measure the distribution of several pigments other than lead and at the same time identify the elementary composition of the painting.

A current drawback of the neutron technique is that the radiation dose to the painting is two orders of magnitude greater at the existing facilities than a typical x-ray examination. Although this is believed to be well below the level that would damage the painting, it cannot be shown that such radiation doses might not result in some deterioration that would not appear until many years in the future. Therefore, it is very important to reduce the radiation dose to as low a level as possible.

A proposal was submitted to the Smithsonian Institution and subsequently a contract was awarded for a design study of a painting autoradiography facility that would reduce the radiation dose received by a painting by an order of magnitude compared to that available at other reactors. The possibility of building such a facility is made feasible by the unique thermal column built into the NBS reactor. The proposed study will result in a detailed design of the facility, a cost estimate for its fabrication, and more detailed estimates of the radiation fields.

For the feasibility study, firstly an experiment was carried out to gather information concerning thermal neutron flux distribution, neutron to gamma ratio, field nonuniformity, size of usable thermal neutron field, radiation shielding requirements, etc..

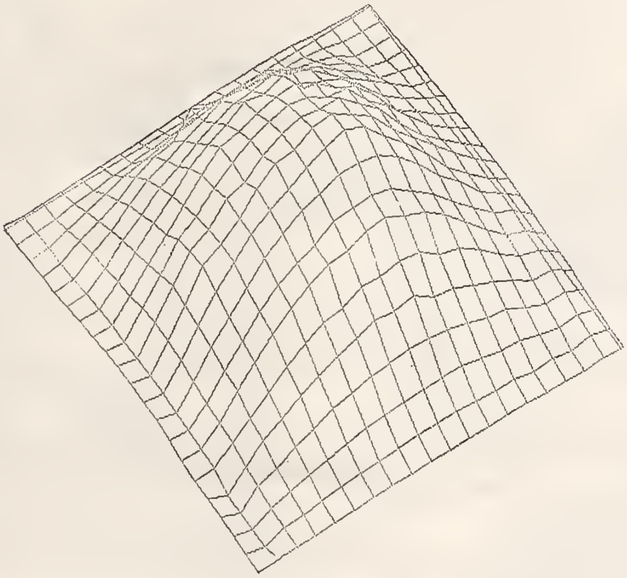

Figure 1. The relative thermal neutron flux distribution of the NBSR thermal column.

The result of thermal neutron flux distribution at the NBSR thermal column surface is shown in figure 1. The field is approximately 54 in. x 54 in. in size and the flux, without any modification, varies by a factor of 4 from column center to the edges. If the nonuniformity of the field is limited to 50 percent, then the usable field size is reduced to a 3 ft. x 3 ft. area with a neutron flux of 6×10^{9} n-cm^{-2}-sec^{-1}. However, this usable field will expand to 5 ft. x 5 ft. area at the proposed first painting irradiation position which is indicated in figure 2, the plan view of the conceptual facility. The usable field will further expand to a 6 ft. x 6 ft. area at the second irradiation position and to 7 ft. x 6 ft. and 8 ft. 4 in. x 7 ft. area at the third and fourth positions respectively.

The goal on one hand is to produce an irradiation field with a thermal neutron flux in the range of 1×10^{9} n-cm^{-2}-sec^{-1} or higher. So the painting can be exposed to a total neutron fluence of 1×10^{13} n-cm^{-2} in a reasonable amount of time; this total fluence is considered necessary to apply the neutron-activation autoradiography technique successfully.

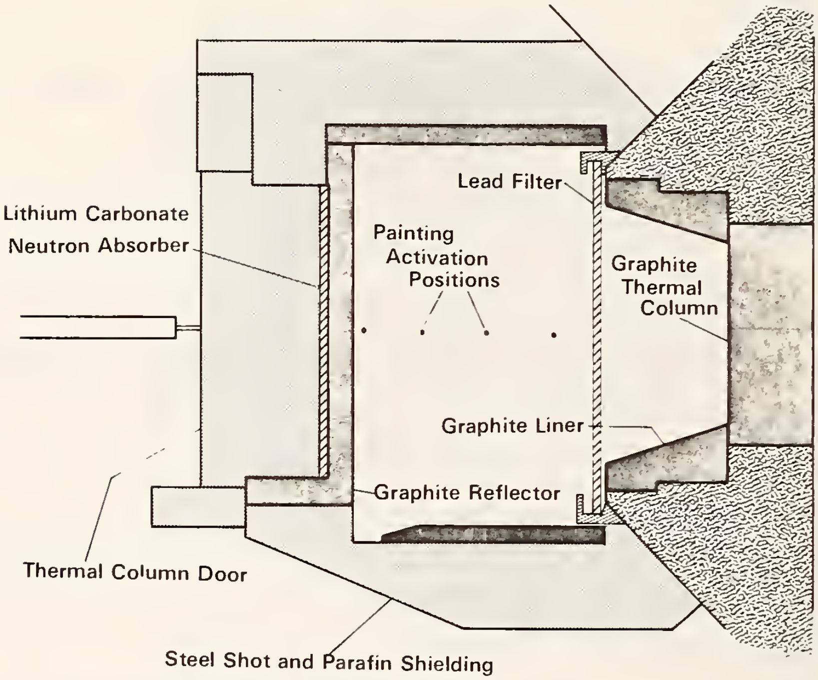

Figure 2. Plane view of the proposed NBSR neutron-activation autoradiography facility.

On the other hand, the emphasis should also be placed upon reducing the unwanted fast neutron and gamma ray doses received by the painting during the activation process. The measurement of the thermal neutron and fast neutron flux at the NBSR thermal column indicates a ratio of < 1,500 which compares very favorably to the ratio of 34 at the BNL medical reactor. This means the fast neutron dose the painting would receive at the NBSR facility will be less than 20 Rads per study. Also shown in figure 2, a 2 in. thick lead sheet is placed between the thermal column and the painting irradiation stations. This serves to decrease the external gamma dosage from an unfiltered value of 200 Rads to an estimated value of 20 Rads for the painting activation process. With more filtering materials, the radiation dosage given to paintings will be further reduced, but the activation time will be proportionally lengthened. Our concept allows the flexibility of changing the thickness and type of filtering materials to tailor the beam for differing needs.

Figure 3 shows the side view of the conceptual facility. The roof sections are of modular design. The section which incorporates the painting

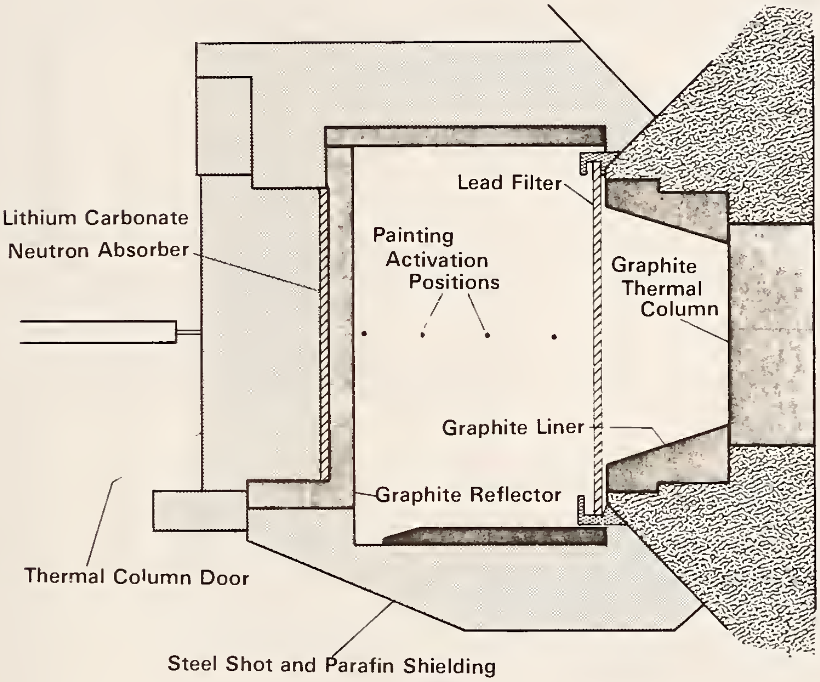

Figure 3. Side view of the proposed NBSR neutron-activation autoradiography facility.

suspension system can be relocated depending on the particular irradiation station selected. A second lead filter, in addition to the one mentioned above and a neutron stopping boral curtain, will be placed between the radiation source and the irradiation station to allow safe installation and removal of the painting. The interior of the facility will be lined with neutron reflecting materials to further enhance the neutron-to-gamma ratio.

Figure 4 shows the concept of the cart which will be used to transport the painting from the irradiation facility to the counting room inside the NBSR building after the painting has been irradiated. It will serve during transportation both as a protection box for the painting as well as a biological shield to attenuate the induced radiation.

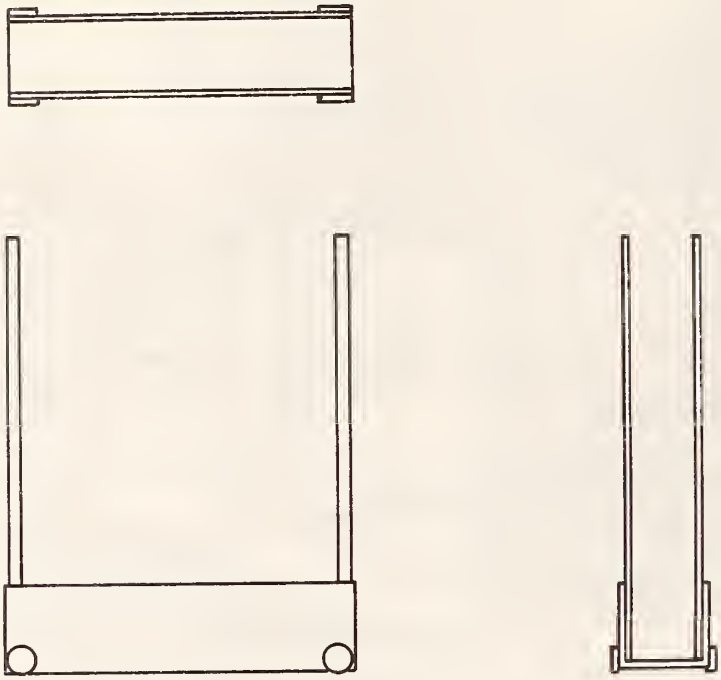

Figure 4. Painting transport cart.

The layout of the counting room is illustrated in figure 5. The irradiated painting will be mounted on a horizontal vacuum table in order to provide intimate contact between films and the painting for the autoradiography process. The table can then be turned to a vertical position for ease of the gamma-ray spectroscopy study. A steel mesh door will separate the painting storage area and the rest of the counting room. In addition, the storage area will also have motion detectors and a fire prevention facility to provide protection for the painting.

In conclusion, the NBSR thermal column, after the suggested modifications, can provide a thermal neutron field suitable for neutron-activation autoradiography studies of paintings while at the same time minimizing the radiation dose received by the paintings. The radiation dose received by a typical painting at the proposed NBSR facility would be about 70 Rads or less which includes an external dose of less than 40 Rads from gamma rays and fast neutrons in the field and a dose of $\sim$ 30 Rads from beta particles and gamma rays emitted by activated elements in the

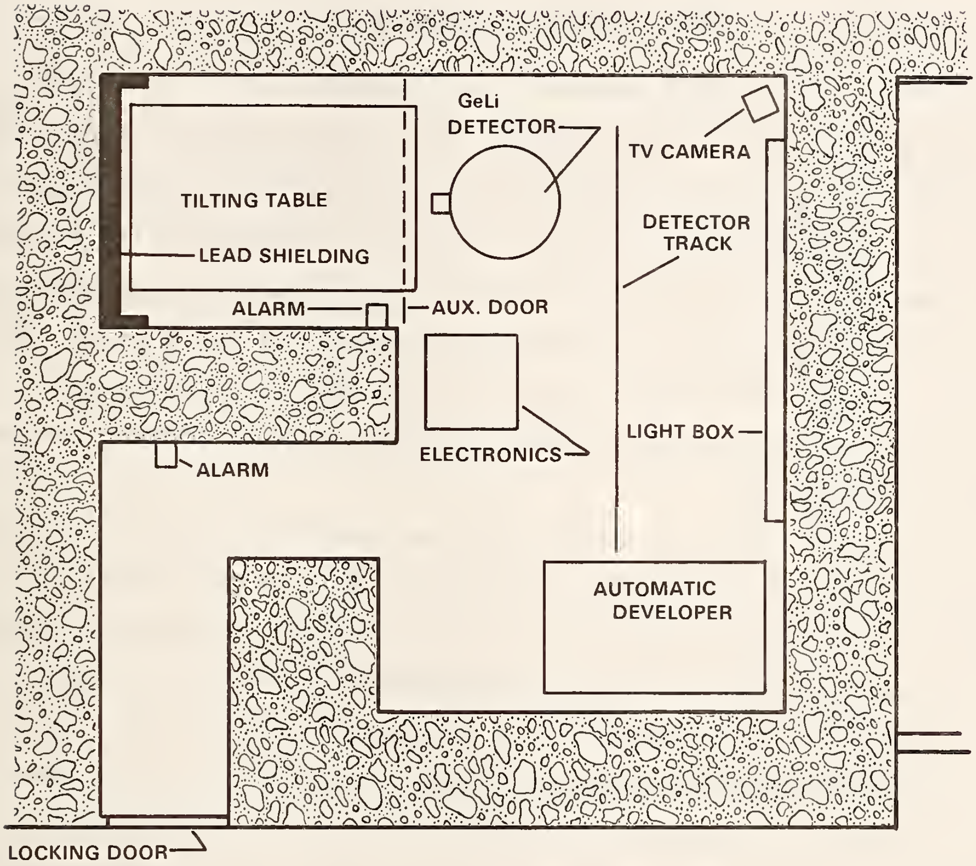

Figure 5. Painting counting room.

painting. This dosage of ∿ 70 Rads is slightly higher than the 20 Rads figure for a comparable x-ray study but well below the doses of ∿ 2,700 Rads from the existing neutron irradiation facilities.

NUCLEAR WASTE MANAGEMENT

Y.T. Cheng & D.A. Garrett

A new program was initiated to study the radiation effects of nuclear waste forms. It is designed to simulate long term radiation damage to the integrities of waste forms and to characterize the structural changes in the waste forms both macroscopically and microscopically. Our purpose is two fold to conduct the feasibility study of 1) using NBSR as a viable irradiation source for radiation damage study; 2) establishing neutron measurement techniques to complement the more common x-ray methods.

Li-6 and B-10 neutron activation methods were chosen to simulate alpha particle and transmutation effects. Activation methods are preferred over the Cm-244 doping process which requires long waiting time and special handling. The use of NBSR research reactor as neutron source gives further flexibility in studying neutron and γ effects.

The total radiation dosage and dose rate given to the waste form can be moderated by varying the amount of Li and B dopants and by putting the sample in different positions in the reactor. This also allows one to change the n/γ or α/γ ratios to qualitatively study synergistic effects.

The waste form currently under study is magnetophimbite ($X^{2+}M_{12}^{3+}O_{19}$). This is one of the four ceramic phases developed to contain high-level waste from the Savannah River Plant operations. Two natural Li doped magnetoplumbite samples ($li_{0.5}La_{0.5}Al_{11}O_{17.5}$) were supplied to us by the Energy Systems Group of Rockwell International.

X-ray and neutron diffraction patterns of the sample were taken as microscopic bench marks for the pre-irradiation characteristics of the sample. Thermal neutron radiography and small angle neutron scattering facilities will be used to characterize the macroscopic properties of the sample. The sample will be enclosed in sealed aluminum containers and be exposed to thermal neutron fluence of $1.2 \times 10^{20} n/cm^2$ to simulate the saturation γ dosage. After irradiation, the sample will be allowed to cool down for 30 days before being examined again by neutron and x-ray techniques to characterize it's post-irradiation conditions.

B. NON-RRD PROGRAMS

ACTIVATION ANALYSIS GROUP FY 81

R. Zeisler

The Activation Analysis Group is part of the Inorganic Analytical Research Division, Center for Analytical Chemistry. The group is located in the reactor building and utilizes the facilities provided here: stable climate counting rooms, clean and radiochemistry laboratories, a class 100 clean room, and the neutron irradiation facilities. The group has an active research program and applies activation analysis to many novel problems. The major research areas are summarized below and more detailed descriptions of important accomplishments are included in this report.

This year's 6th International Conference on Modern Trends in Activation Analysis clearly showed the technique as a versatile and sensitive tool in all branches of science and technology. Though the fundamental principles on which activation analysis is based have remained unchanged, incremental and crucial improvements are achieved by research efforts focused on the evaluation and elimination of errors due to irradiation and counting procedures and errors due to sample handling, and procedures leading to better sensitivity and higher selectivity. The Activation Analysis Group participates successfully in these research efforts and demonstrates the power of this mature technique through its contribution to NBS and other programs. Our goal is to demonstrate that activation analysis can fulfill part of the needs of analytical chemistry for the determination of many components in complex matrices simultaneously and over a broad dynamic range.

Based on the highly characteristic and well-defined nuclear properties of the elements, this technique is close to an ideal nondestructive analytical method. It fulfills the two basic requirements of nondestructive techniques: specificity - the ability to correlate directly and unambiguously the signal with the element sought, and selectivity -

the possibility of measuring the element in question in the presence of other elements which emit signals of the same nature. The Activation Analysis Group is emphasizing research efforts which bring the technique closer to the ideal. We use the different nuclear characteristics of the elements when we apply our various activation analysis techniques: instrumental and radiochemical neutron activation analysis (INAA and RNAA) photon activation analysis (PAA), prompt gamma activation analysis (PGAA), and nuclear track technique (NTT), and we investigate means and ways to determine the specific signals more accurately and more selectively. Concurrently, we are expanding our activities to include questions of general analytical significance, e.g., sampling and sample preparation for analysis.

Recent research accomplishments in the area of activation analysis methodology are highlighted by the development of RNAA procedures for the determination of platinum and tin in biological matrices. In both cases radiochemistry lowers the limit of detection and provides essentially "background-free" counting of the specific signals free of interferences from chemical blanks. Unprecedented low levels of platinum have been determined using this new RNAA technique. Other research efforts are directed towards the determination of light elements as major constituents of complex matrices, the accuracy and precision of PAA and PGAA are currently evaluated. A newly developed RNAA technique for the ultra-trace determination of I-129 will make the issuance of a certified material feasible.

In connection with the pilot National Environmental Specimen Bank (NESB) program research efforts resulted in a better understanding of sampling characteristics of particulate biological matter. We have investigated how to better homogenize these materials and what characteristics determine the subsequent subsampling of analytical test portions in order to obtain meaningful analytical results. Problems involving the appropriate number and size of samples (needed to characterize bulk samples such as a human organ or part of an ecological system) are studied in collaboration with statisticians.

INAA multielement determinations have provided a huge database for the major environmental programs in which we participated during the past year: Chesapeake Bay, NESB, and Hazardous Waste. The dynamic range of activation analysis and its multielement capability is especially useful to analyze varying concentrations and to discover unexpected occurance of elements. INAA is also used for the determination of halogens in organic liquids obtained to analysis from the Recycled Oil Program and from other sources. INAA multielement results have been used for the certification of up to 20 elements in various new SRMs: Bovine Liver, Orchard Leaves, Cast Iron Alloys, Basalt, Obsidian, Reduced Iron Ore, and Fuel Oil. INAA has provided crucial information to another NBS group on fused silica glass insulators.

We continue to emphasize the importance of state of the are equipment to be able to contribute in the same way in the future to the mission of analytcical chemistry at NBS with our strongest competence, that is INAA. Major additions to our counting equipment and the acquisition of a computer will help to follow this route. We also will continue to take advantage of the specifics of nuclear techniques in ultratrace determinations and chemical speciation studies by developing RNAA techniques and applying activation analysis to new problems as in the rapidly expanding field of bio-technology. With the new depth-profiling facility we will enter a new and important field in analytical chemistry.

1. Research in Basic Problems of Analytical Chemistry

a. Application of Sampling Theory to Particulate Biological Samples

S. H. Harrison, B. Kratochvil, K. A. Fitzpatrick, and R. Zeisler

The quality of the analytical sample, as opposed to the quality of the chemical analysis, is a too often disregarded factor in analytical chemistry. The sample on which the results of a chemical analysis are finally based depends very much on the properties of the bulk sample and the analytical test portion taken from the bulk sample [1]. Programs like the pilot National Environmental Specimen Bank (NESB) are critically dependent on the credibility of the analytical results, e.g., on the bulk sample representation found in the analytical test portion. The NESB tasks of evaluating storage conditions and analytical quality are carried out by means of multiple analysis of many samples. This represents an ideal test case for studying the application of sampling theory to the investigation of the properties of particulate biological materials.

Biological specimens, (e.g., human liver, mytilus edulis, etc.) are homogenized at cryogenic temperatures under contamination-free conditions, in Teflon ball and disk mills to provide analytical test portions for comparative analysis. The samples are always handled in a cryogenic state and maintain particulate appearance after homogenization. Assuming a particulate homogenate, the performance of the two types of mills, ball mill and disk mill, was investigated. A radiotracer experiment was carried out and Ingamells' sampling constant, K_s, was determined after collecting the data for a sampling program. Using the ball mill, a $K_s = 32$ g was determined. Based on the K value, one can conclude that the material is not well enough ground or well enough mixed. A result of this experiment was the design of a disk mill which yields a K_s of 0.95g.

To verify the particulate model, efforts were undertaken to actually measure the particle size distribution of the homogenate obtained from the two different milling procedures.

In general, sieving experiments are an easy way to determine particle sizes; however, cryogenic sieving of frozen samples is much more difficult. After some procedure development, the sieving experiments were carried out in a large LN_2 freezer which provided the necessary cold and dry atmosphere to avoid melting and particle agglomeration due to moisture condensation. The results of sieving split liver samples, previously ground in the two different mills, show that the disk mill produces somewhat finer particles with virtual elimination of the course (>40 mesh) fraction. Twenty five percent of the material ground in the ball mill remained in the coarse (>40 mesh) fraction. The obvious effect on subsampling is that smaller particles produce better homogeneity.

Using the information about particle size distribution and some assumptions as to the chemical nature of the liver, the weight of sample required to hold the sampling standard deviation to a preselected level can be theoretically calculated starting with the computation of N, the number of particles. The value of N may be calculated from the relation

$$N = \frac{d_1\ d_2}{\overline{d}}^{\,2} \quad \frac{100\ (P_1 - P_2)}{R\overline{P}}^{\,2} \quad p(1 - p)$$

where d_1 and d_2 are the densities of the two kinds of particles, $\overline{d}$ is the density of the sample, P_1 and P_2 are the percentage compositions of the component of interest in the two kinds of particles, $\overline{P}$ is the overall average composition in percent of the component of interest in the sample, R is the percent relative standard deviation (sampling error) of the sampling operation, and p and 1-p are the fractions of the two kinds of particles in the bulk material [1]. For a two component particle mix made up of cells and fluids, and for 40 mesh particles, the element Na requires a one gram sample to reduce the sampling error to one percent. This is very consistent with our sampling constant of 0.95g.

Table 1. Na and Cl in Mussell Sieve Fractions (concentration in mg/g dry weight)

Sieve Fraction Mesh Range	>40	40-60	60-80	80-100	100-140	140-200	<200	Unsieved
Na	54.0	53.8	57.2	61.9	65.5	70.7	71.8	61.0
Cl	79.8	96.7	102	110	116	121	128	111

In addition, trace element analysis experiments were carried out to provide support data for the theoretical evaluations. In one experiment, ten subsamples of homogenized liver were analyzed for about 30 elements using nuclear methods. The element specific homogeneity was determined to be two to three percent for most elements and one percent or less for Na, Fe, and Zn. In the other experiment, mussel (mytilus edulis) samples were homogenized in a disk mill before being sieved. The sieved fractions were then analyzed by INAA for trace elements. Some interesting results from this experiment are shown in Table 1. The results indicate a salt fraction which is more highly concentrated in the fine particles.

The work shows that theoretical calculations of sampling parameters compare favorably with experimental results. This information can provide important knowledge on the relation of the analytical test portion to bulk material and, therefore, the quality and usefulness of the analysis.

---

1. Kratochvil, B., and Taylor, J. K., Sampling for Chemical Analysis, *Anal. Chem.*, 53 (1981) 924A.

b. Non-Normal Distribution of Blanks in Environmental Samples

R. R. Greenberg, H. M. Kingston, and E. S. Beary.

Many environmental studies involving the chemical analysis of samples collected in the field require the subtraction of blank values arising from filters, acids and other reagent solutions, containers used to store the samples, etc. Typically, a number of blanks are analyzed, the mean used as the most probable value, and the standard deviation used to predict the probability of deviation from the mean. This approach is accurate, however, only when the blanks are normally distributed. Frequently, this is not the case as illustrated by a recent analysis of five 47 mm Millipore filters. Iron concentrations of 0.2, 0.3, 0.3, 0.5, and 1.9 μg/filter were found.

NBS has completed an extensive study of the Chesapeake Bay. As part of this study, 24 blanks were collected and processed with the 102 water samples. These blanks, along with the samples, were then analyzed by the neutron activation analysis. Several of the elements studied, including Fe, Co and Zn, were clearly not normally distributed among the blanks. The use of (normal) means and standard deviations greatly underestimated the probability of elevated blank levels occurring in one or more samples, and could have resulted in erroneous interpretations of some of the data. Much better results were obtained using log-normal distributions to describe the blank behavior of these elements. Fitting log-normal distributions to elements having normal blank distributions, did not significantly affect the results.

2. Improvement and Development of Nuclear Analytical Techniques

a. Ultratrace Determination of Platinum in Biological Materials

R. Zeisler and R. R. Greenberg

Increasing interest in the determination of platinum has been spurred recently by the wide spread use of the element in industrial and medical applications. Two possible major sources contributing to the human body burden are the noble metal catalysts used to reduce automobile emissions, and the administration of platinum containing drugs used in cancer chemotherapy. The intense interaction of platinum and its complexes with biological systems makes it desirable to establish baseline data and to monitor possible increases in human body burden. Previous attempts to measure baseline concentrations of platinum have failed because the reported sensitivities were several ng/g for the various techniques, while the actual concentrations were at least one order of magnitude lower. Many analytical techniques including neutron activation, however, have been successfully applied to monitor elevated platinum levels, e.g., after administration of anticancer drugs consisting of platinum complexes of the cis-($PtCl_2L_2$) type (1).

To measure the naturally occuring concentrations in human tissues and other biological materials, a new neutron activation analysis scheme based upon a radiochemical separation of the activation products has been developed. This method fully utilizes the inherent sensitivity of the activation reaction $^{198}Pt\ (n,\gamma)\ ^{199}Pt$ and counting of the daughter nuclide Au-199 after radiochemical separation. The separation applied here is highly specific for gold, in order to avoid common interferences, as well as to provide "background free" counting of the respective gamma activities. A decontamination factor of $>10^7$ for Na-24 has been achieved. The only remaining interference to be considered is the reaction $^{197}Au\ (n,\gamma)\ ^{198}Au\ (n,\gamma)\ ^{199}Au$ from the naturally occurring gold in the samples. This reaction can be quantitatively assessed with high precision and taken into account by the determination of the gold using the same

Table 1. Platinum and Gold in Biological Standard Reference Materials
CONCENTRATION 10^{-12} g/g

	This work		Literature(2)	
SRM	Pt	Au	Pt	Au
1571, Orchard Leaves	∿ 200	1430 ± 80	89.2×10^3 to 1.2×10^6	970 to 3500
1572, Citrus Leaves	60 ± 30	107 ± 9	NR	NR
1577, Bovine Liver	70 ± 30	56 ± 13	NR	200 to 30000

NR = No data reported previously.

Table 2. Platinum and Gold in Human Liver Specimens

	(Concentration 10^{-12} g/g)	
NESB ID	Pt	Au
B0005	ND	2652 ± 1
B0014	54 ± 13	64 ± 1
B0041 - A	114 ± 23	71.9 ± 0.2
B0041 - B	127 ± 60	143.1 ± 0.3
B0042	240 ± 70	298 ± 1
S0049	ND	496 ± 2

ND = Not detectable.

separation step. This analytical procedure, therefore, also provides excellent results for gold at the 10^{-12} g/g level.

Platinum and gold have been determined in three biological Standard Reference Materials (Table 1). The results for platinum are found to be far below previously reported data (2) for orchard leaves, and below the current limit of detection in this material. The gold values, however, are in good agreement with the previous data, thus confirming the completeness of the analytical scheme. For bovine liver, both elements seem to be inhomogenously distributed, which would explain the wide scatter of the previously reported data for gold. The platinum concentrations found here are the first data reported for a presumably natural baseline in these materials which were collected more than ten years ago. It would be of interest to analyze similar materials collected recently. Possibly an increase of platinum in the environment could be detected.

The application of the technique on human liver specimens collected in the National Environmental Specimen Bank Program will help to establish baseline information on human body burden. Platinum concentrations in human livers have been found at the 0.1 ng/g level (Table 2). The determination of trace elements at these low levels shows again the advantage of the nuclear activation techniques being essentially blank free.

---

1. R. Zeisler, F. Lux, H. Seidenberger, H. Schoenenberger, W. Beck, *Nuclear Activation Techniques in the Life Sciences 1978*, p. 467, IAEA Vienna, 1979.

2. E. S. Gladney, Compilation of Elemental Data for NBS Biological and Environmental Standard Reference Materials, *Los Alamos Scientific Laboratory Informal Report, LA-8438-MS, 1980*, and *Anal. Chem. Acta. 118 (1980)* 365.

b. Precise Determination of Aluminum by Instrumental Neutron Activation

Richard M. Lindstrom and Ronald F. Fleming

Aluminum is the second most abundant cation in the earth's crust, and activates so well with thermal neutrons that Al-28 often greatly predominates in the gamma-ray spectrum of irradiated materials of geological or botanical origin for the first few minutes after irradiation. For both these reasons Al is often useful as the normalizing element, or marker for the crustal component of the sample. Because of the short half-life (2.2405 min), however, the determination of Al is subject to many inaccuracies: variation of irradiation conditions between irradiations, uncertainties in timing, and the effect of high and varying count rate, in addition to other sources of error that must be controlled in work with long-lived nuclides.

We demonstrate here that these errors can all be made smaller than the fundamental limit set by counting statistics, even when that limit is below 0.5 percent. Achieving accuracy of this order requires that the sample basis weight be determined to 0.1 percent, that the sample and standard be irradiated simultaneously with small neutron self-shielding, that counting geometry be controlled to 0.2 mm at 40 cm, that timing be known to 0.2 sec, and that peak integration procedures be stable. In our measurements, samples in disk shape are irradiated between two standard disks of Al foil. The 1779-keV Al-28 gamma activity is assayed with a Ge(Li) dector and multichannel analyzer system adjusted for reliable performance at integral count rates up to 40,000 counts per second, which gives in excess of 10^5 net peak counts in the first of several 80-sec counting intervals.

The transfer function from the observed number of net counts C to the counting rate at the end of irradiation $I_o(0)$ is modeled as the following process:

$$I_o \quad \text{front end} \quad I \quad \text{ADC} \quad I'$$

The relations between these rates are:

$$I_o(t) = I_o(0)\exp(-\lambda t) \qquad \text{(decay)}$$

$$I(t) = I_o(t)\exp(-\alpha I_o(t)) \qquad \text{(extending dead time)}$$

$$I'(t) = I(t)/(1+\theta I(t)) \qquad \text{(nonextending dead time)}$$

The solution to this set of equations is:

$$A(t_1) \equiv \frac{\lambda C\exp(\lambda t_1)}{1-\exp(-\lambda\cdot LT)} \quad \frac{\exp(\lambda\cdot DT)-1}{\lambda\cdot DT} = I_o(0)\exp(-\alpha I_o\exp(-\lambda t_1))$$

where DT = CT-LT is the ADC dead time and the pulse pileup parameter α is determined from a linear fit of $\ln A(t_1)$ vs. $\exp(-\lambda t_1)$. The derivation has been presented elsewhere (1).

The procedure has been applied to the analysis of NBS SRM 1633a Fly Ash. Samples were mixed with spectroscopic-grade graphite and pressed into pellets of constant geometry. The mean concentration and its standard error were 14.085 ± 0.023 percent Al for four determinations (Table 1). Chi-squared tests of intermediate and final results showed no significant variance beyond counting statistics, and hence the procedure is capable of the desired precision.

The accuracy of the method is shown by the analysis of high-purity single-crystal Al_2O_3, in which the amplifier shaping time, masses of sample and standards, sense of the irradiated sandwich (sample-standard-sample vs. standard-sample-standard), and counting geometry were varied without visible effect. The mean concentration observed and its standard error for six determinations was 52.77 ± 0.21 percent Al; the concentration calculated from the stoichiometry is 52.925 percent. The limit to inaccuracy of the method is presently 0.3 percent relative, comparable to the counting statistics obtained in the Fly Ash measurements. It may be concluded that in favorable cases activation analysis can produce aluminum data which are both precise and accurate at better than 0.5 percent relative.

Aluminum in SRM 1633a Fly Ash
(concentrations in percent)

Present Results:

Sample	F1	F2	F3	F4
Concentration	14.120	14.059	14.113	14.050
Standard Deviation	0.045	0.045	0.046	0.044

Mean	14.085
Standard Deviation of Mean	0.023
χ^2/ν	0.065, n = 4

Previous Results

INAA (NBS), Report of Anal. #5210, 5/79	14.07	0.33
PGAA (U. of MD), Anal. Chem., <u>51</u>, 2209 (1979)	14.0	0.2
Certificate (information only)	(14)	

---

1. R. M. Lindstrom and R. F. Fleming, in J. R. Vogt, ed., *Proceedings of the 4th International Conference on Nuclear Methods in Environmental and Energy Research* (Columbia, MO, 1980; in press).

c. I-129 Analysis

G. J. Lutz

Work is currently proceeding towards the certification of a botanical for its I-129 content.

The analysis consists of a pre-irradiation separation, an irradiation in the reactor, and a post-irradiation separation. The pre-irradiation separation involves the combustion of the sample in a stream of oxygen. The off gases are filtered through glass wool to trap out any particulate material and the iodine is collected on activated charcoal. The pre-irradiation filtering is necessary to remove cesium, uranium, and tellurium which interfere *via* the reactions $^{133}\mathrm{Cs}(n,\alpha)^{130}\mathrm{I}$; $^{235}\mathrm{U}(n,f)$ $^{129}\mathrm{I}(n,\gamma)^{130}\mathrm{I}$; and $^{128}\mathrm{Te}(n,\gamma)\overline{^{129}}\mathrm{Te}$ $^{129}\mathrm{I}(n,\gamma)^{130}\mathrm{I}$.

The charcoal trap containing the iodine is sealed in quartz and irradiated in the reactor. Subsequently a few milligrams of inactive iodine carrier and an I-125 spike are added. The major radioactivites are due to chlorine, bromine, and impurities in the charcoal and quartz. The off gases are again passed through a plug of glass wool to filter out particulate material. The collecting trap consists of a bed of hydrated manganese dioxide (HMD) followed by a charcoal trap for collecting the iodine. HMD is one of a series of selective ion retention media developed during the past several years. It is usually used for separations from aqueous solution, but has been applied to gas phase separations.

Over a fairly wide temperature range, a bed of HMD will remove 99.9%+ chlorine and bromine from the oxygen stream while passing $\sim$ 95% of the iodine.

d. Development of a Radiochemical Separation Procedure for Tin

R. R. Greenberg

Although tin has been shown to be essential for mammalian nutrition [1], it can be highly toxic in some forms [2]. Unfortunately, tin cannot be readily determined in biological materials because of the naturally occurring low levels. For example, very few biological reference materials with known tin concentrations are available. None of the eight NBS biological SRMs issued have either certified or "information only" values for tin. Relatively little reliable data concerning the tin concentrations in human and animal tissues and body fluids exists.

Neutron activation analysis can be used to determine tin in most biological materials at the naturally occurring levels if a radiochemical procedure is used to separate tin from interfering elements and the background level of radiation (noise) is reduced. Both the Sn-113 and Sn-117m isotopes can be used to quantify tin if the interfering Tb-160 (for Sn-113) and Sc-47 (for SN-117m) isotopes are removed. This has been accomplished with a separation procedure based on the extraction of SnI_4 into toluene. The sample is initially dissolved with nitric, sulfuric, and hydrofluoric acids along with hydrogen peroxide, followed by a filtration step to remove precipitated oxides and sulfates from the final sulfuric acid solution before extraction into toluene. Carriers are used to assure a quantitative recovery (>99.8%) and maximize the decontamination.

Five samples of SRM 1571 (Orchard Leaves) have been analyzed by the above procedure. The resulting concentration of 290 ± 17 (1s) ng/g agrees favorably with two of the literature values (294 ± 16, 290 ± 20, and 4100 ng/g) compiled by Gladney [3]. The resulting reduction in background radiation was better than a factor of 1000, and no Sc or Tb could be detected using other, more intense, γ-rays, indicating decontamination factors of >20,000 for Sc and >1000 for Tb.

Research is continuing to further improve this method. A small fraction of the selenium, $\sim$1% accompanies the tin through the separation and can elevate the background around the tin peaks in some matrices. Therefore, efforts will be directed at selenium reduction. Other SRMs with lower tin concentrations, such as Bovine Liver (SRM 1577), will be analyzed to evaluate the suitability of this procedure to provide certification quality data for new SRMs.

---

1. Schwarz, K., Milne, D. B., and Vinyard, E., *Biochem. Biophys. Res. Commun., 40,* 22 (1970).
2. Schroeder, H. A., *Environment 13*, 18 (1971).
3. Gladney, E. S., "Compilation of Elemental Concentration Data for NBS Biological and Environmental Standard Reference Materials," *Los Alamos Informal Report LA-8438-MS* (1980).

3. Contributions for Analytical Programs

a. Multielement Analysis of Human Liver Samples

R. Zeisler, S. Harrison, K. Fitzpatrick

The Pilot Environmental Specimen Bank has completed its second year of operation. One of the highlights of this year's accomplishments has been the elemental analysis of 36 of the 300 human liver samples collected. A comprehensive analytical protocol was developed which includes the determination of most of the first-priority elements proposed by the 1978 International Workshop on Monitoring Environmental Materials and Specimen Banking (1). Other elements regarded as possible pollutants have been added to the protocol, as well as biological major elements and trace elements, which can provide information about the "normal" state of the specimen. The analytical protocol includes about 40 elements, which are determined by the following methods: atomic absorption spectrometry (AAS), isotope dilution mass spectrometry (IDMS), neutron activation analysis (NAA), and voltammetry (VOLT). The specific elements determined and the analytical techniques employed for each measurement are summarized in figure 1.

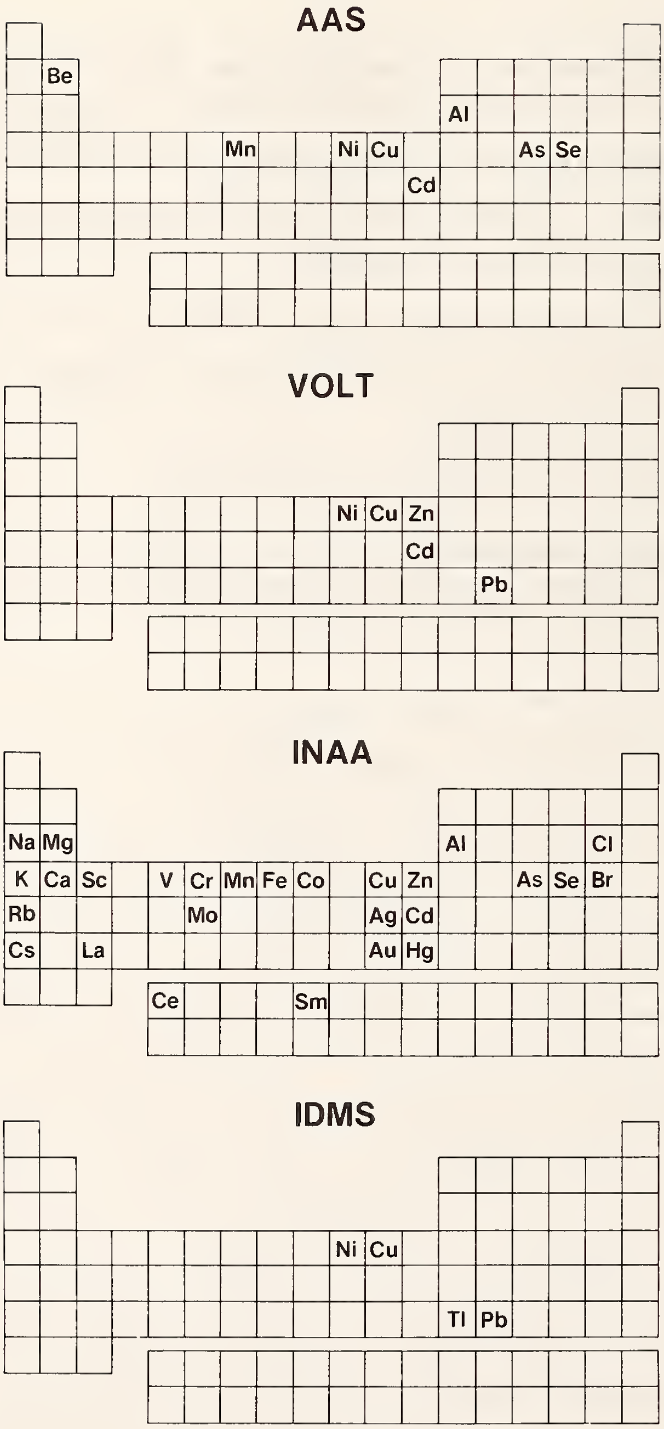

Figure 1. The comprehensive analytical protocol for human livers uses four analytical techniques.

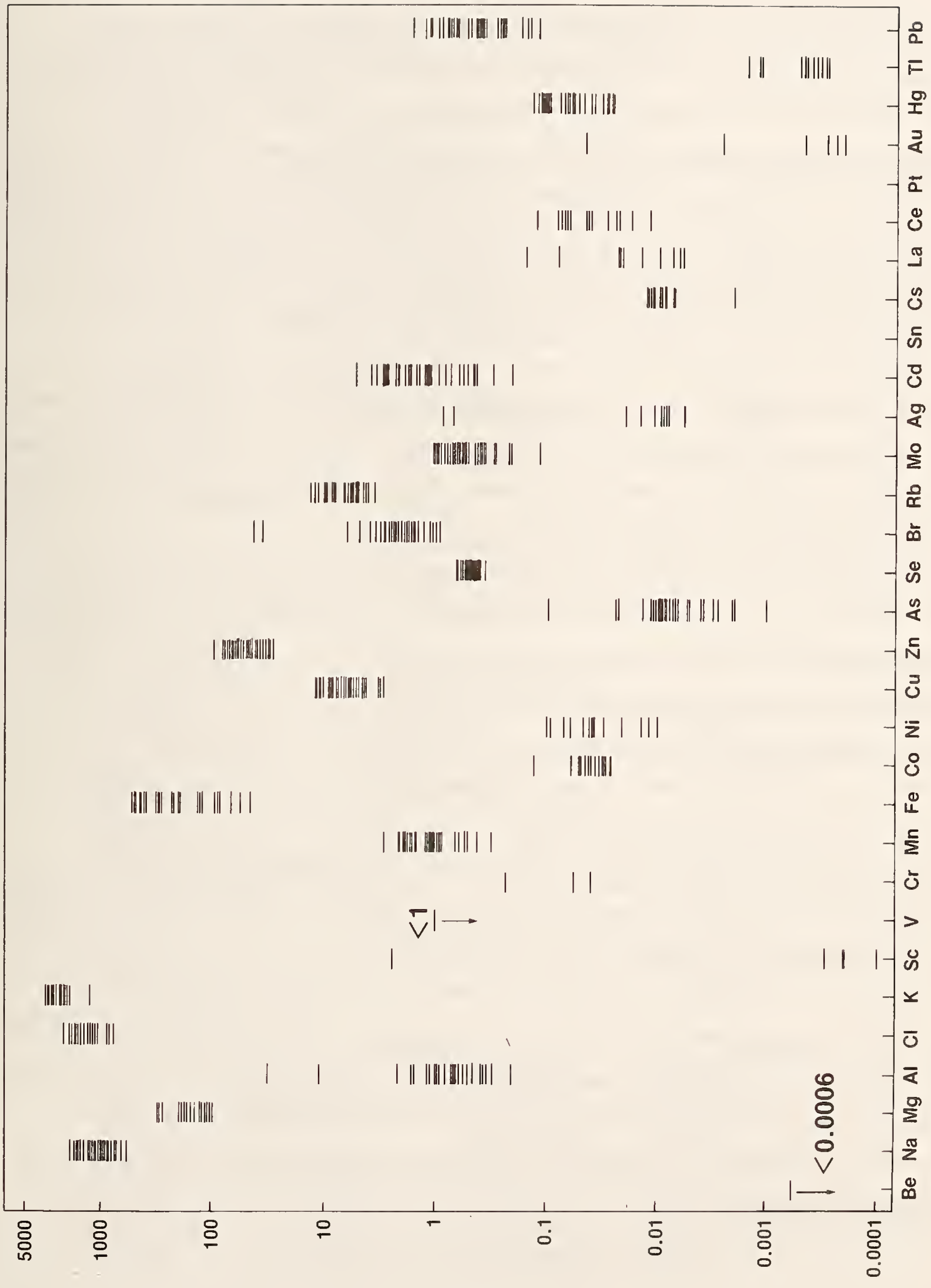

Figure 2. Element concentration (μg/g fresh weight) of 36 liver specimens.

As applied, the analytical protocol is a part of the specimen bank goal of producing a validated and documented chemical measurement system, other parts of which are the sample collection protocol and storage system previously reported. Aspects of the analytical protocol which satisfy these criteria include the relation of the analytical test portion to bulk sample, parallel determinations of Standard Reference Materials, determination of several elements by more than one technique, and the use of high precision, high accuracy techniques, e.g., IDMS.

The data for the 36 liver samples is graphically represented in figure 2. Remarkable is the very narrow spread of some essential trace elements, especially selemium. These results will contribute significantly to the existing trace element data base for human livers for the purpose of biomonitoring and specimen banking.

Nuclear methods other than INAA have been used this year on a select number of liver samples for procedure development and evaluation. A radiochemical procedure (described in section 2a) determines Au and Pt, elements occurring at very low concentrations and of significant medical and environmental interest. In conjunction with workers from the University of Maryland, prompt gamma activation analysis (PGAA) was used to determine H, B, C, N, Na, P, S, Cl, K and Cd in several samples including a homogeneity study. In the homogeneity study, the results of the ten subsamples analyzed by PGAA agreed very well with those of the eight subsamples analyzed by INAA.

Preliminary analyses by INAA of mussel (Mytilus edulis) samples were made this year as part of the development of an analytical protocol for the aquatic accumulator specimen type. The dry weight trace element with the exception of substantially higher concentrations for the lithophilic elements, as would be expected from the sea water and sand fractions in mussels.

b. Determination of Halogens in Organic Liquids by Neutron Activation Analysis

R. Fleming

Significant progress has been made during the past year on the measurement of halogen concentrations in organic liquids.

- We have demonstrated the reliable and accurate, simultaneous determination of chlorine and bromine in a variety of lubricating oils as part of the ASTM/NBS basestock consistency study under the Recycled Oil Program.
- Analysis of total chlorine homogeneity in oils doped with polychlorinated biphenyls has been carried out in the development of the PCB SRM-1581.
- Analysis of the bromine content of deuterated styrene monomer samples to be used in small-angle neutron scattering measurements has been carried out.
- In collaboration with the Tribochemistry Group (561) measurements have been made of the chlorine and bromine contents of the saturated, polar and aromatic fractions resulting from the ASTM D2007 clay-gel separation of various lubricating oils.

Organic liquids provide nearly ideal matrices for neutron activation analysis since carbon, nitrogen, hydrogen, and oxygen produce no countable radioactivity. Each of the halogens, on the other hand, produces an activation product with its own unique half life and gamma ray energy signal, as shown below.

Neutron Activation Products for the Halogens

Element	(Hit) Product	Halflife	Gamma-ray Energies, keV
Fluorine	^{20}F	11.0 sec	1633.8
Chlorine	^{38}Cl	37.2 min	1642.2, 2167.6
Bromine	^{82}Br	35.3 hr	554.3, 776.5, 1044.1
Iodine	^{128}I	25.0 min	442.9

The short halflife of F-20 dictates accurate timing ability and for that reason we have not exploited fluorine analysis routinely. On the other hand, since the fluorine activity will decay away rapidly, its presence at any level does not degrade the measurement of the other halogens. Conversely, because it has the longest halflife, large amounts of bromine will reduce the sensitivity for the other halogens, while bromine can be measured in the presence of any amount of them. In effect, the different halflives accomplish an automatic and complete chemical separation of fluorine, bromine, and the other two halogens. Of course, since modern gamma-ray spectrometry systems have energy resolution of better than 2keV (FWHM), the lines used for quantification are totally resolved.

The dynamic range of the measurements can be from ppb levels to 100%. The measurement reliability demonstrated in the basestock consistency work is $\pm 3\%$ (2σ) relative uncertainty over a twelve month period. Since the technique is non-destructive, the sample can be available after analysis for further measurement by this or other methods. Since the technique is matrix-independent, not depending on chemical species or on physical properties such as viscosity, density, opacity, etc., it is well-suited for the fractionation work. In summary, the increasing need for accurate, sensitive, unambiguous analysis of each of the halogens in organic liquids has prompted the development of activation analysis techniques optimized for this problem.

c. Multielement Determination in Two New Silicious Rock Standards

M. J. Blackman

The analysis of two new silicious rock standards: obsidian (SRM 278) and basalt (SRM 688) by instrumental neutron activation analysis was completed and submitted to OSRM for certification. The elemental concentrations determined are presented in table 1.

Table 1: Elemental Concentrations in Silicious Rock SRMs
(concentrations in mglg, except where noted)

Element	Obsidian SRM 278	Basalt SRM 688
Sc	5.11 ± 0.04	38.1 ± 0.3
Fe%	1.41 ± 0.02	7.24 ± 0.03
Co	1.48 ± 0.03	49.7 ± 0.2
Rb	134 ± 4	n.d.*
Cs	5.50 ± 0.19	n.d.*
Ce	62.2 ± 0.5	13.3 ± 0.7
Eu	0.838 ± 0.024	1.07 ± 0.07
Yb	4.45 ± 0.11	2.09 ± 0.13
Lu	0.725 ± 0.021	0.340 ± 0.014
Hf	8.38 ± 0.13	1.60 ± 0.12
Ta	1.21 ± 0.06	n.d.*
Th	12.49 ± 0.15	n.d.*
Sb	1.45 ± 0.08	n.d.*
Cr	6.1 ± 1.0	332 ± 5
Zn	55 ± 8	58 ± 7
Tb	0.99 ± .10	0.45 ± 0.04

*n.d. = not detected

4. Survey Analysis of Impurities in Silica Glass

R. Lindstrom

Eight samples of fused silica were analyzed by instrumental neutron activation in a search for impurities that would impair the use of the material as a high-temperature electrical insulator. Short-lived activation products were measured after a 5-minute irradiation in the RT4 pneumatic tube and long-lived products after 6 hours in RT3. Several NBS Standard Reference Materials were irradiated and counted under the same conditions as elemental standards, and Hereaus AN grade quartz was used as a blank for aluminum interference by the $^{28}Si(n,p)^{28}Al$ reaction.

The results in table 1 show the concentrations of 28 trace elements in the quartz samples analyzed. The data may be used as an indication of the sensitivity of instrumental neutron activation for the measurement of these elements (in such trouble-free matrices as quartz) with irradiation and counting procedures in common use today at the NBSR.

Table 1. Trace elements in silica glass.

Element	Isotope Used	A	B	C	D	E	F	G	H	Blank 1	Blank 2
Na	Na-24	3.0 ±.1	1.1 ±.1	0.7 ±.2	0.58 ±.03	2.2 ±.1	4.8 ±.2	1.9 ±.1	9.3 ±.4	0.11 ±.01	0.11 ±.01
Mg	Mg-27	<12	<5	<3	<3	<7	<6	<9	<5	--	<3
Al	Al-27	21 ±1	21 ±1	20 ±1	18 ±1	21 ±1	22 ±1	22 ±1	40 ±1	--	0 ±.5
K	K-42	4.0 ±.2	2.4 ±.2	1.5 ±.3	0.7 ±.1	2.0 ±.1	2.4 ±.5	2.0 ±.4	<2	<0.2	<0.2
Ca	Ca-40	<7	<3	<3	<2	<4	<1	<7	6 ± 1	<40	<2
Sc	Sc-46	<7E-4	<8E-4	(4±1)E-4	<3E-4	<4E-4	<.002	<.001	<.002	<4E-4	<3E-4
Ti	Ti-51	<3	<2	<2	<2	<2	<2	<3	<2	--	<1
V	V-52	<.02	<.01	<.01	<.01	<.01	<.02	<.02	<.01	--	<.007
Cr	Cr-51	0.07 ±.02	<.07	0.14 ±.02	<.04	0.19 ±.02	<0.1	<0.1	0.18 ±.03	<.03	<.01
Mn	Mn-56	0.32 ±.05	0.16 ±.01	0.028 ±.002	0.022 ±.003	0.17 ±.01	0.031 ±.003	0.17 ±.01	0.076 ±.006	--	<.01
Fe	Fe-59	<8	<10	<2	<4	<5	<20	<20	<20	<4	<2
Co	Co-60	<.06	<.02	0.006 ±.001	<.01	<.01	<.04	<.04	<.03	<.008	<.003

Table 1. (Cont'd)

Cu	Cu-66	<1	<0.6	<0.6	<0.6	<0.8	<1	<1	<0.8	<1.5	<0.2
Zn	Zn-65	<1	<1	0.5 ±.2	<0.4	<0.6	<3	<2	<3	<0.5	<0.2
As	As-76	<.002	<.001	(4±1) E-4	<.001	<5E-4	<.003	<.002	0.021 ±.002	<5E-4	<3E-4
Br	Br-82	<.003	<.002	<5E-4	<.002	0.0014 ±.0003	<.004	<.004	0.007 ±.002	<7E-4	<3E-4
Sb	Sb-122	0.0024 ±.0002	0.0011 ±.0002	0.0014 ±.0001	0.0007 ±.0002	0.0010 ±.0001	<.002	<.001	0.043 ±.001	<3E-4	<2E-4
Cs	Cs-134	<.02	<.02	<.003	<.006	<.007	<.03	<.02	<.03	<.006	<.003
Ba	Ba-131	<1	<1	<0.2	0.7 ±.3	0.7 ±.3	<2	<2	<2	<0.4	<0.2
La	La-140	0.15 ±.01	0.043 ±.002	0.056 ±.003	0.040 ±.003	0.038 ±.001	0.053 ±.003	0.12 ±.01	0.0021 ±.0004	<8E-4	(9±1) E-4
Ce	Ce-141	0.46 ±.03	0.17 ±.02	0.25 ±.01	0.23 ±.02	0.22 ±.02	0.27 ±.03	0.49 ±.04	<.05	<.02	<.006
Sm	Sm-153	0.072 ±.003	0.031 ±.001	0.043 ±.002	0.054 ±.001	0.044 ±.001	0.057 ±.001	0.086 ±.001	(2.9±0.4) E-4	<4E-5	(2.2±0.5) E-5
Eu	Eu-152m	0.005 ±.002	0.002 ±.001	0.004 ±.002	0.002 ±.001	0.002 ±.001	<.002	0.004 ±.002	<.002	<2E-4	<2E-4

Hf	Hf-181	0.14 ±.02	0.14 ±.02	0.18 ±.02	0.11 ±.03	0.15 ±.04	0.20 ±.05	0.14 ±.02	<.01	<.004	<.002
W	W-187	0.033 ±.002	0.018 ±.002	0.023 ±.001	<.002	<7E-4	<.004	<.004	<.004	<.003	0.0053 ±.0005
Au	Au-198	(2±1) E-5	<3E-6	(3±1) E-5	<2E-6	(2±6) E-5	(1±4) E-5	(2±6) E-5	<6E-6	<1E-6	<7E-7
Th	Pa-233	0.12 ±.01	0.06 ±.01	0.10 ±.01	0.066 ±.003	0.074 ±.005	0.064 ±.005	0.11 ±.01	<.01	<.002	<.001
U	Np-239	0.12 ±.01	0.10 ±.01	0.13 ±.01	0.22 ±.01	0.23 ±.01	0.17 ±.01	0.36 ±.02	<.003	<7E-4	<3E-4

Concentrations are given in μg/g. Uncertainties are the standard deviation computed from counting statistics and from uncertainties in the concentration of the standards.

5. Facilities

a. Neutron Depth Profiling at the NBS Reactor

R. Fleming

Construction work has begun on a neutron depth profiling facility at the BT-3 beam tube. When completed, this analytical tool will make possible the near-surface measurement of concentration distributions of He-3, Li-6, and B-10 as well as the investigation of its application to other elements. A parallel development of an off-line profiling facility for bismuth using in-core irradiation is also underway.

A key component for obtaining an intense, high-quality thermal neutron beam is a good lowpass neutron filter. Therefore, the integrated neutron transmission of room temperature, single crystals of silicon, bismuth, lead and sapphire were measured. As suggested by Nieman, et. al. (1) the sapphire crystals provide the best attenuation of fast neutrons and gamma rays for a given thermal neutron transmission.

The neutron beam is scheduled to be opened early in FY 82. At that time, calibration and characterization of the facility will begin.

b. Facility Enhancements

R. Lindstrom

The primary data acquisition and processing system for the group is a Nuclear Data ND 6620. Data acquisition has become more distributed with the connection of a recent ND66 MCA (belonging to the Smithsonian Institution and the Health Physics Group) and a second ND100 MCA to the system. The ND66 will eventually support four detectors, and the ND100 one in room C003 adjacent to the rabbit receivers. A second 9-track magnetic tape drive has been added. A mofrm hsd been installed to allow remote (off-site) control of all data acquisition and processing via a portable terminal with an acoustic coupler to the commercial telephone network.

---

1. H. F. Nieman, D.C. Tennant and G. Dolling, "Single Crystal Filters for Neutron Spectrometry", *Rev. Sci. Instruments 51,* 1299 (1980).

PRECISION GAMMA-RAY AND X-RAY WAVELENGTHS

E. G. Kessler, Jr., R. D. Deslattes, D. Girard, and W. C. Sauder
(Center for Absolute Physical Quantities)

Gamma- and x-ray wavelengths are measured using crystal diffraction spectrometers. All wavelengths reported to date have been measured with double flat crystal transmission spectrometers equipped with crystals whose lattice spacing has been measured by x-ray/optical interferometry. Diffraction angles are measured interferometrically with a precision of 0.5×10^{-3} sec. A complete description of the instrumentation, measurement procedures, and results published over the past three years is available in reference 1.

A measurement of the wavelength of the electron-positron annihilation radiation[2] (511 keV) which has been promised for a number of years has still not been completed. This is due to the low priority we have assigned this measurement and to problems with the positron source. The proposed positron emitter is Cu-64 and thin sheets of Au plated Cu-64 have been irradiated in aluminum cans filled with D_2O in order to determine the extent of Cu contamination of the D_2O. In a previous irradiation, extensive Cu contamination of the irradiation thimble water occurred.

A Mo-99 sample was obtained in order to measure the wavelength of the 40.6 keV line. This line was used as a calibration line in a recent accurate pion mass determination.[3] The Mo-99 source has a half life of 67 hours and only 2% of the decays produce the 40 keV transition. In addition the low energy of the gamma-ray leads to strong self-absorption in a thick Mo-99 source. Count rates less than 1 per second were achieved. The uncertainty in the measured energy ($E = 40583.47$ eV $\pm$ 4.2 ppm) resulted almost entirely from the counting statistics. The pion mass determination consisted of energy measurements of pionic x-rays from π-P and π-Ti using a bent crystal spectrometer calibrated with the Mo-99 40.6 keV line. The measured value for the pion mass ($m_{\pi^-} = 139567.5 \pm 0.9$ keV) is the most accurate value ever reported.

The gamma-ray sources we have used so far have been long lived sources which were extracted from the NBS reactor for measurement. In order to make high energy measurements (> 2 MeV), it is necessary to use capture gamma-ray sources because of the low efficiency of our spectrometer. We have submitted an instrument proposal to Institute Laue-Langevin (ILL) which requests permission to place a flat crystal spectrometer in front of their 24m bent crystal spectrometer. Our spectrometer will be movable so that both instruments may be used, but not simultaneously. This instrument proposal has been accepted by ILL. The interest in more accurate high energy gamma-ray wavelengths is for detector calibration, as standards for relative measurements, and as possible input to the fundamental constants through a wavelength-mass product.

An extensive number of high Z K x-rays produced at the 4 MeV electron Van de Graaff have been measured during the past year. Measurements have been made on $K\alpha_1$, $K\alpha_2$, $K\beta_1$, and $K\beta_3$ for Ag, Xe, Ba, Nd, Sm, Er, Au, Pb, Th, and U. Comparison of the measured wavelengths with accurate self-consistent field calculations[4,5] provides a test of the theoretical calculations. In an earlier publication[6] using the then best available data, a discrepancy between theory and experiment which was linear in Z was noted. Preliminary analysis of our more extensive data shows a plateau in the discrepancy around Z=60 and a significant decrease in the discrepancy around Z=90. Measurements on Xe are important because it is the only gaseous target which was used. The Xe measurements appear to be consistent with those on the solid targets.

A measurement of the erbium K edge has recently been published. This measurement provided the energy calibration for kaonic potassium x-rays which were measured using the critical absorption technique by Lum and Wiegand of Lawrence Berkeley Laboratory. By comparing the measured and theoretical values for the kaonic x-ray transitions, a value for the kaon mass was deduced. Although the measured mass value ($m_K = 493.640 \pm 0.054$ MeV/c^2) is less accurate than a previous determination, it provides a valuable check because an entirely different experimental technique was employed.[7]

The efficiency of the flat crystal spectrometers is a few x 10^{-11}. Thus only intense gamma- and x-ray transitions can be measured. In order to have the facility measure weaker lines we are upgrading a bent crystal spectrometer we have been given by the University of Colorado.[8] The spectrometer will employ Dumond geometry, have a 4m radius crystal, and an angle interferometer. This instrument will first be used to measure weak x-ray lines such as hypersatellite lines.

---

1. R. D. Deslattes, E. G. Kessler, Jr., W. C. Sauder, and A. Henins, *Annals of Phys.* 129, 378 (1980).
2. W. C. Sauder and R. D. Deslattes, *Jour. Res. NBS* 71A, 347 (1967).
3. D. C. Lu, L. Delker, G. Dugan, C. S. Wu, A. J. Caffrey, Y. T. Cheng, and Y. K. Lee, *Phys. Rev. Lett.* 45, 1066 (1980).
4. K. N. Huang, M. Aoyagi, M. H. Chen, B. Crasemann, and H. Mark, *At. Data Nucl. Data Tables* 18, 243 (1976).
5. J. P. Desclaux (private communication).
6. R. D. Deslattes, E. G. Kessler, Jr., L. Jacobs, and W. Schwitz, *Phys. Lett.* 71A, 411 (1979).
7. G. K. Lum, C. E. Wiegand, E. G. Kessler, Jr., R. D. Deslattes, L. Jacobs, W. Schwitz, and R. Seki, *Phys. Rev. D* 23, 2522 (1981).
8. J. H. Jett, N. S. P. King, D. A. Lind, and P. Henneng, *Nucl. Instr. and Meth.* 114, 301 (1974).

NEUTRON DOSIMETRY FOR REACTOR PRESSURE VESSELS

E. D. McGarry
(Nuclear Radiation Division)

Steel embrittlement due to neutron irraditation in reactor pressure vessels has become an issue of growing concern as many commercial reactors move into their second and third decades of service. An interlaboratory program involving the Hanford Engineering Development Laboratory (HEDL), the Study Center for Nuclear Energy (CEN/SCK at Mol, Belgium), and the NBS has addressed the problem of establishing accurate methods for the neutron dosimetry measurements in the pressure vessel surveillance programs. A reactor pressure vessel (RPV) simulator at the Oak Ridge Pool Critical Assembly (PCA) served as the common irradiation test field for a blind round-robin test of dosimetric measurement methods. The radiometric analysis techniques at HEDL and CEN/SCK have been validated by calibrations against NBS standard gamma sources, neutron fluence standards, and certified fission standards. The latter are certified with respect to fissions in fissionable deposits of known mass with an NBS fission chamber operated at either the CFRMF reactor in Idaho or in the thermal column of the NBS reactor. CEN/SCK performs the radioactivity measurements with a calibrated, transportable 3-in. x 3-in. NaI(Tl) gamma spectrometer system. For the ^{115}In(n,n') reaction, the measurements are "absolute"; for other reactions, they are referenced to benchmark field irradiations in the Mol Cavity, U-235 Fission Spectrum Neutron Field. The CEN/SCK system has been used to make the majority of radiometric measurements for the characterization program.

Table 1 provides an example of the results of a certified-flux irradiation of the 4.5-hour ^{115}In(n,n') reaction at the Cf-252 Fission Neutron Spectrum Facility at NBS. The results were used to validate radiometric measurements of the 4/12 SSC PCA-RPV configuration in November 1980. These measurements were made only by CEN/SCK personnel using the portable NaI(Tl) system. The expression for the flux, as derived from the source strength and a distance measurement, is given near the center of the table. The

Table 1. Compensated beam geometry, certified-fluence irradiation to activate 4.5-hour ^{115}In(n,n') for calibration check of the CEN/SCK NaI(Tl) gamma spectrometer for radiometric-sensor measurements in the LWR-PCA-PV mockup in November 1980.

Results of Certified Flux Radiation:

Sensors: 10-mil thick indium foils (99.999%) ID #1 & #10

Start of Irradiation: Friday, 21 Nov. 1980 at 18:05:00 EST

End of Irradiation: Sunday, 23 Nov. 1980 at 12:20:00 EST

Length of Irradiation: T = 152100 s

Fraction of Saturation: $(1-e^{-\lambda \Delta T}) = 0.9985$

Neutron Source: NBS Cf-252 Source #NS-100

Source Strength: (22 Nov. 1980) $S = 3.837 \times 10^9$ n/s ± 1.4%

Foil-to-Foil Distance: $d = 6.198 \pm 0.041$ cm

Cf-252 Flux Averaged over Foils:

$$\phi = \frac{S}{\pi d^2} \left[\frac{r^2}{p^2} \cdot \mathrm{In} \left(1 + \frac{p^2}{r^2} \right) \right] \quad \& \quad \begin{array}{l} r = d/2 \\ p = 0.635 \text{ cm} \end{array}$$

$$\phi = (3.179 \times 10^7)(0.9796) = 3.11 \times 10^7 \text{ n/cm}^2\cdot\text{s} \pm 1.9\%$$

Corrections for Scattering: The indium reaction rate will require an adjustment to account for scattering of neutrons in the source encapsulation and holding structures. It is estimated, by calculation, that because of this scattering the 4.5-hour indium activity will be 0.6% ± 0.8% too large.

Results of Radioactive Foil Analyses:

Foil Weights: ID #1 = 0.2272 g

ID #10 = 0.2270 g

U-235 Equivalent Flux: $7.30 \times 10^6/0.2271 = 3.21 \times 10^7$ n/cm$^2\cdot$s ± 2%

Conversion Factor to Cf-252 Flux: 1.05

Observed Cf-252 Flux: $3.21 \times 10^7/1.05 = 3.06 \times 10^7$ n/cm$^2\cdot$s

Table 2. Summary of Cf-252 standard neutron field irradiations in the period 1979 to 1980 to benchmark reference neutron characterization measurements of the PCA-RPV mockup facility.

		^{235}U Fission Equivalent Fluxes		
Date	Foil ID	HEDL(a)	Mol(b)	NBS(c)
		^{115}In(n,n')^{115m}In Reaction		
9/21/79	4	2.031×10^7	2.028×10^7	$2.02 \times 10^7 \pm 2.2\%$
9/21/79	5	2.027×10^7	2.027×10^7	$2.02 \times 10^7 \pm 2.2\%$
9/21/79	6	2.062×10^7	2.060×10^7	$2.05 \times 10^7 \pm 2.2\%$
9/21/79	7	2.044×10^7	2.061×10^7	$2.05 \times 10^7 \pm 2.2\%$
11/23/80	1	N/A	3.21×10^7	$3.27 \times 10^7 \pm 2.4\%$
11/23/80	10	N/A	3.21×10^7	$3.27 \times 10^7 \pm 2.4\%$
		^{58}Ni(n,p)^{58}Co Reaction		
9/21/79	BR	2.033×10^7	2.033×10^7	$2.01 \times 10^7 \pm 2.5\%$
9/21/79	BP	1.994×10^7	2.011×10^7	$2.01 \times 10^7 \pm 2.5\%$

(a) Derived from HEDL-measured absolute reaction rates per nucleus and evaluated average uranium-235 fission spectrum cross sections of 189 mb for indium, 108.5 mb for nickel and 0.705 mb for aluminum.

(b) Derived from benchmark-field calibration at Mol U-235 Fission Spectrum; absolute reaction rates also obtained for indium and nickel.

(c) NBS values are based upon compensated-geometry irradiations and, therefore, are derived from a source strength S-252, the average counting rate of a pair of foils and the distance d between them:

$$\phi_{eq} = \frac{\bar{\sigma}^{252}}{\bar{\sigma}^{235}} \; \frac{S^{252}}{d^2} \left[\frac{r^2}{p^2} \cdot \ln \left(1 + \frac{p^2}{r^2} \right) \right]$$

where: $r = d/2$

p = foil radius

For the ^{115}In(n,n')^{115m}In reaction, $\bar{\sigma}^{252}_{In} / \bar{\sigma}^{235}_{In}$ = 1.05 % 0.03

For the ^{58}Ni(n,p)^{58}Co reaction, $\bar{\sigma}^{252}_{Ni} / \bar{\sigma}^{235}_{Ni}$ = 118 mb/108.5 mb

Table 3. Summary of other U-235 standard neutron field irradiations in the period 1978 to 1980 to benchmark reference PCA dosimetry.

		^{235}U Fission Equivalent Fluxes		
Date	Foil Id	HEDL(a)	Mol(b)	NBS(c)
		^{115}In(n,n')^{115m}In Reaction		
11/9/78	2	N/A	1.89×10^{10}	$1.87 \times 10^{10} \pm 2.4\%$(c)
	3	N/A	1.89×10^{10}	$1.86 \times 10^{10} \pm 2.4\%$
	4	N/A	1.87×10^{10}	$1.86 \times 10^{10} \pm 2.4\%$
11/17/78	N7(A)(d)	1.94×10^{10}	1.88×10^{10}	$1.92 \times 10^{10} \pm 2.7\%$
	N8(B)	1.86×10^{10}	1.88×10^{10}	$1.93 \times 10^{10} \pm 2.7\%$
		^{27}Al(n,α)^{24}Na Reaction		
11/17/78	M1	1.91×10^{10}(d)	1.88×10^{10}	$1.90 \times 10^{10} \pm 3.5\%$(e)
		^{58}Ni(n,p)^{58}Co Reaction		
Spring 1979	CD	1.97×10^{10}(f)	1.95×10^{10}(f)	$2.00 \times 10^{10} \pm 3.5\%$

(a)(b) See footnotes (a) and (b) Table 2.

(c) All fluxes reported here have been reduced by 2.0 ± 1.5% to account for excess ^{115m}In (4.5-hour) activity caused by scattering within the NBS U-235 Cavity Fission Source.

(d) This set is slightly suspect because of questions about the actual indium foils sent, as indicated by the foil ID in brackets.

(e) No adjustment for scattering in the cavity fission source were made to the NBS-reported flux. It is believed that in-scattering effects are balanced by inelastic scattering removal in the 40-mil thick aluminum foil.

(f) Values of foil disintegration rates reported by HEDL and Mol, respectively, were 8257 dps ± 1.8% and 8164 dps ± 1.7%, on January 29, 1979, 10 a.m. (Mol time). A second group from Mol reported 8373 dps ± 1.8%. Fluxes were derived on the basis of $\bar{\sigma}_{Ni}^{235}$ = 108.5 mb.

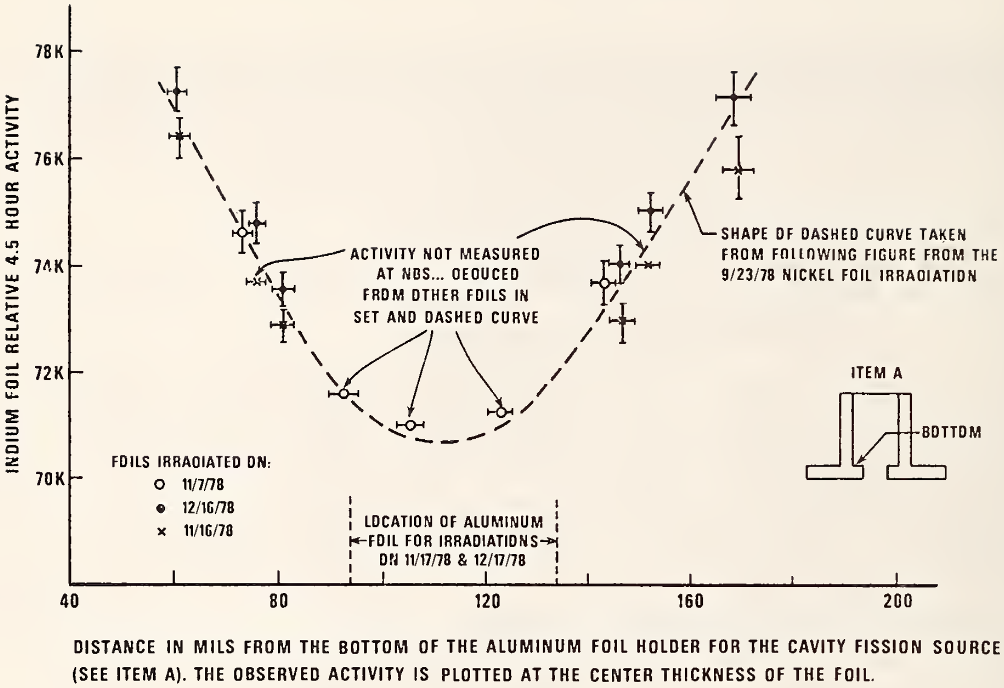

Figure 1. Comparison of results of indium foil irradiated in three different cavity fission source certified fluence runs.

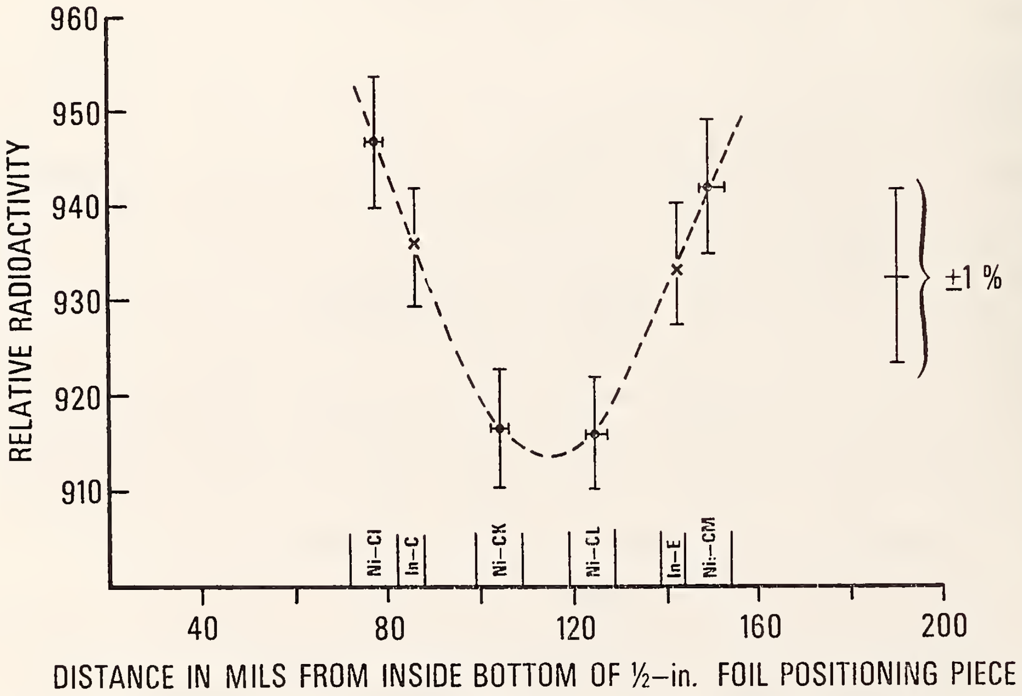

Figure 2. U-235 cavity fission irradiation of nickel foils CJ, CK, CL, and CM. (Irradiation time: 112380 s, 9/23/81, 21:37:00 EST).

expression enclosed in square brackets is an adjustment for the fact that the foil, of radius p, is a disk and not all points on its surface lie on a sphere of radius r.

Table 2 and 3 are summaries of similar types of irradiations, some in the Cf-252 and others in the U-235 standard neutron fields at NBS. Certain significant aspects of these tables should be recognized. First, at least one type of dosimeter, namely the ^{115}In(n,n')^{115m}In reaction, was measured in every period of significance, as defined by the run-to-run monitoring activities reported earlier. Second, for all reactions checked: ^{115}In(n,n')^{115m}In, ^{58}Ni(n,p)^{58}Co, and ^{27}Al(n,α)^{24}Na agreement is good to excellent, to within 2.5%, over the three-year period. In some cases, however, this agreement is not overly significant because the Mol and HEDL fluxes are derived from reported reaction rates; and agreement with the NBS-reported flux depends upon the exact spectrum-averaged cross section used. The details are given in the footnotes of Table 2 and 3.

As opposed to the derivation of fluxes from spontaneously fissionable point sources such as Cf-252, those obtained from thermal-neutron driven U-235 sources require considerable more effort to certify. Some explanation of techniques and reproducibility of results is afforded by Figures 1 and 2. One problem area, identified by the larger uncertainty of $\pm$ 3.5% on the ^{27}(n,α)^{24}Na irradiation, resulted from the larger thickness of the aluminum foil (40 mil compared to routinely used 5 to 10 mil thicknesses). Consequently, estimating the true flux within the foil volume is more of a problem.

OBSERVATION OF FIELD PARAMETERS FOR THE INTERMEDIATE-ENERGY STANDARD NEUTRON FIELD (ISNF)

R. Dallatore, C. Eisenhauer, D. Gilliam, J. Grundl,
G. Lamaze, and E. D. McGarry
(Nuclear Radiation Division)

Currently the ISNF is receiving increased interest as a dosimetry standard field in several areas of application from cross-section adjustment studies for fast reactor applications, to damage evaluations in light-water reactor pressure vessels, which is the subject of an ongoing program at ORNL being sponsored by the Electric Power Research Institute.

In the past year two ISNF field parameters were subject to secondary experimental checks of limited accuracy in order to improve general confidence regarding design principles and primary neutron flux measurement methods.

1. Central neutron fluence based on neutron source strength of fission disk drivers

This flux determination is a direct and absolute check of the neutron transport calculations for ISNF but it is complicated and not amenable to high accuracy.

The measurement steps are as follows:

1. Relative neutron source strength of the eight driver disks (see Figure 1) -- relative gross gamma counting of irradiated fission disks.
2. Absolute number of fissions produced in a single disk during a monitored ISNF irradiation.

   a. Prepare U-235 fission activation counting standard in thermal column cavity irradiation. Establish number of fission produced in disk on basis of absolute fission chamber monitor in the cavity.

   b. Determine total fissions produced in a single disk during ISNF irradiation with a Pu-239 fission chamber operated in the central ISNF field.

   -- Counting of Ba-140 fission-product activity in disk relative

It is to be noted that the primary method for establishing the ISNF central flux is that of neutron flux transfer from the NBS Cf-232 fission neutron irradiation facility. The accuracy of that technique is close to ± 3%.

2. Experimental check of superposition principle applied to ISNF geometry

Spherical symetry in the ISNF system is an important property for a standard neutron field whose neutron spectrum is specified on the basis of neutron transport calculation and the physical and nuclear parameters of its constituents. The eight fission disks are placed at a fixed radius in the cavity -- see figure 1 -- but physically are only small sections of the complete shell source which is entered into the transport calculation. Because there is only radial dependence of material densities in the ISNF, angular position of sources must be indistinguishible for source neutrons which arrive at the center of the system. All paths from source to center remain the same if the source is rotated about the center. Thus each fission disk contributes to the central neutron flux according to its source strength alone, not to its position.

There are some minor departures from spherical symetry in the ISNF (instrument penetration for example). The extent to which these departures are negligible is not difficult to check in principle since the ISNF can be operated with a single fission source disk. A sensitive spectral index observed for a one-disk ISNF irradiation should be the same as for an eight-disk irradiation. The spectral index chosen for this test was $S_{U235/U238}$ and has the following characteristics in the INSF spectrum:

to the fission activation counting standard.

3. Integrated neutron source strength for monitored ISNF irradiation

$$\begin{matrix}\text{integrated number}\\ \text{of neutrons}\end{matrix} = \underset{\text{- step 2 -}}{\begin{bmatrix}\text{total fissions}\\ \text{in disk \#3}\end{bmatrix}} \times \underset{\text{- step 1 -}}{\left[\frac{\text{fission in all 8 disks}}{\text{fission in disk \#3}}\right]} \times \begin{bmatrix}\bar{\nu}\text{, total neutrons}\\ \text{per fission}\end{bmatrix}$$

The neutron transport calculations yield a central ISNF flux per source neutron. Applying this value to the observed integrated source strength gives the expected neutron fluence for a particular monitored irradiation.

$$\begin{bmatrix}\text{central ISNF}\\ \text{neutron flux}\end{bmatrix} = \overset{\begin{matrix}\text{source}\\ \text{neutrons}\end{matrix}}{\underset{\text{- step 3 -}}{\left[1.1\text{x}10^{15}\right]}} \times \underset{\text{calculation}}{\left[0.001385\ \frac{\text{central flux}}{\text{1 neutron/sec}}\right]}$$

$$= 1.5_2\text{x}10^{12}\ \text{neutrons/cm}^2$$

The monitor for this irradiation was a fission chamber operated with a 105 μg deposit of Pu-239 and 248 μg deposit of U-238. The ISNF spectrum-averaged cross section for Pu-239 from the transport calculation provides the necessary parameter to obtain an ISNF fluence from the observed fission/gm from the chamber

$$\begin{bmatrix}\text{central ISNF}\\ \text{neutron flux}\end{bmatrix} = \left[6.63\text{x}10^{9}\ \text{fis/gm}\right] \times \left[1.82\ \text{barns}\right] \times \frac{0.602}{239}$$

$$= 1.45\text{x}10^{12}\ \text{neutrons/cm}^2$$

The difference between the neutron fluence based on fission disk source strength to that obtained with a Pu-239 fission chamber is close to 5%. It is estimated that the accuracy of this involved experiment is no better than ± 5%.

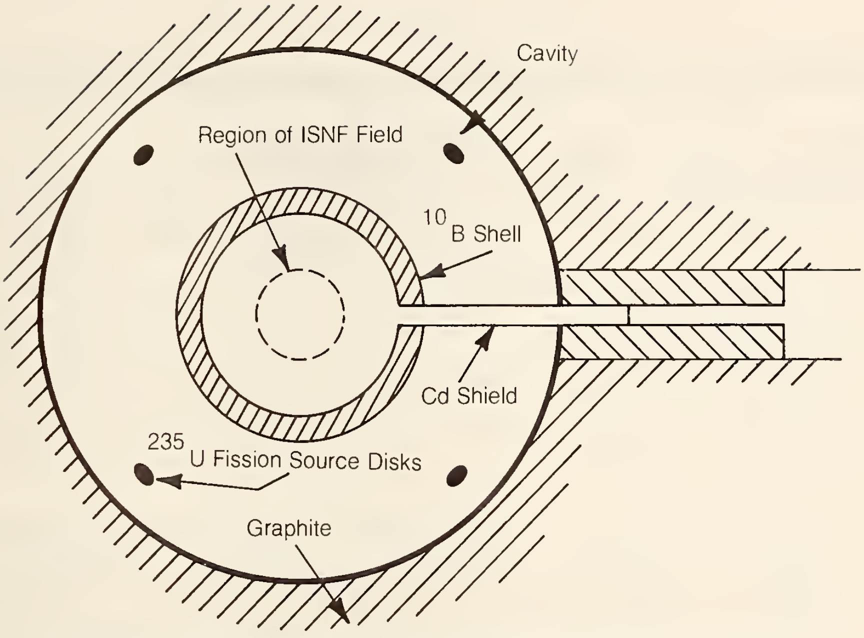

Figure 1. A schematic drawing of the ISNF spherical cavity.

	90% response range		
	E_{low}	E_{median}	E_{high}
ISNF spectrum:	8.3 keV	0.59 MeV	3.5 MeV
U235(n,f) response:	0.9	0.26	3.1
U238(n,f) response:	1400	2.3	5.9

The spectral index measurement was carried out with a double fission chamber and included chamber rotations and separate measurements of backgrounds with 1 disk and with eight disks. The final result obtained was:

$$\text{U235/U238 spectral index:} \quad \frac{\text{ISNF w/8 driver disks}}{\text{ISNF w/1 driver disk}} = 1.016 \pm 1\ 1/2\%$$

The accuracy for this result is dominated by the reactor background for the 1-disk run which was 12% and 21% for the U235 and U238 detectors, respectively. This is to be compared with normal reactor backgrounds for eight disk runs of 1.4% and 2.8% for those detectors.

FISSIONABLE DEPOSIT MASS ASSAY FOR ABSOLUTE FISSION RATES IN THE FFTF

D. M. Gilliam
(Nuclear Radiation Division)

One part of the Fast Flux Test Facility (FFTF) Reactor Characterization Program was a measurement of absolute fission rates of eight major fuel isotopes at two different positions within the reactor. The instruments employed in these tests were fission ionization chambers for which the absolute efficiency and fissionable deposit mass assay have been rigorously established.

Most of the fifteen fissionable deposits used in these tests were vacuum-evaporated fluoride deposits made by the CBNM laboratory at Geel. The U-238 deposits were oxide deposits prepared at Los Alamos National Laboratory; one Pu-239 deposit and the Pu-241 deposit were made at the Oak Ridge National Laboratory. Mass assay of these deposits was carried out by comparison to NBS reference deposits. Both alpha counting and fission counting comparisons (in both thermal neutron beams and fast neutron fields) were employed. The reference deposit mass assay was based on two or more independent methods wherever possible. Absolute alpha assay was employed in every case, and the isotope dilution mass spectrometry was used for U-235, U-238, Pu-239, and Pu-240. The deposit masses and estimated errors along with lists of isotopic impurities are given in table 1.

TABLE 1

FFTF-RCP ABSOLUTE FISSION CHAMBER REFERENCE FISSION FOILS

ISOTOPE	DEPOSIT ID	PRINCIPLE ISOTOPE MASS		BATCH IMPURITY COMPOSITION (ATOM PERCENT)	
Th-232	02N-9	621 μg	± 2 %	-	
Np-237	37K-05-1	68.3	± 1.1 %	-	
U-233	23K-02-8	30.71	± 1.5 %	U-232	<0.6. ppm
				U-233	99.76
				U-234	0.018
				U-235	0.009
				U-236	<1.0 ppm
				U-238	0.21
U-235	25A-03-1	30.96	± 0.77%	U-234	0.1822
	25A-03-2	30.91	± 0.77%	U-235	99.0829
				U-236	0.0353
				U-238	0.6996
U-238	28G-5-1	735.7	± 1.2 %	U-234	0.00016
				U-235	0.01755
				U-236	<0.00001
				U-238	99.9823
U-238	28NC-5-1	651.7	± 0.9 %	U-234	0.0054
				U-235	0.7194
				U-238	99.2752
Pu-239	49K-005-1	0.0983	± 0.8 %	Pu-238	<0.001
	49K-001-3F	1.788	± 0.6 %	Pu-239	99.978
	49K-0-3F	4.893	± 0.6 %	Pu-240	0.021
	49K-02-3F	25.33	± 0.5 %	Pu-241	0.0005
	49K-03-2F	35.10	± 0.5 %	Pu-242	0.0005
	49K-4-1	468.1	± 0.6 %	Pu-244	<0.0002
Pu-240	40L-2-3F	221.4	± 0.8 %	Pu-238	0.0109
				Pu-239	0.6727
				Pu-240	98.5191
				Pu-241	0.4289
				Pu-242	0.3679
				Pu-244	0.0006
				Am-241	0.17
Pu-241	41K-03-1(L)	8.71	± 2.5 %	Pu-238	0.001
		(10/13/80)		Pu-239	0.972
				Pu-240	0.255
				Pu-241	98.653
				Pu-242	0.118
				Pu-244	0.002
				Am-241	15.0

NEUTRON PERSONNEL DOSIMETER CALIBRATION AND TESTING

R. B. Schwartz
(Nuclear Radiation Division)

The reactor filtered beams, with energies of 2 keV, 24 keV, and 144 keV, together with the thermal column beam, were used for several important neutron dosimeter tests, as well as for the calibration of a Bonner sphere set.

In October 1980, a new neutron dosimeter, developed by the Israel Atomic Energy Commission, was tested at the three filtered beams. This dosimeter was designed to act as a simple neutron spectrometer so that, unlike all other dosimeters, it would not be necessary to know anything about the neutron spectrum in order to evaluate the reading. The NBS filtered beams comprised the only facility in the world where this important concept could be experimentally evaluated. The tests done at the reactor and at the NBS californium facility showed that the concept did, indeed, work. The results of these tests allowed the designers to "fine-tune" the design, so that in later field tests it gave quite accurate results. This dosimeter is now available commercially from an American company and is being considered for use at at least one reactor power station. Further tests will be done on the commercial version.

The filtered beams are also being used to help evaluate the possibilities of using dye dosimeters for personnel protection. Since these dosimeters are generally sensitive to gammas, the 144 keV beam was especially valuable since it has the highest ratio of neutron-to-gamma dose equivalent of any of the NBS neutron calibration facilities (∿ 100:1). This work is being done by both the NBS Radiation Physics Division and by a commercial company. The work is still in the preliminary stages, and the results so far have been rather inconclusive. Since the dyes offer the promise of high sensitivity and nearly tissue equivalent response, much more work will be done with these dosimeters.

NON-RRD PROGRAMS

Tests were also done at the filtered beams and with the thermal column beam, of the use of silicon diodes as dosimeters. In principle, the resistivity should change with dose, but the sensitivity turned out to be too low to be of practical use. No further tests of these particular devices are planned.

Routine calibrations of more conventional dosimeters were performed for several DOE laboratories, commercial companies, and one hospital, using the four reactor beams. In addition the Aberdeen Proving Ground Bonner sphere set was calibrated at thermal and with the 24 keV beam.

FLUX MEASUREMENT IN THE SMALL ANGLE NEUTRON SCATTERING FACILITY

G. Lamaze and D. Gilliam
(Nuclear Radiation Division)

On April 1, 1981, a flux measurement was made using an NBS double fission chamber containing a deposit of U-235 in one chamber and a deposit of Pu-239 in the other. The principal parameters and calculations are given below:

Mass of Pu-239 deposit (49I-1-4) = 104.4 μg: $N = 2.63 \times 10^{17}$ atoms (±0.4%)

Counting rate with extrapolation to zero and dead-time correction: R = 5956 c/sec (±0.3%)

Correction for self absorption of fission fragments: C1 = 1.0054 (±0.35%)

Correction for neutron scattering : $C2 = (1.054)^{-1}$ (±2.0%)

flux = R x C1 x C2/(N x Sigma)

flux = 2.16×10^{-14} (±2.1%)/Sigma

where Sigma is the spectrum averaged cross section in cm^2.

Mass of U-235 in deposit (25k - 1 - 2) = 132.2 μg: $N = 3.39 \times 10^{17}$ (±0.5%)

R = 6164 c/sec (±0.3%)

C1 = 1.0072 (±0.35%)

$C2 = (1.054)^{-1}$ (±2.0%)

Correction for Pt transmission loss: T = 1.066 (±0.7%)

flux = R x C1 x C2 x T/(N x Sigma)

flux = 1.85×10^{-14} (±2.2%)/Sigma

Sigma has been estimated by assuming a Maxwellian distribution with a temperature of 30 meV (∿ 75 °C) and a sharp cutoff at 5.3 meV (lambda = 3.93 Å). This yields the following values:

Sigma(Pu) = 2138 b

Sigma(U) = 1817 b

If there are transmission losses in the beam tube that are 1/v in nature, the spectrum shape will be changed resulting in a different value of Sigma. Assuming different values for the transmission at 3 meV, the following values were obtained:

Trans	Sigma(Pu)	Sigma(U)	flux (n/cm^2/sec)
100%	2138 b	1817 b	1.01×10^7 ($\pm$4%)
75%	2072 b	1760 b	1.05×10^7 ($\pm$4%)
50%	2009 b	1707 b	1.08×10^7 ($\pm$4%)

A flux measurement of the fine beam was also made and it was found to equal 16.0% of the principal beam. This value was in good agreement with a measurement of this beam made on March 4, 1981.

PREPARATION OF A CERTIFIED FISSION PRODUCT COUNTING STANDARD

D. M. Gilliam
(Center for Radiation Research)

Standards of this kind are comprised of foils of fissionable material which are activated by neutrons while an active fission chamber running simultaneously is employed to determine the number of fissions/per gram of fissionable material. These standards are provided to reactor dosimetry laboratories for calibration of radiometric fission product analysis systems.

In the present case, a natural uranium activation foil was irradiated in the well-thermalized neutron field of the NBSR thermal column cavity. Fission products were generated only by the U-235 component of the natural uranium foil, while the U-238 served only as a passive diluent.

Table 1 gives details of the calibration method and table 2 lists the irradiation parameters and the certified integrated fission count.

Table 1. Fission counting standard calibration.

Back-to-back Active Monitor Deposit: 2-5U-4-4-9

On 5.5 mil Pt backing, supplied by N. Dudey (formerly) of ANL.

Effective mass (including any contamination in the fission chamber):

96.6×10^{-9} g of U-235.
± 0.8%

Established by comparisons to both an enriched U-235 deposit and a normal uranium deposit. These independent comparisons were consistent within 0.3%.

Accumulated Monitor Counts: 8.594×10^{8} fissions

With corrections for (2.3 ± 0.8)% dead-time, 1.1% printing time (118 printing intervals), and (0.23 ± 0.2)% extrapolation to zero pulse height.

Monitor fissions/g = 8.896×10^{15}
± 1.14%

Foil-Backing Self-Shielding Correction:

$(\text{Fiss/g})_{\text{act. foil}}/(\text{Fiss/g})_{\text{monitor dep}} = 0.9966 \pm .2\%$

Ref: ILRR 9th Prog. Rept. p. NBS-24.

U-235 Mass of Activation Foil: 471.5 ± 3 mg total U x .007104 wt%U-5

→ 3.349 g U-5 in the activation foil.

± 0.81%

Integrated Fission Count for the Activation Foil:

$(8.896 \times 10^{15}\text{fiss/g} \pm 1.14\%) \times (3.349\text{ mg} \pm 0.81\%) \times (0.9966 \pm 0.2\%)$

$= 2.970 \times 10^{13}$ fissions

± 1.4%

Table 2. Results.

Irradiation Start (1/2 power): 18:58:59 EDT 12-22-80

Irradiation Finish (1/2 power): 15:03:51 EDT 12-23-80

Irradiation Length: 72,392 ± 15 sec

Start-up Time: ∿ 40 sec.

Shut-down Time: ∿ 35 sec.

Power Variation: ± 0.8%

Integrated Fission Count: $\boxed{2.970 \times 10^{13} \text{ fissions} \pm 1.4\%}$

Foil Composition: Nat. Uranium Metal Foil

Foil Mass: 471.5 ± 3 mg

Foil Thickness: 0.196 mm (7.7 mils)

Neutron Field: NBSR Thermal Column Cavity

Fissioning Isotope: U-235 > 99.5%

Energy Spectrum of Neutrons Inducing Fission: Thermal

RECYCLED OIL PROGRAM

D. A. Becker
(Office of Recycled Materials)

The reactor facility has been utilized for the past several years for activation analysis on recycled oil samples, by the Activation Analysis Group/Center for Analytical Chemistry. In particular, R. Fleming has provided analytical results on the accurate determination of chlorine and bromine in many such samples where there was no other acceptable method available.[1]

Because of the writers' long experience and continuing interest in the neutron activation analysis technique, he has maintained a capacity for research in this field. This brief report will describe the equipment used, followed by a short description of his on-going areas of research.

1. Equipment

The equipment currently used includes a Nuclear Data ND-60 pulse height analyzer, with a Texas Instruments Model 745 electronic data terminal readout. At present, a Ge(Li) detector approximately 60 c.c. in active volume is being shared with the FDA. The detector has a 1.86 keV resolution for the 1.333 MeV gamma-ray of Co-60, and an absolute peak efficiency as shown in table 1.

Table 1. Absolute peak efficiency for 60 cc (Ge(Li) detector**

Nuclide	E_γ (MeV)	γ/s*	Total Net Counts	Absolute Efficiency (%)
^{137}Cs	0.662	4105	8004	0.355
^{60}Co	1.172	3732	4105	0.200
^{60}Co	1.333	3736	3707	0.180

---

* NBS point source SRM, corrected for decay

** At 5.0 cm geometry (β holder)

2. Research

Current research efforts are focussed on two problems. The first is the development of separation methods to evaluate halogen speciation in re-refined oils. Since it is known that the halogens occur in used oils in both the inorganic and organic forms, it appears necessary to be able to assess the relative effects on lubrication performance of each of these forms. This effort is also being addressed in different ways by the Tribochemistry Group/CMS and the Activation Analysis Group/CAC.

In addition to the above, an accurate and reliable method for the determination of aqueous solutions of tin organometallics is being evaluated, in cooperation with the Chemical Stability and Corrosion Division/CMS. Such a method is necessary in order to establish the viability of a speciation technique developed in their laboratory.

---

1. D. A. Becker, "Research Methodology in Used Oil Recycling," in Proceedings, Conference on Atomic and Nuclear Methods in Fossil Energy Research, (In Press).

C. REACTOR OPERATIONS AND SERVICES

Routine round-the-clock operation was resumed following the lengthy shutdown of the previous year. Except for a 2-month shutdown to install and connect the new cooling tower and secondary cooling system, reactor operations was almost continuous for the balance of the year. Most of the technical effort this year was directed towards extensive modernization of the reactor and the preparation of safety analyses and environmental appraisal in connection with upgrading the reactor to 20 MW.

In December 1980, application was made to the Nuclear Regulatory Commission to double reactor power to 20 MW and to renew the operating license for another period of 20 years. Extensive documentation in support of the application were prepared and submitted. After publishing its intent to consider the application, the NRC determined that an Environmental Impact Statement would be required because the higher power level put the NBS reactor in a different class. Additional documentation had to be supplied and a public hearing was held on the scope of the Environmental Impact Statement. The NRC is continuing its safety evaluation of the application for upgrade and a decision is expected early in 1982. Once the new license is issued, it will make the NBS reactor the highest powered licensed research reactor in the country. This will permit major expansion of current programs and initiation of new programs not previously possible at the lower power level.

Application and use of the reactor continued to be very extensive and wide ranging. More than 50 major organizations from within and outside NBS are involved. There are now 25 simultaneously operable experimental and irradiation facilities contributing more than 125,000 instrument hours per year.

2. Reactor Operations

The reactor operating schedule returned to normal this year following the lengthy shutdown of the previous year. The first batch of new high performance elements were loaded into the reactor this year. The new fuel element design has considerably increased operating cycle time resulting in significant cost savings. It is projected that the average fuel element lifetime will increase from the previous 300 operating days to more than 400 operating days. This is more than 33 percent gain in fuel utilization efficiency. A summary of overall operating statistics for the period July 1, 1980 to June 30, 1981 is presented in the following table. While the on-line time was 65 percent for the whole year, the actual operating efficiency was an outstanding 80 percent if the planned extra shutdown time is excluded. The more than two thousand irradiations made involved tens of thousands of samples and specimens. Overall, the operating record for last year was one of the best in the history of the facility.

NBSR OPERATING SUMMARY FY 80

No. of days at 10 MW	238
On-line time at 10 MW	65%
Average U-235 burnup	52%
No. of Irradiations	2600
Hours of Irradiations	3300
Hours per Irradiation	1.3

2. Irradiation Services

Heavy utilization of the reactor for activation analysis and irradiation services resumed after the lengthy shutdown of the previous year. Again multitudes of samples involving foods, drugs, environmental monitoring, geological and mineral studies, forensic investigation, and standard reference materials were irradiated at the NBS reactor.

High precision measurements to detect extremely low level changes in the environment were initiated. A three-fold program is being carried out independently by NBS, other government agencies, and universities. This involves world-wide sampling for man-made or natural phenomenon of specific concern. Included among these is the study of the effect of the eruption of Mount St. Helen on the environment. A comprehensive study of trace and toxic elements has been carried out over the entire length and depth of Chesapeake Bay. Extensive data are currently being evaluated in collaboration with the Environmental Protection Agency.

A new procedure has been developed to determine the platinum concentration in biological materials at the currently natural occurring levels of 10^{-10} to 10^{-11} g/g. This is the first time ever that a certifiable number for platinum has been generated which will be incorporated in several important standard reference materials. This development is a significant breakthrough as it will provide base-line data for monitoring of platinum concentration in the environment and to detect changes as a result of the introduction of catalytic converters in automobiles, for example.

Finally, one of the more important analyses recently completed using the NBS reactor was the examination by the FBI of evidence involved in the shooting of the President.

3. Engineering Services

Besides regular engineering and design services provided to reactor operations, experimenters, and users, the engineering staff was heavily involved in a comprehensive program of reactor modernization. A new high efficiency cooling tower was installed, tested, and is operational, utilizing two speed motor controls, providing energy conservation. The entire secondary cooling system, including pumps, piping, and controls, was redesigned and modified to provide for more efficient and smoother operation. Old booster pumps were utilized as main pumps to save costs of new pumps. A 24 inch return line was installed from the heat exchangers to the cooling tower to reduce the pressure on the pumps to provide more flow. Two separate suction lines with sumps were installed to increase the suction pressure at the pump intakes to eliminate possible cavitation. This also makes it possible to use one set of pumps to reverse flow through the heat exchangers to clean heat exchanger tubing. The new cooling tower was raised four feet higher than the old tower to further increase the suction pressure on the pumps. Major portions of the reactor console are being redesigned to introduce modern, up-to-date equipment and components. Detector elements such as force balance type transmitters for flow, level, and pressure measurements are being replaced with the latest state-of-the-art strain gauge electronic transmitters. Old recording instruments are being replaced with modern recorders. When the entire modernization program is completed, it will provide for greatly improved, more efficient, and reliable operation and will clear the way for the 20 MW conversion as soon as the license amendment is received.

D. SERVICE PROGRAMS

ACTIVATION ANALYSIS PROGRAM OF THE FOOD AND DRUG ADMINISTRATION AT THE NBSR

W. C. Cunningham and W. B. Stroube, Jr.
(Food and Drug Administration, Washington, DC)

The Food and Drug Administration maintains a neutron activation analysis (NAA) unit in the Reactor Building of the National Bureau of Standards. The neutron activation program at FDA includes both research and analytical support for special projects. This report will focus upon one research project. In addition, examples are given where NAA has been used as an analytical support tool.

1. Research

Multielement Analysis by Neutron Activation of Tissues from Swine Administered Copper Supplemented Diets

Many swine diets are supplemented with Cu at high dietary concentrations to improve weight gain and feed efficiency. A number of researchers have demonstrated that dietary Cu concentrations of 250 ppm cause a large elevation of Cu in liver and to a lesser extent in kidney.

The main objective of the present study was to obtain additional data on levels of Cu and other elements in liver primarily for pigs with dietary copper levels near 60 ppm. Neutron activation analysis (NAA) was chosen for this study because the elements of interest could be determined non-destructively at the levels expected in the tissues.

In this study, eighty-four weanling crossbred pigs were divided into three replicate groups and randomly allotted to seven treatments to provide 21 pens of four pigs per pen. Copper sulfate was added to the basal diet to provide dietary treatments ranging from 15 to 154 ppm and feed and water were constantly available. The animals were slaughtered at 95 kg average body weight.

Table 1. Ranges of elemental abundances in swine liver, dry matter basis.

Dietary Cu, ppm	Cu(ppm)	Fe(ppm)	Co(ppb)	Mg(ppm)	Mn(ppm)	Se(ppb)	Zn(ppm)
15	20-58	400-756	70-169	700-1060	11-19	310-600	202-617
37	25-69	392-770	72-118	570-1060	10-18	360-690	228-525
54	25-60	258-724	66-274	550-1080	10-16	260-680	178-332
68	24-52	290-671	76-167	680-1180	10-15	250-640	175-435
82	25-265	185-582	81-216	660-1180	9-16	360-650	180-382
95	26-146	313-751	73-205	670-1150	8-18	300-1280	217-393
154	25-272	258-958	58-128	660-1290	10-18	460-900	222-387

Table 1 gives the range for the elemental abundances of the elements determined in the liver tissues. All values are given in either ppm (μg/g) or ppb (ng/g) and are expressed on a dry matter basis. The observed difference within groups fed the same level of dietary copper is attributed to animal-to-animal variability.

The data in table 1 illustrate that some animals in the three highest dietary copper groups had elevated copper abundances in the liver. While these three groups had an approximately even distribution of values between the low and high copper values in the tissues, the means for these groups were significantly higher. It can also be seen that even at 95 and 154 ppm dietary copper, some animals had no increase in copper levels in the tissues. While this study was limited to seven dietary levels with twelve animals per level, the data show that at dietary copper values of about 80 ppm, liver copper abundance increases for certain animals.[1]

2. Service

An example of the NAA Lab's service to other divisions within FDA is its cooperation during the past year with the Division of Nutrition. The NAA Lab assisted the Division of Nutrition by analyzing infant formulas for several metals. This was part of a compliance study of infant formulas to verify their contents. The study was prompted by the occurrence of several cases of metabolic alkalosis which resulted from chloride-deficient formula.

A related study involved the NAA analyses of pig blood, urine and tissue samples for chlorine. This was part of a pilot study to observe the effects of chlorine deficient diets upon the animals.

The following are additional examples of service projects performed during the past year.

- Determination of Sb at the one ppb level in coffee.
- Multielement analysis of volcanic ash.
- Determination of F and Na in feed contaminants.

---

1. W. B. Stroube, Jr., W. C. Cunningham, J. T. Tanner, B. D. Bradley, and C. Graber, "Multielement Analysis by Neutron Activation of Tissues from Swine Administered Copper Supplemented Diets," *Journal of Radioanalytical Chemistry*, accepted June 1981.

POSITRON ANNIHILATION IN Cu ALLOYS

L. M. Pecora and A. C. Ehrlich
(Naval Research Laboratory, Washington, DC)

For the past several years we have been performing positron annihilation experiments in Cu-based alloys by measuring the angular correlation of γ-rays emitted from a single crystal sample. We continued this work in the past year by examining several Cu-Ge and Cu-Zn alloys in the fcc α-phase. Our method consists of using the samples themselves as positron sources (Cu-64 is the source). This is accomplished by irradiating each sample in the NBS reactor for the appropriate time. Typical activities range from 10 to 20 Curies. The active samples are transported to the Naval Research Laboratory where they are placed in a Hot Cell between two Tantalum Tube collimators which allow only γ-rays at certain angles to pass through and be detected. The detected γ-rays are coincidence counted by standard nuclear instrumentation. Figure 1 shows the geometry of the apparatus.

The coincidence counts are proportional to an integral over the electronic momentum density of the sample along a line in momentum space (see Fig. 1). We have shown[1] how to "invert" the data thus reconstruct the momentum density $\rho(\vec{p})$ in a plane in momentum space which can be interpreted as representing the quantum mechanical probability of finding an electron with momentum $\vec{p}$, i.e. $\rho(\vec{p}) = X^*(p)X(p)$ where $X(p)$ is the electronic wave function in momentum space.

SERVICE PROGRAMS

1. Experiments

During the past year we have measured angular correlations of γ-rays on the following samples in the respective planes shown: Cu (111), $Cu_{92}Ge_8$ (111), $Cu_{92.5}Zn_{7.5}$ (110), $Cu_{85}Zn_{15}$ (110), and $Cu_{75}Zn_{25}$ (110). All samples were cylindrical in shape and single crystals. The cylinder axis of the sample determined the plane sampled in momentum space. The momentum density was reconstructed in each respective plan. The CuGe experiments completed a "full set" of experiments which were begun the previous year (1979-1980) on the alloys $Cu_{97}Ge_3$ (110), $Cu_{94}Ge_6$ (110), and $Cu_{92}Ge_8$ (110) and allowed us to examine the change in $\rho(\vec{p})$ of Cu upon alloying with Ge.

2. Results

Reconstruction of $\rho(\vec{p})$ in a particular plane for each alloy allows us to examine $\rho(\vec{p})$ as a function either in single directions, i.e. sections of $\rho(\vec{p})$, or as a function of two momentum variables i.e. as a surface. We have presented some examples of typical $\rho(p)$ results for pure Cu and $Cu_{92}Ge_8$ in both the (110) and the (111) planes.

Figure 2 shows sections of $\rho(\vec{p})$ in three high symmetry directions in $(1\bar{1}0)$ for pure Cu. Obvious structures are the Fermi break between 5 and 6 mrad, the positron annihilation enhancement peaks just below the Fermi breaks, the anisotropy between (001) and (110) in the core contribution between 6 and 8 mrad, and the higher momentum components on [002] in the [001] direction. Figure 3 shows the same function in the entire plane. Note that three of the four Cu necks are evident here.

Figure 4 shows $\rho(\vec{p})$ in $(1\bar{1}0)$ for $Cu_{92}Ge_8$. Although there are subtle changes in the Fermiology which are reflected in $\rho(p)$, the greatest change is the vanishing the trough along [001] at about 7 mrad (see Fig. 3) and its replacement by a bulge in $\rho(p)$. This constitutes a reversal of the [110] - [001] core anisotropy seen in Cu. Causes of this will be discussed in the next section.

Figure 5 shows sections of $\rho(p)$ for Cu in (111) and Figure 6 shows the associated 2-D surface which represents $\rho(p)$ in the entire (111) plane.

Changes in $\rho(p)$ in this plane were mostly in Fermiology and not as radical as the (110) changes noted.

Figure 6 shows changes in Fermi radii upon alloying Cu with Ge.

At present the CuZn data is being analyzed and is not in a form for presentation.

2. Comparison with Theory

In order to determine what changes in the wave functions are necessary to cause the [110] - [001] anisotropy changes in $\rho(\vec{p})$ which occur in CuGe alloys and which were mentioned in the previous section we obtained self consistent APW results[2] and used these to generate momentum-space wave functions in a tight binding-like scheme. A typical wave function looked like

$$\chi(p) = C_s\phi_s + C_p\phi_p + C_d\phi_d = \sum_{\ell=o}^{2} C_\ell\phi_\ell$$

where ϕ_s, ϕ_p, and ϕ_d are s, p, and d atomic orbitals and C_s, C_p, C_d are the appropriate coefficients for their admixture to make up $\chi(p)$. Since $\rho(p) = |\chi(p)|^2$ we now have the possibility of determining how the coefficients C_ℓ change on alloying Cu with Ge, i.e. we can estimate changes in wave function hybridization. The APW wave functions showed that although the bands which contribute to $\rho(p)$ in the core region in the area of the anisotropy are primarily of d character ($C_d^2 \approx 1$), the s and p orbital values are quite large and hence small changes in s and p admixture will readily show up. The reason for the original [110] - [001] anisotropy in pure Cu is that the wave function along [110] has more p mixed in than does the wave function along [001] which has no p at the brillouin zone boundary by symmetry. This causes $\rho_{[110]} > \rho_{[001]}$ in the core region (6-8 mrad). However, this anisotropy reversed in $Cu_{92}Ge_8$ and we have $\rho_{[001]} > \rho_{[110]}$. The only possibility is that the s component along [001] must increase. This means that we now have evidence for a change in s-d hybridization in CuGe alloys. This work was recently published in Physical Review Letters, June 1, 1981 issue.[3]

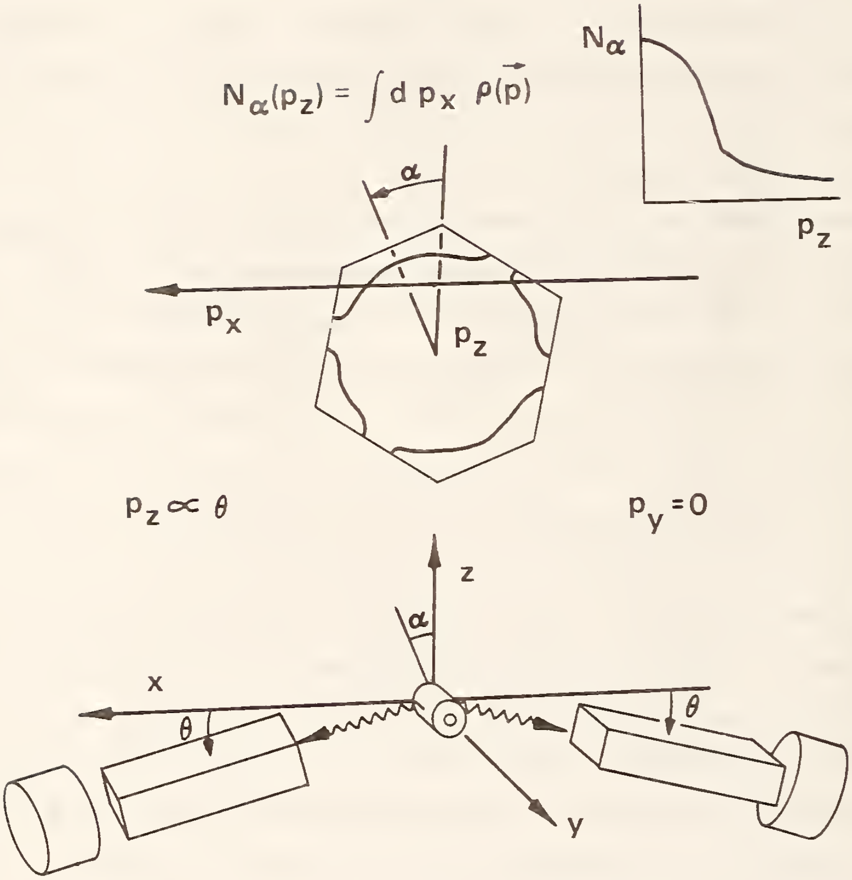

Figure 1. Schematic of the Geometry and appropriate coordinate systems used in the experiment. A slice of the Cu (110)·plane in momentum space is shown as an example of sampling of ρ(p) by a measurement at a particular collimator angle.

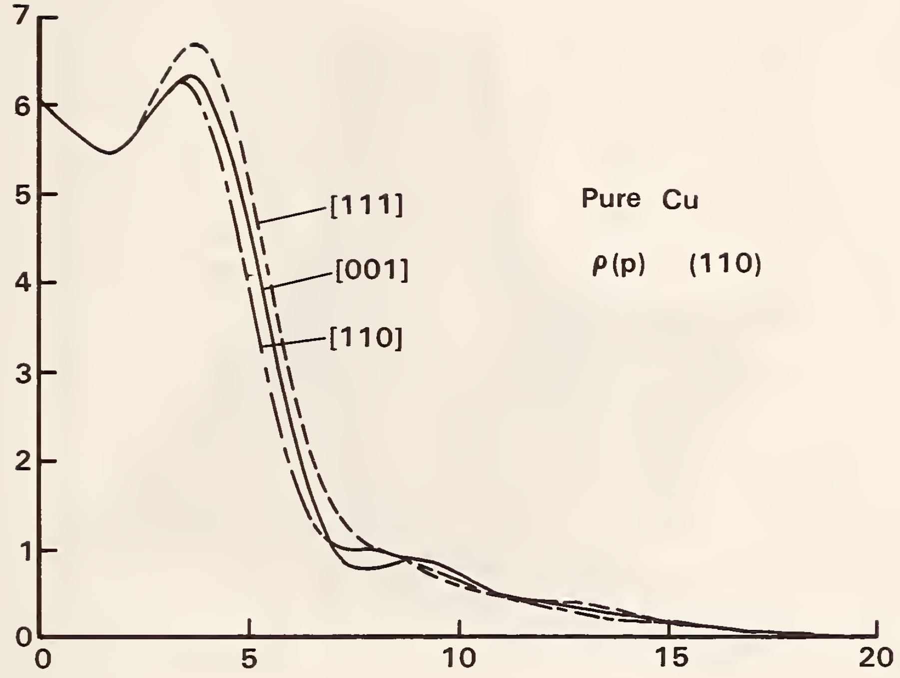

Figure 2. Sections of ρ(p) along three high symmetry directions in (110) for pure Cu.

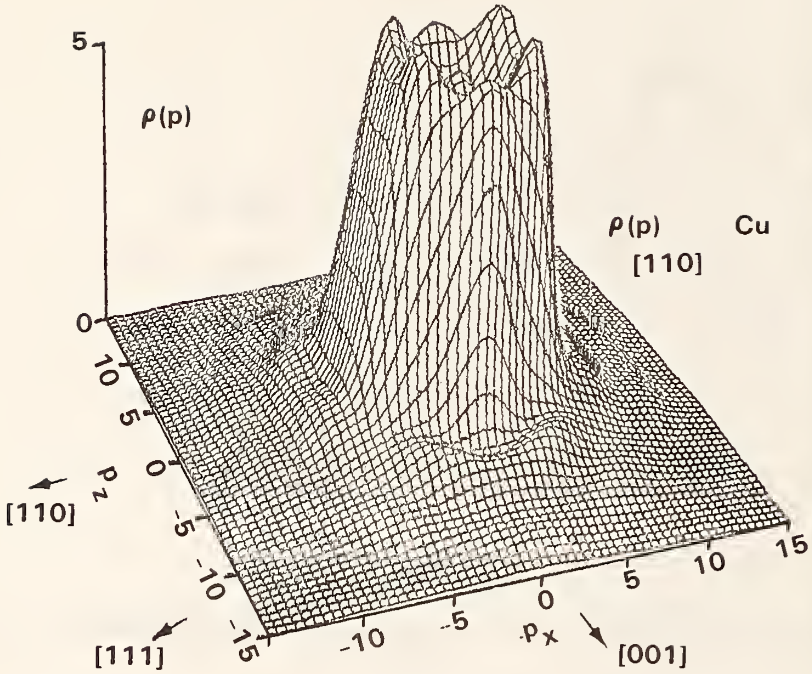

Figure 3. ρ(p) reconstructed in the entire (110) plane for Cu.

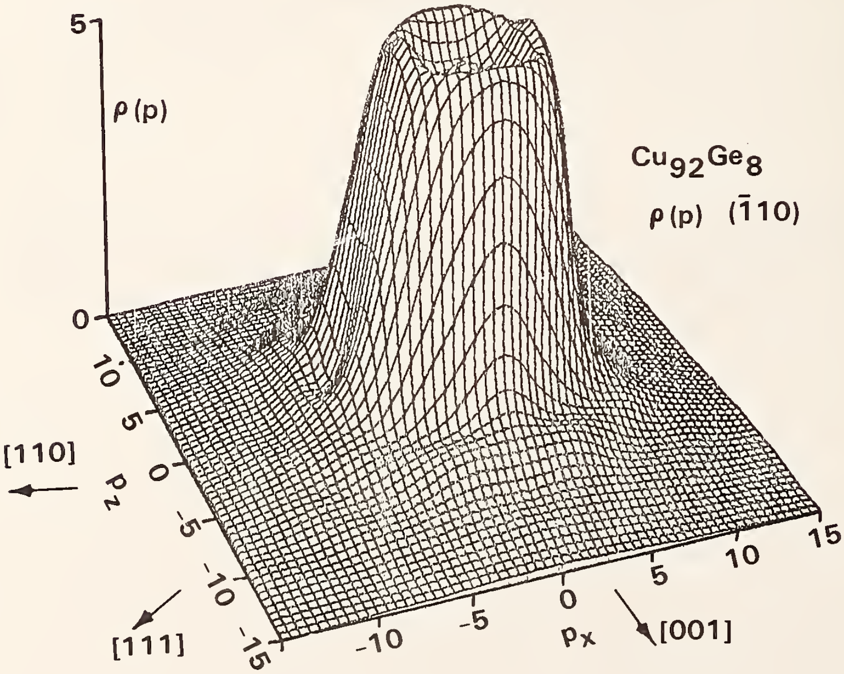

Figure 4. Same as 3 except for $Cu_{92}Ge_8$ (110).

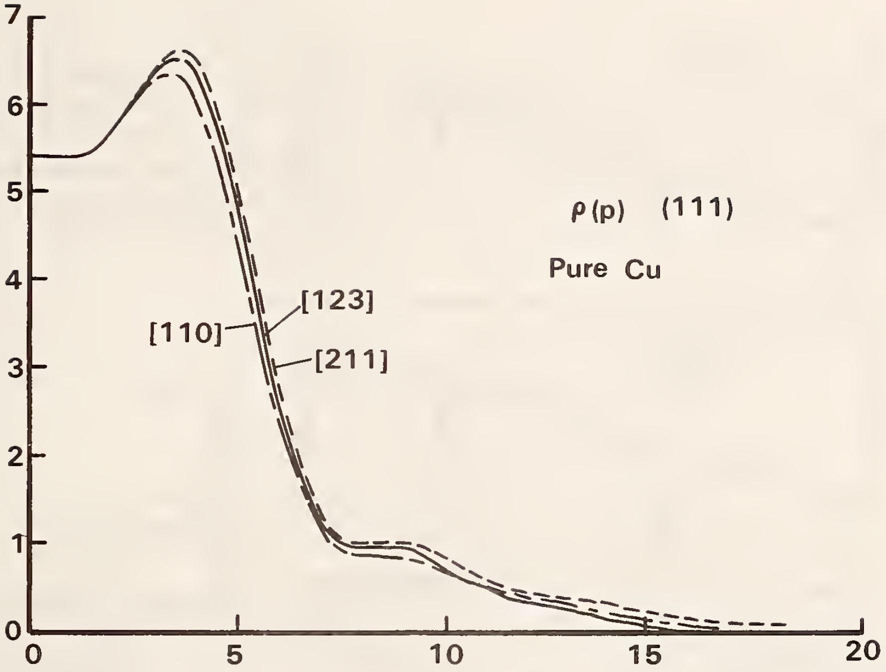

Figure 5. Sections of ρ(p) in 3 directions in the (111) plane for pure Cu.

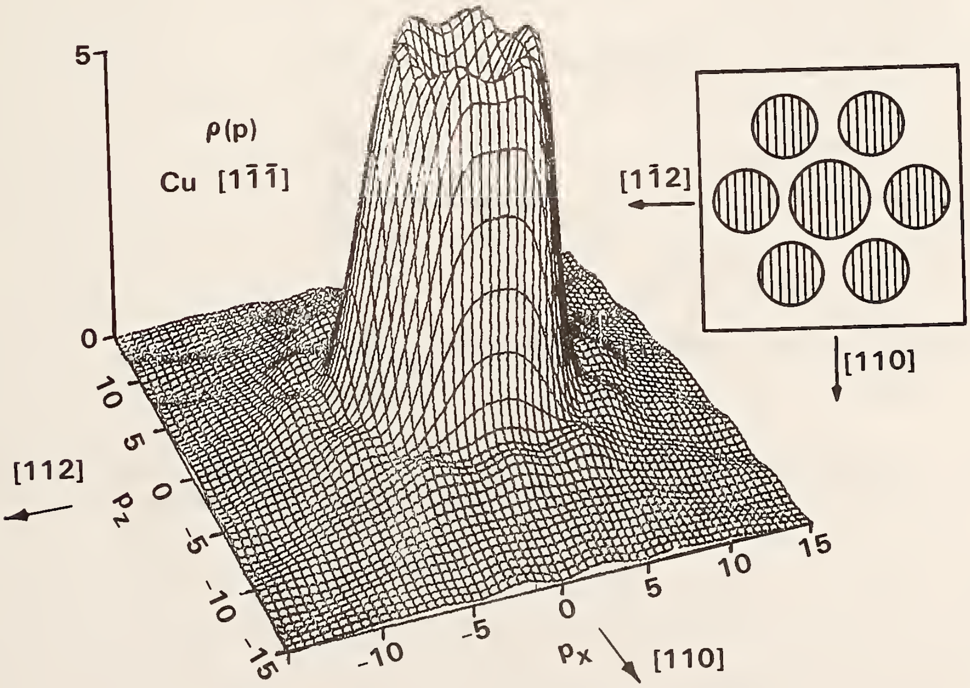

Figure 6. Surface plot of ρ(p) in (111). Note the 6 higher momentum components and the 6 core maximum between them at 8 mrad around the main conduction band peak.

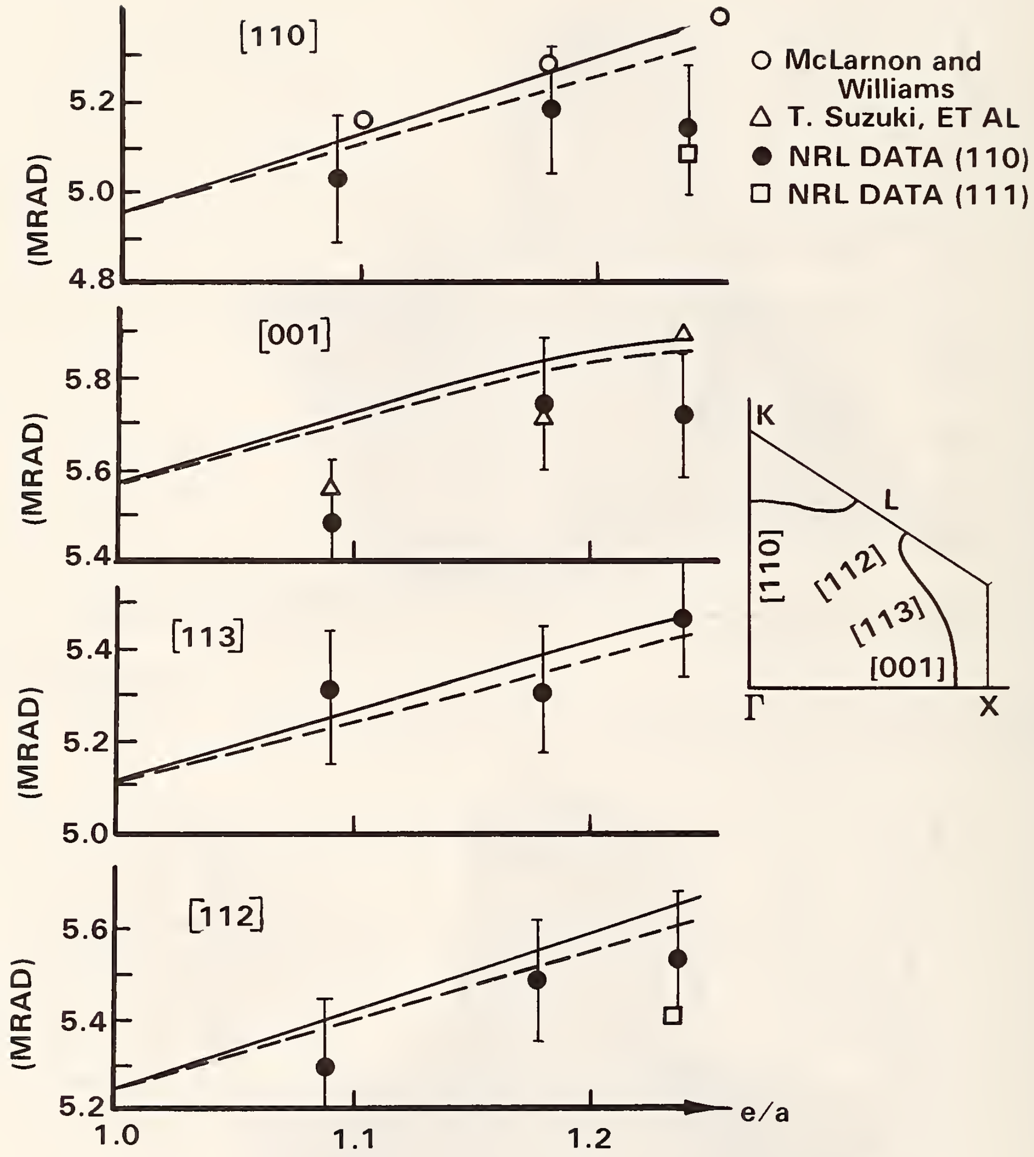

Figure 7. Graphs of Fermi radii from the CuGe data plotting p_F, Fermi radii, as a function of electrons per atom (e/a).

---

1. L. Pecora and A. C. Ehrlich, *Phys. Rev. B*, 19, 719 (1979).
2. D. A. Papaconstantopoulos, et al., *Phys. Rev. B*, 15, 4221 (1977).
3. L. M. Pecora and A. C. Ehrlich, *Phys. Rev. Lett.* 46, 1476 (1981).

U.S.G.S. ACTIVATION ANALYSIS PROGRAM

P.A. Baedecker, L.J. Schwarz
C.A. Palmer, and G.A. Wandless
(U.S. Geological Survey, Reston, VA)

1. Instrumental Neutron Activation Analysis

a. The Geological Survey has an ongoing program of automated INAA which provides data for 24 to 30 elements in 3000 to 4000 rock mineral and coal samples per year. The technique is applied to studies related to: 1) the characterization of tectonic setting; 2) magma chamber eruptive sequences; 3) trace element partitioning to study petrologic history; 4) mechanisms of ore deposition; 5) alternation studies; 6) the formation of Mn nodules and metal rich sediments; 7) the origin of coals and peats; 8) compilation of a baseline of coal compositions; and 9) trace element studies to assist other geologic and geochemical investigations. In addition to neutron irradiation at the NBS reactor, epithermal irradiations using the JEEP-II reactor in Kjeller, Norway are used for the analysis of rocks with high Uranium and/or Phosphorous contents, or to improve the sensitivity for certain elements.

b. INAA is being applied to the determination of 35 major and trace elements in various minerals found in coal and fly ash. Size and density separates of fly ash and low temperature ashed coal are being analyzed. This data in conjunction with x-ray diffraction and scanning electron microscopy can be used to identify the association between trace elements and their host minerals. Size and density separations of whole coal are also being analyzed to help determine the citing of trace elements for coal utilization.

2. Radiochemical Neutron Activation

We continue to supplement our INAA determinations by group separations for the rare earth elements in those materials where REE abundances are very low, particularly in mafic and ultramafic rocks and some separated minerals. New procedures using x-ray fluourescence analysis have been developed for chemical yield determinations for our group separation procedures.

E. PERSONNEL ROSTER

REACTOR RADIATION DIVISION

566

R. S. Carter
T. M. Raby, Deputy Chief
*E. C. Maxwell, Admin. Officer
*L. Sprecher, Secretary
T. Mangum, Secretary

Division Staff
D. Alger, IPA
R. Casella
B. Mozer
F. Shorten

Reactor Operations
T. M. Raby, Chief
J. F. Torrence, Deputy Chief

*T. Hatley, Secretary

Reactor Operators

R. Beasley
M. Bell
N. Bickford
H. Brake
J. Browning
A. Chapman
H. Dilks
W. Mueller
J. Ring
R. Stiber
A. Toth
D. Wilkison

Engineering Services
J. H. Nicklas, Chief

Mechanical Design

E. Guglielmo
J. Sturrock

Electronics

R. Conway
W. Crummer (Coop)
R. Hayes
L. Shuman

Neutron S-S Physics
J. J. Rush, Chief

S. Long, Secretary

Crystallography

#C. Choi
D. Fravel (1/2)
J. LaRock (1/2)
E. Prince
W. Rymes (1/2)
A. Santoro

Metal Hydrides and Molecular Materials

D. Fravel (1/2)
#A. Magerl
#H. Prask
J. Rowe (1/2)
W. Rymes (1/2)
#S. Trevino

Biological Materials

#L. Sjolin
A. Wlodawer

Magnetic and Amorphous Materials

#H. Alperin
#N. Koon
+J. Lynn
J. Rhyne
#R. Williams

Advanced Neutron Methods

N. Berk
S. Bai, IPA
C. Glinka
J. LaRock (1/2)
J. Rowe (1/2)
S. Singhal, IPA

Neutron Radiography
Donald A. Garrett

Neutron Radiography

M. Dorsey
M. Ganoczy
T. Cheng

*Part-time
+Intermittent
#Guest Worker

NON-RRD NBS STAFF LOCATED AT REACTOR

Division 354

J. Arras
P. Cassidy
D. Hoaney
I. Jensen
F. Moore
J. Shubiak

Division 532

R. A. Dallatore
C. Eisenhauer
D. Gilliam
J. A. Grundl
S. T. Hwang
G. Lamaze
L. Li
E. McGarry
I. G. Schroder
R. Schwartz
W. Slater
V. Spiegel

Division 500

B. Carpenter

Division 551

D. Allen
R. Fleming
K. Fitzpatrick
S. Harrison
J. Langland
R. Lindstrom
G. Lutz
J. Mitchell
T. Mitlehner
L. Pilione
M. Vinocur
R. Zeisler

GUEST WORKERS AND COLLABORATORS

Division 501

H. Berger

Division 506

D. Becker

Division 520

E. Kessler
W. Sauder

Division 522

R. Dove

Division 532

A. Wasson

Division 533

R. Placious

Division 541

J. Kelly
T. Madey

Division 544

D. Tsai

Division 545

R. Kavanagh

Division 553

H. Rook

PERSONNEL ROSTER

Division 561

E. N. Pugh

Division 562

F. Biancanello
E. Case
J. Early
R. Fields

Division 563

R. Bowen
C. Han
M. Mathew
S. Takagi
R. Waterstrat

Division 564

R. Reno
R. Shull

Division 565

C. Hubbard
A. Mighell
R. Roth

Aberdeen Proving Ground

C. Heimbach

Argonne National Laboratory

T. Brun
H. Flotow
O. Hinks
S. Susman
J. Viccaro

Battelle, N. W.

L. Brackenbush
G. Endres

Brookhaven National Laboratory

P. Levy

Federal Bureau of Investigation

R. Asbery
R. Bilko
D. B. Davies
J. Haverkost
J. W. Kilty
E. Mitchell
C. Peters
J. P. Riley

Food and Drug Administration

M. Allegrini
W. Cunningham
W. Stroube, Jr.
J. Tanner

National Gallery of Art

B. Miller
C. Parkhurst

National Institutes of Health

D. Davies
R. Frank
J. Weinstein

Naval Research Laboratory

P. D'Antonio
A. Ehrlich
M. Fatemi
W. Hendricksen
J. Karle
N. Koon
L. Pecoia

Naval Surface Weapons Center

H. Alperin
M. Lia
G. Riel
R. Williams

PERSONNEL ROSTER

Oak Ridge National Lab

F. Kam
H. Smith

Carnegie Institute of Washington

B. K. Kothari

Institute Laue Langevin, France

M. Marezio
J. Hodeau

Smithsonian Institution

M. Blackman
T. Chase
J. Mishara
J. Olin
L. Zacherman

U. S. Geological Survey

P. Baedecker
J. Morgan
G. Wandless

KFA Jülich, Germany

D. Richter

American University

J. Malamas

Iowa State University

R. Shelton

Massachusetts Institue of Technology

B. Averbach
C. Skarda
B. Wuenscher

Reed College

W. Parker

Technical University of Munich

H. Metzger
H. Wipf

University of Antwerp

K. Michel

University of Arizona

R. Salemme
P. Weber

University of Alabama

J. Segrest

University of California
(Lawrence Livermore Laboratories)

D. Hankins

University of Chicago

E. Anders
R. Wolf

University of Connecticut

J. Budnick

University of Grenoble, France

J. Hodeau
M. Marezio

University of Houston

S. Moss

University of Illinois

H. Zabel

University of Maine

H. Patterson

PERSONNEL ROSTER

University of Maryland

D. Anderson
N. Aras
J. Baca
D. Ballantine
C. Barley
D. DeLozier
D. Demers
I. Gokman
G. Gordon
J. Lynn
J. Parrington
J. Phelan
W. Sonnefeld
M. Thompson
G. Tuncel
W. Walters
J. Weber
W. Zoller

University of Missouri (Columbia)

D. Alger

University of Missouri (Rolla)

W. James

State University of New York

H. Herman

University of Pittsburgh

R. Buttera
S. Malik
W. Wallace

University of Rhode Island

S. Pickart

University of Wisconsin

J. Hinkley
H. Yu

Allied Chemical Corporation

G. Leibowitz
G. Fish
A. Maeland

Bicron Corporation

R. Culp

B-K Dynamics

N. Chesser

EG & G Idaho Falls

V. Gupta

General Electric Company

J. L. Provo

Israel AEC Soreq Nuc. Res. Center

Y. Eisen

Metronic, Inc.

P. Skarstad

Monsanto Research Corporation

W. Brotherton

ManTech Corporation

D. Bracher

Oklahoma Memorial Hospital

D. W. Anderson

Sandia Corporation

J. Harris

Siemens Gammasonics, Inc.

R. Oswald

PERSONNEL ROSTER

Nuclear Energy Center, Mol, Belgium

A. Fabry

Westinghouse-Hanford Corp.

W. McElroy
J. Rawlins

F. PUBLICATIONS

COLLABORATIVE PROGRAMS

ALPERIN, H. A., MELAMUD, M., and HOROWITZ, A., "Neutron Scattering Study of Spinwaves in the Antiferromagnet $RbMnCl_3$," *J. Appl. Phys.* 52, 2225 (1981).

BARKIGIA, K. M., RAJKOVIC-BLAZER, L. M., PEPE, M. T., PRINCE, E., and QUICKSALL, C. O., "Molybdoarsinate Heteropoly Complexes. The Structure of the Hydrogen-tetramolybdodimethylarsinate (2-) Anion by X-ray and Neutron Diffraction," *Inorg. Chem.* 19, 2531-2537 (1980).

BIZZARO, W., YARMUS, L., ROSENTHAL, J., and BERK, N. F., "EPR Linewidth of Triplet Excitons in Molecular Crystals, II, Tetracene," *Phys. Rev* B23, 5673 (1981).

BERK, N. F., BIZZARO, W., ROSENTHAL, J., and YARMUS, L., "EPR Linewidth of Triplet Excitons in Molecular Crystals. I. Theroy and Experiment: Pyrene," *Phys. Rev.* B23, 5661 (1981).

CASELLA, R. C., "Detection of Impurity Tunneling in Solids via Coherent Phonon Coupling and Direct Neutron Scattering," *Proc. of International Conference on Phonon Physics* (submitted).

CASELLA, R. C., "Theory of Neutron Scattering from Hydrogen in Metals Involving Transitions to Excited Tunnel-Split States, *Phys. Rev. B* (submitted).

CHOI, C. S. and PRASK, H. J., "Texture, Nondestructive Characterization," *Ency. Matls. Sci. and Eng.* (in press).

CHOI, C. S., "Refinement of 2-Nitroguanidine by Neutron Powder Diffraction," *Acta Cryst.* (in press).

CHOI, C. S., PRASK, H. J., and PRINCE, E., "Phase Transitions in Ammonium Nitrate," *J. Appl. Cryst.* 13, 403-409 (1980).

CHOI, C. S. and MARINKAS, P. L., "Refinement of Dipara-anthracene," *Acta Cryst.* B36, 2491-2493 (1980).

FERNANDEZ-BACA, J. A. and LYNN, J. W., "Neutron Scattering Studies of the Magnetic Superconductor $(Ce_{1-x}Tb_x)Ru_2$," *J. Appl. Phys.* 52, 2183-2185 (1981).

GARRETT, D. A. and BRACHER, D. A., "Real-Time Radiologic Imaging: Medical and Industrial Applications STP-716," *American Society for Testing and Materials* (1980).

PUBLICATIONS

GLINKA, C. J., "The National Bureau of Standards Small Angle Neutron Scattering Spectrometer," *Proc. of Symposium on Neutron Scattering* (submitted).

GLINKA, C. J., PRASK, H. J., and CHOI, C. S., "Neutron Diffraction and Small-Angle Scattering as Nondestructive Probes of the Microstructure of Materials," *Mechanics of Nondestructive Testing*, pp. 143-164 (1980).

HARDMAN, V. K., RHYNE, J. J., PRINCE, E., SMITH, H. K. MALIK, S. K., and WALLACE, W. E., "Magnetic and Structural Properties of $Th_6Mn_{23}D_x$ and $Y_6Mn_{23}D_x$," *The Rare Earths in Modern Science and Technology, Vol. III* (in press).

HARDMAN, V. K., RHYNE, J. J., and JANES, W. J., "Magnetic Structures of $Y_6(Fe_{1-x}Mn_x)_{23}$ Compounds," *J. Appl. Phys.* 52, 2049 (1981).

HARDMAN, V. K., RHYNE, J. J., SMITH, K., and WALLACE, W. E., "Structural Investigation of $Th_6Mn_{23}P_{16}$ by Neutron Diffraction," *J. of Less Common Metals* 74, 97-102 (1980).

KELLEY, R. D., CAVANAGH, R. R., RUSH, J. J., and MADEY, T. E., "Neutron Inelastic Scattering Study of C_2H_4 Absorbed on Raney Nickel," *Surface Science* 97, L335 (1980).

KOON, N. C. and RHYNE, J. J., Ground State Spin Dynamics of $ErCo_2$," *Phys. Rev.* B23, 207-214 (1981).

LONG, G. J., HARDMAN, V. K., and JAMES, W. J., "A Mössbauer Effect Study of the Manganese-Rich $Y_6(Fe_{1-x}Mn_x)_{23}$ Compounds," *Solid State Commun.* 34, 253 (1980).

LYNN, J. W., ERWIN, R. W., RHYNE, J. J., and CHEN, H. S., "Spin Glass-Ferromagnetic Phase Transition in Amorphous $(Fe_xNi_{1-x})_{0.75}P_{0.16}B_{0.06}Al_{0.03}$," *J. Appl. Phys.* 52, 1738-1740 (1981).

LYNN, J. W., "Neutron Scattering Studies of Ternary Magnetic Superconductors," *Ternary Superconductors*, p. 51 (1981).

MAGERL, A., ROWE, J. M., and RICHTER, D., "Oservation of Low-Energy Excitations in NbD: A Single Lattice-Dynamical Model," *Phys. Rev. Lett.* B23, 1605-1608 (1981).

MAGERL, A., and ZABEL, H., "Phonons in Graphite-Potassium Intercalation Compound: $C_{36}K$," *Phys. Rev. Lett.* 26, 444 (1981).

MICHEL, K. H. and ROWE, J. M., "On the Existence of an Orientational Glass State in $(KCN)_x(KBr)_{1-x}$ Mixed Crystals," *Phys. Rev.* B22, 1417-1428 (1980).

PUBLICATIONS

NICHOLSON, W. L. and PRINCE, E., "A Robust/Resistant Technique for Crystal Structure Refinement," *Acta Cryst.* (submitted).

PLACIOUS, R. C., GARRETT, D. A., KASEN, M. B., and BERGER, H., "Dimensioning Flaws in Pipeline Girth Welds by Radiographic Methods," *J. Am. Soc. for Nondestructive Testing* 39, 755 (1981).

PRASK, H. J., CHOI, C. S., and TREVINO, S. F., "Nondestructive Testing of Armament-System Components by Means of Neutron Diffraction," *Proc. of the Army Science Conf.* (1980).

PRINCE, E., "Comparison of Profile and Integrated Intensity Methods in Powder Refinement," *J. Appl. Cryst.* (in press).

PRINCE, E., "Comparison of the Fits of Two Models to the Same Data Set," *Acta Cryst.* (in press).

RHYNE, J. J., HARDMAN, V. K., MALIK, S. K., and WALLACE, W. E., "Magnetic Properties of Cubic and Hexagonal $HoMn_2$," *The Rare Earths in Modern Science and Technology, Vol. III* (in press).

RHYNE, J. J., "Magnetic Materials," *Encyclopedia of Physics,* pp. 547-550 (1981).

RHYNE, J. J., "Magnetic Inelastic Neutron Scattering Studies of Rare Earth Metals and Laves-Phase Compounds," *Science and Technology of Rare Earth Metals,* pp. 261-290 (1980).

ROWE, J. M., RUSH, J. J., PYNN, R., HEIDEMANN, H., and MICHEL, K. H., "Observation of Critical Dynamics in ND_4Br by High-Resolution Neutron Spectroscopy," *J. Chem. Phys.* 74, 5323-5324 (1981).

RUSH, J. J., MAGERL, A., ROWE, J. M., HARRIS, J. M., and PROVO, J. L., "Tritium Vibrations in Niobium by Neutron Spectroscopy," *Phys. Rev.* (submitted).

RUSH, J. J., ROWE, J. M., and MAELAND, A. J., "Neutron Scattering Study of Hydrogen Vibrations in Polycrystal and Glassy TiCuH," *J. Phys.* F10, L283-L285 (1980).

RUSH, J. J., ROWE, J. M., GLINKA, C.J., VAGELATOS, N., and FLOTOW, H. E., "Coherent Neutron Scattering Study of the Vibrations of Interstitial Deuterium in α-$VD_{0.7}$," *Phys. Rev.* B21, 5613-5616 (1980).

SANTORO, A., ROTH, R. S., and AUSTIN, M. C., "Powder Neutron Diffraction Study of the Nonstoichiometric Solid Solution of Lithium Tantalate $9LiTaO_3$:Ta_2O_5," *Acta. Cryst.* (submitted).

PUBLICATIONS

SANTORO, A., CAVA, R. J., MURPHY, D. W., and ROTH, R. S., "Use of the Pearson Type VII Distribution in the Neutron Profile Refinement of the Structures of $LiReO_3$ and Li_2ReO_3," *Proc. of Symposium on Neutron Scattering* (submitted).

SANTORO, A., CAVA, R. J., MURPHY, D. W., and ROTH, R. S., "Structural Aspects of Lithium Insertion in Oxides: Li_xReO_3 and $Li_2FeV_3O_8$," *Proc. of International Conference on Fast Ionic Transport in Solids* (in press).

SANTORO, A., MIGHELL, A. D., and RODGERS, J. R., "Determination of the Relationship Between Derivative Lattices," *Acta Cryst.* A36, 796-800 (1980).

SANTORO, A., and D'Antonio, P., "Powder Neutron Diffraction Study of Chemically Prepared β-PbO_2," *Acta Cryst.* B36, 2394-2397 (1980).

SANTORO, A., MAREZIO, M., ROTH, R. S., and MINOR, D. B., "Neutron Powder Diffraction Study of the Structure of $CeTaO_4$, $CeNbO_4$, and $NdTaO_4$," *J. Solid State Chem.* 35, 167-175 (1980).

SINGHAL, S. P., ALPERIN, H. A., BIANCANELLO, F., and HERMAN, H., "Phase Decomposition in the NiRich Side of Ni/Ni_3Al Miscibicity Gap: A Small-Angle Neutron Scattering Study," *Scripta Metall.* (submitted).

SINGHAL, S. P., HERMAN, H., and KOSTORZ, G., "Small-Angle Neutron Scattering Study of Nonlinearity of Spinodal Reaction in a Symmetric Au-60 at % Pt Alloy," *Proc. of International Conference on Solid-Solid Phase Transformation* (submitted).

SINGHAL, S. P., "The Au-Pt (Gold Platinum) System," *Alloy Phase Diagram Bulletin #4* (1981).

SJÖLIN, L., and WLODAWER, A., "Improved Technique for Peak Integration for Crystallographic Data Collected Using Position-Sensitive Detectors: A Dynamic Mask Procedure," *Acta Cryst.* (in press).

STROUBE, JR., W. B., CUNNINGHAM, W. C., TANNER, J. T., BRADLEY, B. D., and GRABER, C., "Multielement Anaysis by Neutron Activation of Tissues from Swine Administered Copper Supplemented Diets," (to be published).

STROUBE, W. C., BOYER, K. W., JONES, J. W., LINSCOTT, D., WRIGHT, S. K., "Trace Element Levels in Tissues from Cattle Fed Sewage Sluge-Amended Diet," *Journal of Toxicology and Environmental Health,* 8:281-295 (1981).

PUBLICATIONS

STROUBE, W. B., JR. and TANNER, J. T., "Application of Neutron Activation Analysis in a Regulatory Agency," *Proceeding of the Fourth International Conference on Nuclear Methods in Environmental and Energy Research,* ed. J. R. Vogt, (1980).

TAYLOR, H. C., RICHARDSON, D. C., RICHARDSON, J. S., WLODAWER, A., KOMORIYA, A., and CHAIKEN, I. M., "Active" Conformation of an Inactive Semisynthetic Ribonuclease-S," *J. Mol. Biol.* 149, 313-317 (1981).

TREVINO, S. F. and RYMES, W. H., "A Study of Methyl Reorientation in Solid Nitromethane by Neutron Scattering," *J. Chem. Phys.* 73, 3001-3006 (1980).

TREVINO, S. F., PRINCE, E., and HUBBARD, C. R., "Refinement of the Structure of Solid Nitromethane," *J. Chem. Phys.* 73, 2996-3000 (1980).

TSAI, D. H. and TREVINO, S. F., "Thermal Relaxation in a Liquid Under Short Compression," *High Pressure Science and Technology,* p. 1051 (1980).

ROSENTHAL, J., YARMUS, L., and BERK, N. F., "Triplet Exciton Annihilation and Triplet Spin Relaxation in Molecular Crystals," *Phys. Rev. B*23, (1981).

WIPF, H., MAGERL, A., SHAPIRO, S. M., SATIJA, S. K., and THOMLINSON, W., "Neutron Spectroscopic Evidence for Hydrogen Tunneling States in Niobium," *Phys. Rev. Lett.* 26, 947 (1981).

WIPF, H., MAGERL, A., SHAPIRO, S. M., SATIJA, S. K., and THOMLINSON, W., "Neutron Scattering Measurements of Low-Temperature Hydrogen Tunneling in Niobium," *Proc. of Coral Gables Conf. on Hydrogen in Metals* (1981).

WLODAWER, A., BOTT, R., and SJÖLIN, L., "The Refined Crystal Structure of Ribonuclease A at 2.0 Å Resolution," *J. Biol. Chem.* (submitted).

WLODAWER, A. and HENDRICKSON, W. A., "A Procedure for Joint Refinement of the X-ray and Neutron Single-Crystal Diffraction Data for Macromolecules," *Acta Cryst.* (submitted).

WLODAWER, A. and SJÖLIN, L., "Improvement of the Quality of the Data Collected Using a Position-Sensitive Detector," *J. Nucl. Instrum. and Methods* (in press).

WLODAWER, A., SJÖLIN, L., and SANTORO, A., "Refinement of the Crystal Orientation Matrix for the Flat-Cone Diffractometer," *J. Appl. Cryst.* (in press).

WLODAWER, A. and SJÖLIN, L., "Improvement of the Quality of the Data Collected Using a Position-Sensitive Detector," *Nucl. Instrum. Meth.,* (in press).

PUBLICATIONS

WLODAWER, A. and SJOLIN, L., "Orientation of Histidine Residues in Ribonuclease-A: A Neutron Diffraction Study," *Proc. of National Academy of Science, USA* 78, 2853-2855 (1981).

WLODAWER, A., "Studies of Ribonuclease-A by X-ray and Neutron Diffraction," *Acta Cryst.* *B*36, 1826-1831 (1980).

PUBLICATIONS

INDEPENDENT PROGRAMS

ANDERSON, D. L., FAILEY, M. P., ZOLLER, W. H., WALTERS, W. B., GORDON, G. E., and LINDSTROM, R. M., "Facility for Non-Destructive Analysis for Major and Trace Elements Using Neutron-Capture Gamma-Ray Spectroscopy," *J. Radioanal. Chem.,* 63, 97 (1981).

EISENHAUER, C., and SCHWARTZ, R., "Difficulties in Calculating Spectrum-Average Values of Dose Equivalent," *Health Physics* (1981).

GILLIAM, D. M., FULLER, J. L., GRUNDL, J. A., and DAUGHTRY, J. W., "Absolute Fission Rates in the FFTF, *Trans. Am. Nucl. Soc.,* 37, (November 1981).

EISENHAUER, C. M., and SHWARTZ, R. B., "The Effect of Room-Scattered Neutrons on the Calibration of Radiation Protection Instruments," *Proceedings of the Fourth Symposium on Neutron Dosimetry* (1981).

GILLIAM, D. M., FULLER, J. L., GRUNDL, J. A., and RAWLINS, J. A., "FFTF Reactor Characterization Program: Absolute Fission Rate Measurements," TC-1963, Hanford Eng. Dev. Lab. (1981).

GILLIAM, D. M., and BAUN, M., "Calibrating the FFTS," *Dimensions* (1981).

EISENHAUER, C. M., and GRUNDL, J., "Benchmark Referencing of Neutron Dosimetry Measurements, LWR-PV Irradiation Surveillance Dosimetry," *Prog. Report,* NUREG/CR-1240, Vol. II (1981).

GREENBERG, R. R., and KINGSTON, H. M., "Simultaneous Determination of Twelve Trace Elements in Estuarine and Sea Water Using Pre-Irradiation Chromatography," *J. Radioanal. Chem.,* (in press).

GREENBERG, R. R., ZOLLER, W. H., and GORDON, G. E., "Atmospheric Emissions of Elements on Particles from the Parkway Sewage-Sludge Incinerator," *Environ. Sci. Technol,* 15, 64 (1981).

GRUNDL, J., EISENHAUER, C., MCGARRY, E. D., and SPIEGEL, V., with MCELROY, W., et al., "LWR Pressure Vessel Surveillance Dosimetry Program, Eighth Reactor Safety Research Information Meeting," *NRC Annual Report,* NUREG/CR-1747 (April 1981).

HARRISON, S. H., ZEISLER, R., ANDERSON, D. L., "Evaluation and Analysis of Environmental Specimen Bank Samples by Nuclear Methods," *J. Radioanal. Chem.* (to be published).

PUBLICATIONS

HARRISON, S. H., ZEISLER, R., WISE, S. A., eds., "Pilot Program for the National Environmental Specimen Bank - Phase 1," (1981).

HARRISON, S. H., GILLS, T. E., MAIENTHAL, E. J., ROOK, H. L., WISE, S. A., ZEISLER, R., and GOLDSTEIN, G. M., "The National Environmental Specimen Bank Pilot Program," *Proc. of the 14th Annual Conference on Trace Substances in Environmental Health,* Columbia, MO., p. 329. (1980).

LINDSTROM, R. M., and FLEMING, R. F., "Accuracy in Activation Analysis: Count Rate Effects," *Proc. of the 4th Int. Conf. Nucl. Method in Env. and Energy Res.,* (1980).

MCGARRY, E. D., FABRY, A., GOLD, R., KELLOGG, L., and KAM F., "Current PCA Specifications for Transport Theory Validation, LWR-PV Surv. Dos. Improvement Program, NUREG/CR-1861, Section 8 (1981).

MCGARRY, E. D., FABRY, A., and GRUNDL, J., "Experimental Program: Integral Measurements in LWR Pressure Vessel Surveillance Dosimetry Improvement Program, PCA Experiments and Blind Test," NUREG/CR-1861, Section 2.0, 2.1, 2.3 and 4.0 (1981).

MCGARRY, E. D., "Determination of the Effective Mass of U-235 in the Fission Chamber Used for Absolute Core Power Measurements in PCA, LWR-PV Irr. Surv. Program," Progress Report, NUREG/CR-1241, Vol. II (1981).

MCGARRY, E. D., "Test of Radiation Exposure Calculations for Reactor Pressure Vessels," *Dimensions* (1980).

POWELL, L. J., MURPHY, T. J., and GRAMLICH, J. W., "The Absolute Isotopic Abundance and Atomic Weight of a Reference Sample of Silver," (to be published) in *J. of Res. Nat. Bur. Stand.*

SCHWARTZ, R. B., and EISENHAUER, C. M., "Use of a D_2O Moderated ^{252}Cf Source for Dosimetry Testing and Calibrations," *Proceedings of Eighth DOE Workshop on Neutron Dosimetry* (1981).

SPIEGEL, V., EISENHAUER, C. M., WINKLER, G., and SMITH, D. L., "Measurement of the Average Activation Cross Section for the Reaction $^{63}\text{Cu}(\eta,\alpha)^{60}\text{Co}$ in the Spontaneous Fission Neutron Field of Californium-252, *Nucl. Sci. & Eng.* 78, No. 4, p. 415 (1981).

ZEISLER, R., "Trace Element Analysis," in Pilot Program for the National Environmental Speciman Bank - Phase I, p. 29, *NTIS*, Springfield, VA (in press).

PUBLICATIONS

ZEISLER, R., and GREENBERG, R. R., "Ultratrace Determination of Platinum in Biological Materials Via Neutron Activation and Radiochemical Separation," *J. Radioanal. Chem.* (to be published).

NBS-114A (REV. 2-80)

U.S. DEPT. OF COMM. **BIBLIOGRAPHIC DATA SHEET** *(See instructions)*	1. PUBLICATION OR REPORT NO. NBS TN 1160	2. Performing Organ. Report No.	3. Publication Date June 1982

4. TITLE AND SUBTITLE

NBS Reactor: Summary of Activities
July 1980 Through June 1981

5. Edited by:
Frederick J. Shorten

6. PERFORMING ORGANIZATION *(If joint or other than NBS, see instructions)*

NATIONAL BUREAU OF STANDARDS
DEPARTMENT OF COMMERCE
WASHINGTON, D.C. 20234

7. Contract/Grant No.
None

8. Type of Report & Period Covered
July 1980 through June 1981

9. SPONSORING ORGANIZATION NAME AND COMPLETE ADDRESS *(Street, City, State, ZIP)*

Same as #6

10. SUPPLEMENTARY NOTES

☐ Document describes a computer program; SF-185, FIPS Software Summary, is attached.

11. ABSTRACT *(A 200-word or less factual summary of most significant information. If document includes a significant bibliography or literature survey, mention it here)*

This report summarizes all those programs which depend on the NBS reactor. It covers the period from July 1980 through June 1981. The programs range from the use of neutron beams to study the structure and dynamics of materials through nuclear physics and neutron standards to sample irradiations for activation analysis, isotope production, radiation effects studies, neutron radiography, and nondestructive evaluation.

12. KEY WORDS *(Six to twelve entries; alphabetical order; capitalize only proper names; and separate key words by semicolons)*

Activation analysis; crystal structure; diffraction; isotopes; molecular dynamics; neutron; neutron radiography; nondestructive evaluation; nuclear reactor; radiation.

13. AVAILABILITY

☒ Unlimited
☐ For Official Distribution. Do Not Release to NTIS
☐ Order From Superintendent of Documents, U.S. Government Printing Office, Washington, D.C. 20402.
☒ Order From National Technical Information Service (NTIS), Springfield, VA. 22161

14. NO. OF PRINTED PAGES
204

15. Price

USCOMM-DC 6043-P80

✰U.S. GOVERNMENT PRINTING OFFICE: 1982-360-997/2118

NBS TECHNICAL PUBLICATIONS

PERIODICALS

JOURNAL OF RESEARCH—The Journal of Research of the National Bureau of Standards reports NBS research and development in those disciplines of the physical and engineering sciences in which the Bureau is active. These include physics, chemistry, engineering, mathematics, and computer sciences. Papers cover a broad range of subjects, with major emphasis on measurement methodology and the basic technology underlying standardization. Also included from time to time are survey articles on topics closely related to the Bureau's technical and scientific programs. As a special service to subscribers each issue contains complete citations to all recent Bureau publications in both NBS and non-NBS media. Issued six times a year. Annual subscription: domestic $18; foreign $22.50. Single copy, $4.25 domestic; $5.35 foreign.

NONPERIODICALS

Monographs—Major contributions to the technical literature on various subjects related to the Bureau's scientific and technical activities.

Handbooks—Recommended codes of engineering and industrial practice (including safety codes) developed in cooperation with interested industries, professional organizations, and regulatory bodies.

Special Publications—Include proceedings of conferences sponsored by NBS, NBS annual reports, and other special publications appropriate to this grouping such as wall charts, pocket cards, and bibliographies.

Applied Mathematics Series—Mathematical tables, manuals, and studies of special interest to physicists, engineers, chemists, biologists, mathematicians, computer programmers, and others engaged in scientific and technical work.

National Standard Reference Data Series—Provides quantitative data on the physical and chemical properties of materials, compiled from the world's literature and critically evaluated. Developed under a worldwide program coordinated by NBS under the authority of the National Standard Data Act (Public Law 90-396).

NOTE: The principal publication outlet for the foregoing data is the Journal of Physical and Chemical Reference Data (JPCRD) published quarterly for NBS by the American Chemical Society (ACS) and the American Institute of Physics (AIP). Subscriptions, reprints, and supplements available from ACS, 1155 Sixteenth St., NW, Washington, DC 20056.

Building Science Series—Disseminates technical information developed at the Bureau on building materials, components, systems, and whole structures. The series presents research results, test methods, and performance criteria related to the structural and environmental functions and the durability and safety characteristics of building elements and systems.

Technical Notes—Studies or reports which are complete in themselves but restrictive in their treatment of a subject. Analogous to monographs but not so comprehensive in scope or definitive in treatment of the subject area. Often serve as a vehicle for final reports of work performed at NBS under the sponsorship of other government agencies.

Voluntary Product Standards—Developed under procedures published by the Department of Commerce in Part 10, Title 15, of the Code of Federal Regulations. The standards establish nationally recognized requirements for products, and provide all concerned interests with a basis for common understanding of the characteristics of the products. NBS administers this program as a supplement to the activities of the private sector standardizing organizations.

Consumer Information Series—Practical information, based on NBS research and experience, covering areas of interest to the consumer. Easily understandable language and illustrations provide useful background knowledge for shopping in today's technological marketplace.

Order the **above** *NBS publications from: Superintendent of Documents, Government Printing Office, Washington, DC 20402.*

Order the **following** *NBS publications—FIPS and NBSIR's—from the National Technical Information Services, Springfield, VA 22161.*

Federal Information Processing Standards Publications (FIPS PUB)—Publications in this series collectively constitute the Federal Information Processing Standards Register. The Register serves as the official source of information in the Federal Government regarding standards issued by NBS pursuant to the Federal Property and Administrative Services Act of 1949 as amended, Public Law 89-306 (79 Stat. 1127), and as implemented by Executive Order 11717 (38 FR 12315, dated May 11, 1973) and Part 6 of Title 15 CFR (Code of Federal Regulations).

NBS Interagency Reports (NBSIR)—A special series of interim or final reports on work performed by NBS for outside sponsors (both government and non-government). In general, initial distribution is handled by the sponsor; public distribution is by the National Technical Information Services, Springfield, VA 22161, in paper copy or microfiche form.

U.S. DEPARTMENT OF COMMERCE
National Bureau of Standards
Washington, D.C. 20234

OFFICIAL BUSINESS

Penalty for Private Use, $300

POSTAGE AND FEES PAID
U.S. DEPARTMENT OF COMMERCE
COM-215

U.S.MAIL

SPECIAL FOURTH-CLASS RATE
BOOK